533516

Research on High Temperature Ceramic Insulation for Electrical Conductors

by

Eric R. Kreidler, Associate Professor
Materials Science and Engineering
The Ohio State University

and

Vidya Praveen Bhallamudi, M. S.
The Ohio State University

Final report on

Grant Number NAG 3-2090
NASA Glenn Research Center
21000 Brookpark Rd
Cleveland, OH 44135

June 6, 2001

Research on High Temperature Ceramic Insulation for Electrical Conductors

by

Eric R. Kreidler, Associate Professor
Materials Science and Engineering
The Ohio State University

and

Vidya Praveen Bhallamudi, M. S.
The Ohio State University

Final report on

Grant Number NAG 3-2090
NASA Glenn Research Center
21000 Brookpark Rd
Cleveland, OH 44135

June 6, 2001

Contents

Summary and Recommendations for Future Work

Three methods for applying ceramic coatings to wires were examined in depth and a fourth (chemical vapor deposition) was studied briefly. Three of the methods are reported in Vidya Praveen Bhallamudi's M. S. Thesis, which is attached. CVD coatings were not reported in the thesis because it was realized early in the study that the deposition rate of the coatings* was too slow to be used in a commercial process.

Of the methods reported in the thesis, slurry coating was the most promising. This method consists of slowly drawing a platinum wire through a thixotropic slurry of alumina in a vehicle composed of polyvinyl butyral, methyl ethyl ketone, and toluene. The coatings produced by this method were continuous and free of cracks after sintering (see pg. 97 of the thesis). The sintered coatings crack when the wire is bent around sharp corners (pg. 98), but most of the coating remains in place and still provides electrical insulation between the wire and any metallic structure to which the wire may be attached. The coating thickness was 0.61mil (16μ). The electrical resistivity of the intact coating was 340MΩ-cm at 800°C and 23MΩ-cm at 1050°C. Therefore, these coatings more than meet the electrical requirements for use in turbine engines. Although adherence of the coating to the wire was generally excellent, a problem was noted in localized areas where the coating flaked off. Further work will be needed to obtain good coating adherence along the entire length of the wire.

The next most promising coatings were made by electrophoretic deposition (EPD) of Al_2O_3 onto platinum wires, using mixtures of ethanol and acetone as the suspending liquid. These EPD coatings were made only on short lengths of wire because the coating is too fragile to allow spooling of the wire. The coatings were uniform and free of cracks after drying (pg. 76), but developed regularly spaced transverse cracks after sintering (pg. 76). The thickness of the EPD coatings was controlled by varying the deposition time and current. The coating, shown on page 76, was 4.8mil thick after sintering. The average crack width was 3-4mil and the average spacing of the cracks was 20.7mil. The crack width is too small to allow contact between the wire and any metallic structure that supports the wire. The coating adheres well to the wire (pg. 77). When the wire is bent, no coating is lost because bending occurs only where the coating is already cracked (pg. 57). We estimate that the wire shown on page 76 could be bent 90° around a corner, having a radius of 0.044", without stretching the platinum wire. The electrical resistivity of the EPD coatings was 70MΩ-cm at 900°C and 3MΩ-cm at 1050°C. Although the resistivity of the EPD coatings is lower than that of the slurry coatings, the EPD coatings still provide effective electrical insulation. As shown on pg. 83, the cracks can be covered up by a second EPD coating if desired. The pre-cracked EPD coatings are effectively similar to using fish spine beads strung onto wires to provide electrical insulation. However, the big advantage of the pre-cracked EPD coatings is that the overall diameter

* Silica coatings were made by decomposing gaseous tetraethyl orthosilicate on a platinum wire.

of the insulated wire (~16 mil for the case on pg.76) is much smaller than that possible with fish spine beads (~62 mil). The micrograph on page 77 suggests that the cracks initiate on the outermost surface of the coating. Based upon the micrographs on page 76, the estimated volume shrinkage due to sintering is 54%. Since the sintered coatings are at theoretical density, the unfired EPD coating had a packing fraction of 0.46, which is relatively low and consistent with the flocculated nature of the starting suspension..

The worst coatings were those made by electrophoretic deposition from aqueous suspensions. Due to generation of gas bubbles at the electrodes, the coatings contained large pores and the thickness was not uniform (pg. 66). The gas bubbles are due to the electrolysis of water and are unavoidable in aqueous EPD. The dried coatings contained transverse cracks similar to those, which occur after sintering wires EPD coated from organic suspensions. A very undesirable crack pattern, involving both transverse and longitudinal cracks was observed in thin coatings (pg. 64). Because of the defects noted above, we do not recommend further development of aqueous EPD coatings.

Continuous slurry coating of wire was achieved, but due to lack of suitable equipment, the wire had to be cut into short (~one foot) lengths for sintering. We recommend that a wire handling system be built which can continuously feed wire through a high temperature furnace at rates appropriate for binder burn out and sintering of the coating. We also recommend that studies be undertaken to determine the maximum feed rates that can be used to process the coatings. Once this is accomplished, we will be able to provide long lengths of wire for evaluation in engineering tests. We recommend further development of the slurries used to coat the wires. The current slurries have short shelf life and it is hard to control their viscosity. This means that it is not easy to control the coating thickness. Slurries should be developed which use water or other solvents having lower vapor pressures than methyl ethyl ketone and toluene. By reducing the evaporation rate of the solvents, we can obtain slurries whose rheological properties are less variable during coating. Further work must be done on wire cleaning techniques to eliminate localized areas having poor coating adherence. In the work, reported in the thesis, the wire was cleaned by passing it through an ultrasonic bath containing acetone. Some localized contaminants, were apparently not removed by this process and these later led to areas having poor coating adherence. We recommend that, in addition to solvent cleaning, the wire be heated to ~1000°C to remove carbonaceous or other insoluble materials.

We recommend further development of organic EPD coatings with the main objective being to make this a continuous process. Our results show that deposition from organic suspensions is fast enough to be used in a continuous process. EPD coating has several potential advantages over slurry coating. In slurry coating, the viscosity of the suspension must be exactly right to obtain good coatings of the desired thickness. In EPD coating, it is much easier to simply adjust the time and current needed to obtain a desired thickness. EPD coating also has a potential advantage in continuous firing because very

little organic material is present in the dried coating. Slurry coated wires contain a large amount of organic binder and burning out this binder will probably be the rate limiting step in firing the coatings. Since little or no binder has to be burned out of the EPD coatings, we expect that higher sintering speeds will be possible. Further work needs to be done on the relationship between crack frequency and thickness of EPD coatings. We also recommend that a study be carried out to determine if cracking is related to the degree of dispersion of the alumina particles while they are still in suspension. More disperse systems should yield higher packing density in the unfired coating, but this may not be the optimum condition. We note that our suspensions, used in slurry coating, were gelled (i.e., highly flocculated) and this should lead to relatively low packing density in the green coating. As noted earlier, these coatings did not develop cracks when sintered whereas the more densely packed green EPD coating did develop cracks.

In conclusion, both the continuous coatings and those having regularly spaced transverse cracks may be useful as high temperature electrical insulation. We recommend continued development of both types of coating. After long lengths of coated wire are produced, using the continuous coating and firing procedures we envision, they should be tested to determine their suitability for use in engines. We recommend that only pure platinum or platinum-rhodium alloys be used as the substrate wires. These materials have high melting points and do not oxidize in air at high temperatures. This allows the alumina coatings to be sintered to high density without contamination from the wire. The thermal expansion of Al_2O_3 and platinum are well matched, making it possible to obtain highly adherent coatings. We have found that platinum-10% nickel wires (suggested for use in engine instrumentation) oxidize in air at 800°C, producing a layer of NiO on the surface of the wire. At elevated temperatures, NiO reacts with Al_2O_3 and forms $NiAl_2O_4$ spinel. The electrical properties of this spinel are inferior to those of pure α-Al_2O_3.

Application of Ceramic Insulation on High Temperature Instrumentation Wire for Turbine Engines*

by

Eric R. Kreidler, Associate Professor
Vidya Praveen Bhallamudi†, M.S.

Dept. of Materials Science & Engineering
The Ohio State University
Columbus, Ohio

Sponsor

NASA Glenn Research Center
Cleveland, Ohio
Grant # NAG 3-2090

Presented May 29, 2001
at
2001 International Nano Ceramics/Crystal Forum
and
International Symposium on Intermaterials
Hanyang University
Seoul, Korea

---

* Submitted for publication in the Journal of Ceramic Processing Research published by the International Organization for Ceramic Processing.

† At the time this work was done he was a candidate for the Master of Science Degree.

Abstract

Problems with the mineral insulated, metal sheathed lead wires used to instrument aircraft engines have become more severe at the increased operating temperatures of today's engines. To solve these problems, we have applied high purity Al_2O_3 directly onto platinum wires. Three coating methods have been studied, electrophoretic deposition (EPD) from ethanol suspensions, slurry coating, and EPD from aqueous suspensions. The coatings were sintered to theoretical density at 1500-1600°C. Highly adherent, crack free, coatings were obtained by the slurry coating process. When bent, the coating cracked in localized areas, but very little of it was dislodged from the wire. The wires coated by EPD from ethanol suspensions were free of cracks after drying but after sintering, regularly spaced cracks perpendicular to the wire axis developed. These cracks allow the wire to be bent around corners while still retaining the sintered coating. The coatings obtained by EPD from aqueous suspensions contained large voids due to the gas bubbles generated by electrolysis of water. After drying, these coatings exhibited two different crack patterns. One pattern was similar to that seen in sintered coatings obtained by EPD from organic systems. The other crack pattern occurred in thin coatings and consisted of an interconnected network of longitudinal and perpendicular cracks. The latter cracking pattern is undesirable. The deposition rates of the coatings were studied as functions of the variables in the processes. Although all three coating methods were sufficiently rapid to serve as the basis for a commercial process, aqueous EPD coatings are not recommended for this application. The electrical resistivity of the sintered coatings was studied as a function of temperature from 800 to 1050°C. The resistivities of the coatings at 800°C were 3.4-7.5x$10^8\Omega$-cm, depending upon coating type.

Introduction

The efficiency and performance of jet aircraft improves as the engine operating temperature increases. Consequently, there has been a steady trend to increase the operating temperature of turbine engines. In the design and development stage, engines may be equipped with dozens of sensors including, thermocouples, strain gauges, and blade tip clearance detectors, to monitor conditions at critical points in the design. The signals from these sensors are led out of the engine through mineral insulated metal sheathed wires. These wires have a central metal conductor surrounded by particulate insulation, which is held in place by an outer metal sheath. The insulating materials are usually MgO or Al_2O_3, of mineral origin, and are not very pure. The wires are produced in various sizes by conventional wire drawing methods, and during this operation the insulation may be further contaminated by abrasion of material from the metal conductor and the sheath. Engineers, who are responsible for engine instrumentation, estimate that up to 90% of the sensor failures can be traced to problems with the lead wires. At the high operating temperatures (>800°C) of engines currently under development, sensor failures have become excessive, and attention has been focused on lead wire failures and

other instrumentation concerns through PIWG*. Lead wires fail for several reasons. The insulation may become electrically conducting at high temperatures or it may be dislodged due to intense acoustic vibrations. The latter problem is most likely to occur at sharp bends in the wire. In either case the result is an electrical short between the conductor and the sheath.

The failures caused by high temperature conductivity of the MgO or Al_2O_3, used in mineral insulated wires, must be due to contamination by impurities, either present in the raw materials or picked up during wire manufacture. This must be the case because pure Al_2O_3 and MgO have very high resistivity even at high temperatures. The resistivity of polycrystalline Al_2O_3 at 1000°C is $1.78 \times 10^7 \Omega$-cm and that of MgO is $1.17 \times 10^7 \Omega$-cm[1]. These values are more than adequate for use in lead wires. Dislodgment of insulation by mechanical vibrations is exacerbated by the fact that the insulation is present as a packed powder layer. Applying high purity insulation directly to the conductor wire and then sintering it in place to form a dense ceramic coating, could eliminate both problems. However, for this approach to work, several conditions must be met. The insulation must not become chemically contaminated during manufacture of the wire. The insulation must not react with the conductor wire during sintering. The conductor must not oxidize in air at high temperatures. The sintered insulation must strongly adhere to the wire, so that when the wire is bent very little insulation is lost. Any cracks or openings in the sintered insulation must be so small that metal to metal contact is impossible either between adjacent wires or between wires and engine components. To be used in an engine, the wire must be flexible and have a small diameter i.e. a pair of wires must have a combined diameter <0.060 inch.

To meet the list of requirements, we chose high purity alumina as the insulating material and platinum or platinum-rhodium alloys as the conductor. This combination of materials has several advantages. The thermal expansion coefficients are well matched, and this will promote good adhesion of the Al_2O_3 coating to the Pt wire. The materials will not react chemically with each other at high temperatures, and the metal will not oxidize in air at engine operating temperatures. The melting points of the metals are high enough to allow the alumina coatings to be sintered to theoretical density. Alumina was selected because it has the highest resistivity of all oxides except BeO.

The methods used to apply the coatings were electrophoretic deposition and slurry coating. These methods can be carried out in chemically pure systems and can yield high purity coatings. Since mechanical forming operations such as wire drawing have been eliminated, the purity of the coatings can be maintained throughout the manufacturing process.

* The Propulsion Instrumentation Working Group, organized by the Ohio Aerospace Institute, has members from NASA and all of the major producers of aircraft turbine engines in the United States.

Experimental Procedures

The alumina powders used in this work are listed in Table 1. The particle size, specific surface, and purity varied from one powder to the next, and where necessary, coating formulations were adjusted to take account of these differences. In general, the chemical purity was very high and total metallic impurities did not exceed 180ppm. Substrate wires were either pure platinum or platinum-10% rhodium alloys having diameters of 5-10mil. The wires were cleaned in an ultrasonic bath containing acetone prior to coating with alumina.

Water based suspensions for electrophoretic deposition (EPD) contained 10-40wt.% (2.7-10.1vol.%) alumina. Doubly distilled water was used for all preparations and an ammonium salt of polyacrylic acid* was used as the dispersant. In aqueous media the dispersant dissociates to give $R\text{-}COO^-$ ions. These ions are absorbed onto the alumina surface and give the particles a negative charge. The dispersant was added at a rate of 0.5mg per square meter of alumina surface. The suspensions were ball milled in 1000ml, wide mouth, high density, polyethylene, bottles for 24-48 hours. The milling media were 1/2" alumina spheres.

The suspensions used for non-aqueous EPD were prepared with mixtures of ethanol and acetone. When pure ethanol was used, deposition was not observed at 250Volts, the limit of our power supply†. Addition of acetone lowered the deposition voltage, but because of its high vapor pressure, the amount of acetone was kept at or below 25% by volume. A typical suspension contained 35wt.% alumina and 65wt.% ethanol-acetone mixture (75vol.% ethanol, 25vol.% acetone). No dispersants were used in these suspensions. The suspensions were ball milled for 24 hours in polyethylene bottles.

The suspension used for slurry coating and its preparation is outlined in Table 2. This suspension was based on a tape casting formulation reported by Faber[2]. This slurry had shear thinning characteristics, and its viscosity curve extrapolated to 38,500cP at zero shear rate.

The apparatus for EPD coating consisted of a 500ml beaker and a stand for holding the sample and counter electrode in fixed positions. The counter electrode was a 20mil platinum wire and the samples to be coated were two-inch lengths of Pt or Pt 10% Rh wire. The distance between the electrodes was ~1.5 inches. The voltage source could be operated in either constant current or constant voltage mode, all of our coatings were made using constant current conditions. Coating thickness was controlled by limiting the deposition time and current. The slurry was agitated with a magnetic stirrer to minimize settling of the alumina particles. After the desired coating thickness was obtained, the wires were removed from the slurry and air dried while hanging in a vertical position.

---

* Rohm and Haas Company, Duramax D-3021.
† E-C Apparatus Corporation model EC 250-90.

This was done to prevent distortion of the fragile wet coating by contact with a supporting surface.

The apparatus used for slurry coating is shown in Figure 1. The wire was fed from a spool through an ultrasonic bath filled with acetone and then through the slurry. A stainless steel "J" tube lined with teflon was used to lead the wire under the surface of the slurry. The immersed end of the "J" tube contained a stainless steel orifice (15mil diameter) to serve as a wire guide. The slurry container was tightly sealed except for this orifice and a 1/8" diameter exit hole for the wire. This was done to minimize solvent loss and changes in slurry viscosity. After exiting the slurry the coated wire was passed between two 3-foot long, quartz, infrared heaters. The dried wire was taken up on a motor driven spool. We controlled the velocity of the wire through the coating machine by changing the speed of the drive motor. The coater was capable of wire speeds of 0.2 to >10.0cm/s.

After the coatings had dried, the wires were sintered in air at 1500-1600°C, and held at the maximum temperature for 0.5-2.5 hours. To provide time for the binder to burn out, the slurry coated wires were heated at 2°C/min to 500°C, held at 500°C for one hour, and then heated to the final sintering temperature at a rate of 10°C/min. Since the EPD coatings did not contain a binder they could be heated to the sintering temperature at a rate of 10°C/min with no hold at 500°C. Upon completion of sintering, the furnace was shut off and allowed to cool with the samples still inside. To minimize damage to the coatings during sintering, the samples were hung from 1/8" diameter alumina rods supported by the rim of a large alumina crucible.

The macrostructure of the samples was examined using a stereozoom microscope equipped with a video printer. The coatings were examined after drying and also after sintering, and typical coating structures were photographed. The microstructures of the coatings were examined with a Philips XL-30 FEG scanning electron microscope. To prevent charging, the samples were coated with a thin film of carbon. Thickness measurements of the coatings were obtained by measurements taken on micrographs, having known magnification.

The electrical resistance through the thickness of the coatings was measured in one of two ways depending upon the structure of the coatings. For crack free coatings the sample configuration shown in Figure 2 was used. A short length of the coated wire was attached to a polycrystalline alumina plate with platinum paste. Care was taken to ensure that the entire surface of the coating was coated with the paste. A second platinum lead wire was attached to the platinum paste and the entire assembly was cured at 1200°C. The core wire and the second lead were attached to a Hewlett Packard multimeter and the resistance of the coating was measured as a function of temperature in the interval 800-1050°C. The temperature was raised in 50°C increments and the sample was held at each temperature for 20-30 minutes to allow the temperature to stabilize.

The resistance values were recorded on a computer. A resistance reading was taken every two seconds until 200 values had been accumulated. The average and standard deviations for each set of readings were calculated. These values were later converted to resistivity using the equation $\rho = (R2\pi l(r_o+t/2))/t$ where R is the measured resistance, r_o is the radius of the uncoated wire, t is the coating thickness, and l is the length of the coated wire covered by platinum paste. Depending upon sample temperature, the measured resistance values ranged from 0.66MΩ at 1050°C to 9.60MΩ at 800°C. The standard deviations were consistently about 30% of the average readings.

The cracked EPD coatings could not be measured by the method used for crack free coatings because the Pt paste entered the cracks and made contact with the wire. To measure the resistance of these coatings, the configuration shown in Figure 3 was used. A "hairpin" shaped piece of Pt wire, having a known distance between the legs was EPD coated and sintered. The bend in the hairpin was then cut away and the resistance of the coating, remaining between the legs, was measured with a Keithley electrometer (model 6517). The sample was held 30min at each temperature before a reading was taken. The resistance was not stable and the most frequently observed values were recorded. Measured resistance ranged from 10MΩ at 1050°C to 222MΩ at 900°C. The resistivity of the coatings was calculated using the approximation $\rho = Rd_otl$ where R is the measured resistance, d_o is the diameter of the uncoated wire, l is the length of the coating, and t is the separation between the two wires.

Results and Discussion

Observations on the Coating Processes

Although EPD from aqueous suspensions did not produce the best coatings, this method was studied in greater detail than EPD from organic suspensions. The reason for this was that charging of the particles was more easily controlled in aqueous suspensions. The rate of coating deposition was measured at constant currents of 1.0, 2.0, and 3.0mA in a slurry containing 40wt.% Al_2O_3. As seen in Fig. 4, the deposition rate is constant with time at each current level, as would be expected. However, the rate saturates at about 2.0mA and does not increase significantly with further increases in current. This behavior is probably related to changes in conditions at the anode, where the particles are deposited. As the current increases, the voltage drop through the suspension increases and since the force on the particles increases, one would expect that the deposition rate would also increase. However, most of the potential drop occurs in a thin sheath about the anode, eventually the suspension within this region becomes depleted of alumina particles, and the deposition rate is limited by the diffusion rate of particles to the anode. Under these conditions a greater fraction of the current is carried by the ions in the electrolyte. This means that the rate of electrolysis of water increases, and the anode

becomes covered with a layer of oxygen bubbles. The bubble layer restricts access of particles to the surface of the growing deposit and the deposition rate is further slowed. As will be seen, photomicrographs clearly show that gas bubbles locally restrict deposition of alumina particles. Due to these effects, the quality of the coatings was lower at high deposition rates. The coatings produced under these conditions contained large pores and had uneven or "hilly" surfaces. As shown in Fig. 5, the deposition rate increased as the concentration of alumina particles increased. The effect is not linear, and a fourfold increase in alumina concentration leads to only a 36% increase in coating thickness after 25 seconds of deposition.

Since the EPD coatings made from aqueous suspensions were poor in quality, we decided to abandon this approach and to use organic solvents to formulate the suspensions. Organic solvents do not electrolyze and gasses are not produced at the electrodes. As noted earlier, no dispersants or charging agents were added to the slurries based on ethanol-acetone mixtures. Nevertheless, the alumina particles were sufficiently charged to undergo electrophoretic deposition. The conductivity of the ethanol-based suspensions was measured as the solids content increased. The data in Figure 6 show that the conductivity is linearly related to the alumina concentration. Sarkar and Nicholson[3] have proposed a mechanism for the charging of Al_2O_3 in ethanol. The first step is the adsorption of ethanol molecules at basic surface sites. The adsorbed molecules then dissociate into protons and $C_2H_5O^-$ ions. The $C_2H_5O^-$ ions dissolve into the liquid phase and the protons remain adsorbed on the alumina surface. The alumina particles therefore acquire a positive charge and the solvent becomes more conductive due to the higher concentration of $C_2H_5O^-$ ions. This charging mechanism explains the conductivity seen in Fig. 6 and the fact that the alumina particles are deposited at the cathode.

An attempt was made to control the dispersion of alumina particles in ethanol suspensions by changing the pH. The pH was adjusted by adding small quantities of glacial acetic acid or n-butylamine. The pH of the suspensions was measured as well as the thickness of coatings deposited in 25 seconds at a current of 1.0mA. The pH readings were corrected for the non aqueous environment by the method in reference 3. The data are shown in Figure 7. Increasing the pH had a small effect on the coating rate under these conditions. What is more important is that the coating rate overall is faster ($\sim 7.6 \times 10^{-3}$ mm/s) than that under similar conditions in an aqueous system (9.6×10^{-4}mm/s, Fig.4). This is important because it shows that deposition of alumina from ethanol-acetone mixtures is a rapid process.

The ethanol-based slips were not very stable, the alumina settled rapidly but the resulting sediments were easily re-dispersed. These are characteristics of partially flocculated suspensions. Flocculation occurs when the particle charge is small and the repulsive energy barrier between approaching particles is small. This same energy barrier must be surmounted when particles deposit on the cathode. We believe that the low energy barrier is the reason for rapid deposition in this system.

Slurry coating was studied as an alternative method for applying alumina directly onto platinum wires. The viscosity of the slurry and the speed of the wire through the slurry determine the structure and thickness of the coating. If the viscosity was too low, the coating broke up and became a "string of beads" on the wire. This was caused by Rayleigh instability, the same phenomenon responsible for the break up of a falling stream of water into spherical droplets. The beads were spaced about four diameters apart and left too much exposed wire to be useful for electrical insulation. On the other hand, if the viscosity was too high or if the speed of the wire was too high, the coatings were too thick and too uneven to be useful. With the slurry in Table 2, smooth cylindrical coatings about 0.6mil thick were made when the wire speed was 0.5cm/s. This slurry produced the best results of any tried, and as Figure 8 shows it was thixotropic, having shear-thinning behavior. As the wire was drawn through the slurry, the liquid near the wire was sheared, the viscosity in the sheared zone decreased, and a thin smooth layer of suspension coated the wire. Shortly after leaving the bath, the shearing of the liquid stopped and the viscosity increased due to the thixotropic effect. In addition, solvent evaporation occurred and this also contributed to an increase in viscosity of the suspension adhering to the wire. If the viscosity increased rapidly enough, the coating set up before Rayleigh instability could cause it to break up into a string of beads.

Structure of the Coatings

The structure of a typical dried coating produced by EPD from an aqueous slurry is shown in Figure 9. The coating contains "craters" where it grew around oxygen bubbles attached to the anode surface. When the bubbles break away, the coating tends to fill in the craters but this process is often incomplete and the surface of the coating has irregular undulations which are relicts of the incompletely filled craters. We believe that the large-scale variations in coating diameter, seen in Fig. 9, are caused by this process. The wet coatings are free of cracks, and this indicates that the cracks seen in Fig. 9 are caused by drying shrinkage of the constrained coating. All of the defects seen in Fig. 9 remain in the coating after the wire has been sintered. The drying cracks become wider during sintering due to firing shrinkage. The spacing of the cracks is fairly regular over the length of the coated wire. Detailed studies[4], not reported here, indicate that the crack spacing is influenced by the wire diameter, coating thickness, wire type, and surface roughness of the wire. If the coating is thin, a more complex system of cracks develops as shown in Figure 10. The cracking pattern shown in Fig. 10 is undesirable since the coating flakes off the wire when it is bent around corners. As will be shown later, the regular transverse cracks (Fig. 9) may be useful since they prevent coating loss when the wire is bent.

The coatings produced by EPD from alcohol-based suspensions behave differently than those made from aqueous suspensions. Figure 11 shows that the coatings can be dried without cracking, but when sintered, these coatings develop regularly spaced cracks similar to those found in aqueous EPD coatings. Chiu, Garino and Cima[5,6] have analyzed the stresses developed during drying of constrained ceramic films. Their analysis

indicates that the drying stress in a constrained coating is due to surface tension forces. Since acetone and ethanol have only 1/3 the surface tension of water, the drying stresses in alcohol-acetone based EPD coatings are apparently too low to cause cracking as the coating dries. Furthermore, since no gas bubbles were evolved during the coating process, the coatings had smooth cylindrical surfaces of constant diameter. The dimensions of the coating before and after sintering were used to calculate the radial and longitudinal firing shrinkage. The radial firing shrinkage was 33% and the longitudinal firing shrinkage was 16%. The volume shrinkage on firing was 54%, which is rather large and indicates that the dried coatings had a packing fraction of only 0.46. This is consistent with the earlier observation that the alumina-ethanol-acetone suspensions were flocculated.

The cracks in a sintered coating can be filled by a second EPD coating as shown in Figure 12. However, the second coating develops a new set of cracks, which are located over the intact regions of the first coating. Apparently, the initial cracks serve as "anchoring points" for the second coating. As the second coating shrinks during sintering, new cracks develop between these anchor points. In any case, no exposed metal wire is visible through these double coatings.

The structure of a sintered, slurry coated specimen is shown in Figure 13. The coating has a smooth surface and is free of cracks. The thickness of the coating was 0.61mil. The same specimen is shown at higher magnification in Figure 14. The micrograph shows that the coating was sintered to theoretical density since it is free of porosity. The fine structure within individual grains was caused by thermal faceting of high energy surfaces on the particles, and is often observed in alumina after sintering at high temperatures. The microstructure in Fig.14 was also observed in sintered coatings made by EPD from both alcohol and water based suspensions.

Coating Adherence

Wires must be bent around sharp corners when installed in an engine. Since all ceramics are brittle, they crack when bent. However if the cracks are small and if the alumina coating adheres very strongly to the wire, the coating will remain in place after cracking and continue to provide electrical insulation. To qualitatively assess coating adherence, we bent sintered wires 360° around 1/16 inch drill rod and then examined them under a microscope. Figure 15 shows what happens when a pre-cracked coating is bent. The wire, bridging the cracks, bends and stretches but the wire inside sintered segments of coating remains straight. On the inside radius of the bend, the cracks close while on the outside radius they open up. Since all of the bending strain occurs within the wire, bridging the cracks, none of the alumina coating is lost nor are new cracks formed. Because the widest opening of the cracks is only 250μ (9.8mil), engine components beneath the wire or adjacent wires are unlikely to make contact with the central conductor. Therefore, although the coatings are cracked, such wires may be useful if the coating can withstand the intense acoustic vibrations found in turbine engines. Future

tests are planned to determine how well the coatings will withstand conditions within an operating engine.

The response of a sintered, slurry coated wire to a sharp bend is shown in Figure 16. The coating develops a series of narrow transverse cracks whose spacing is proportional to the local bend radius. However, very little of the coating spalls off the wire and the coating can still provide electrical insulation. The most severe damage occurs at the apex of the bend, but even here, nearly all of the coating remains attached to the wire. Whether it will continue to remain attached when subjected to intense engine vibrations is an open question, which will be answered in the future by testing bent wires in an acoustic chamber, which simulates engine vibrations.

A longitudinal section through a sintered, EPD coated wire is shown in Figure 17, this is the same type of wire shown in Fig. 11. The bright diagonal band is the platinum wire, the coating (including cracks) is the lower brightness region next to the wire, and outside of this (and filling the cracks) is the polymer material used to mount the sample for polishing. The cracks in this coating developed during sintering. The average coating thickness is 4.8mil and the average crack width is 3-4mil. The outer edges of the coating segments are bowed away from the central wire. At the ends of the segments the coating has pulled away from the wire leaving small gaps parallel to the Pt-Al_2O_3 interface. The geometry of the coating segments is an indication that a strong bond exists between the coating and the platinum wire. The frictional forces at the central portions of the segments were sufficiently large to prevent shrinkage of the alumina next to the interface. However, the outer surfaces of the segments were unconstrained and shrank. As a result, the outer surface of the coating was in tension and the part next to the wire was in compression. Eventually these stresses increased to the point where they exceeded the tensile strength of the Pt-Al_2O_3 bond. The bond then ruptured, gaps opened along the interface, and the ends of the coating bowed outward by plastic flow. Despite the gaps, most of the interface remained strongly bonded and the alumina segments were held firmly to the wire.

Wire Flexibility

The minimum bend radius of a wire having a pre-cracked coating can be estimated based upon the following criteria. To prevent damage to the platinum wire, its centerline fiber must remain at constant length, that is the wire should not be stretched. To prevent additional cracks and coating loss, bending should cease when the edges of the cracks come into contact with each other. The geometry for this situation is shown in figure 18. The bend angle (θ) which can be accommodated at each crack is $\tan(\theta/2) = w/(2(t + r_o))$ where w = the average crack width before bending, t = the coating thickness, and r_o = the radius of the uncoated wire. The number of segments (n) needed to bend the wire in a circle can be calculated from $n = 360/\theta$, and therefore the circumference (C) of the circle at the centerline of the wire is $C = nL_s$ where L_s is the average distance between cracks,

measured at the crack centers. The radius (r_c) of the circle at the centerline of the wire is given by $r_c = C/2\pi$ and the minimum radius (r_{min}) at the inside edge of the coating is $r_{min} = r_c - t$. The minimum bend radius for the wire shown in Figs. 11 and 17 was estimated to be 0.044″. In other words, the wire could be bent around a corner, having this radius, without creating new cracks or stretching the conductor wire. The minimum bend radius can be used as a measure of the flexibility of wires having pre-cracked coatings. The flexibility is inversely related to the minimum bend radius.

A similar calculation cannot be done for wires having continuous, crack free, coatings since there are no pre-existing cracks. However, since the coatings are thin, they offer little resistance to bending and the slurry coated wires, in this sense, are quite flexible. A more practical criterion, which cannot be evaluated at present, is how small the bend radius can be without resulting in excessive damage to the coating.

Coating Resistivity

The high temperature resistivity of typical coatings is summarized in Table 3. The measured resistances (and dimensions) of the coatings are included in the table to show that the resistance values themselves are in the Mega Ohm range at temperatures up to 1050°C. Both the slurry coatings and the alcohol-based EPD coatings have high temperature resistivities, which greatly exceed the PIWG target of $1x10^6\Omega$-cm at 800°C. Hence in terms of resistivity alone, either type of coating will be useful in modern turbine engines. The resistivity of a pure, sapphire single crystal[7] is shown in Table 3 for comparison to our coatings. Our coatings do not approach the ultimate resistivity of alumina. There are several potential reasons for this, but the most likely explanation is that our values are dominated by surface resistivity, since we took no special precautions to clean the coatings prior to making measurements. In addition, the platinum paste contains impurities (oxides) to improve its adherence, and we did not use guard rings to intercept and eliminate the contribution of surface currents to our measured resistance values. Moulson and Popper[7] have shown that all of these factors contribute to lowering of measured resistivity. However, since none of these precautions will be taken when wires are installed in engines, our values are indicative of what can be expected in practice.

At 1050°C the resistivity of the slurry coating is about seven times that of the EPD coating. Figure 19 shows that the resistivity values for the two types of coatings converge at lower temperatures and become equal at ~850°C. The difference in high temperature resistivity is in part due to the much longer path that surface currents must traverse in slurry coated samples. In the slurry coated samples this path is at least several centimeters long since it includes the entire length of alumina coating not covered by the platinum paste electrode (see Fig. 2). In contrast, the path length for surface currents in an EPD coated specimen is only 0.055cm, the separation distance between the two embedded wires (see Fig. 3).

The resistivity values were converted to conductivity and a plot of $\ln(\sigma)$ versus 1/T was used to extract the activation energies for conduction. For the sapphire single crystal, the EPD coating, and the slurry coating these values were 3.69, 2.8, and 1.4eV respectively. Since the band gap of alumina is 8.8eV, all of the samples mentioned are conductive by virtue of impurity states in the band gap or by surface conduction. The higher activation energy for the EPD coating (2.8eV) compared to the slurry coating (1.4eV) may be due to impurities in the platinum paste, used to cover a portion of the slurry coated sample. At the curing temperature of the paste (1200°C), these oxide impurities could diffuse into the alumina and introduce additional energy states into the band gap which are more easily populated by thermally excited electrons or holes. The net result would be to reduce the activation energy for conduction.

Despite all the limitations, one can conclude from our measurements that both types of coatings exceed the electrical requirements for use in engines.

Conclusions

Short lengths of platinum wire were coated with alumina by slurry coating and by electrophoretic deposition from alcohol based suspensions. The coatings were sintered to theoretical density at 1500-1600°C. Two types of coatings resulted. One type, prepared by slurry coating, was about 0.6mil thick and free of cracks and other defects. When bent, this coating fractures but virtually all of the alumina remains attached to the wire. The electrical resistivity of this type of coating was $3.4 \times 10^{8}\Omega$-cm at 800°C. The other type, prepared by electrophoretic deposition, was about 5.0mil thick and had regularly spaced transverse cracks about 3.0mil wide. These cracks relieve the stress when the wire is bent, no coating is lost, and no new cracks are formed. The minimum bend radius for such a coating, without damage to the Pt wire, is about 0.45mil. The electrical resistivity of this type of coating was $7.5 \times 10^{8}\Omega$-cm at 800°C. These coatings meet or exceed most of the targets set by PIWG for new lead wire technology, to be used in advanced turbine engines. These targets were; good wire flexibility, coating resistivity of $1.0 \times 10^{6}\Omega$-cm at 800°C, low conductor resistance, diameter for a wire pair less than 63mil, the insulation is not degraded at 800°C, and joining by soft soldering or spot welding. The coated wires, we have produced, are very flexible and greatly exceed the resistivity requirement on the insulation. The resistivity of pure platinum is low ($1 \times 10^{-5}\Omega$-cm at 25°C) and the diameter for a pair of wires is between 14 and 30mil, depending upon wire type. Alumina is one of the materials most resistant to chemical attack and environmental degradation. The joining of our wires by soldering or spot welding has not been tested, but should be possible once methods are developed for stripping the alumina insulation. Although many of the PIWG targets have been met, there are several questions remaining unanswered. The most important ones are; the resistance of the insulation to dislodgment by the intense acoustical vibrations found in operating engines, and the effect of cracks in

the insulation on its electrical resistivity in an engine environment. Tests are planned to answer both of these questions. Finally, the coated wires are sufficiently promising to justify further development of the techniques needed to manufacture them. In particular, pilot scale facilities should be developed which will allow production of long lengths of coated wire.

Acknowledgements

This material is based upon work supported by the NASA Glenn Research Center Award No. NAG 3-2090. Any opinions, findings, conclusions, or recommendations expressed in this publication are those of the authors and do not necessarily reflect the views of the NASA Glenn Research Center. We thank the Members of the Propulsion Instrumentation Working Group (PIWG) and the Ohio Aerospace Institute for calling our attention to the problem. We particularly thank Dr. Jih-Fen Lei of NASA Glenn for her support and encouragement of this project.

References

1. A. A. Bauer and J. L. Bates, Battelle Memorial Inst. Report #1930, July 31, 1974.
2. T. E. Faber, Fluid Dynamics for Physicists, 295, Cambridge University Press (1995).
3. P. Sarkar and P.S. Nicholson, "Electrophoretic deposition (EPD): Mechanisms, Kinetics, and Applications to Ceramics", J. Am. Ceram. Soc. 79 [8], 1987-2002 (1996).
4. Vidya Praveen Bhallamudi, Coating high temperature lead wires with electrically insulating alumina by electrophoretic deposition and slurry coating, M.S. Thesis, The Ohio State University (2000).
5. R.C. Chiu, T.J. Garino, and M.J. Cima, "Drying of granular ceramic films: I, Effect of processing variables on cracking behavior", J. Am. Ceram. Soc. 76 [9], 2257-2264 (1993).
6. R.C. Chiu and M.C. Cima, "Drying of granular ceramic films: II, Drying stress and saturation uniformity", J. Am. Ceram. Soc. 76 [11], 2769-2777 (1993).
7. A.J. Moulson and P. Popper, "Problems associated with the measurement of the volume resistivity of insulating ceramics at high temperature", Proceedings Brit. Ceram. Soc. (1968) No.10, 41-50.

Table 1. Identification and specifications for the alumina powders used in this work.

Alumina Code	Product Code*	Particle Size (μm)	Specific Surface (m^2/gm)	Total impurity content** (ppm)
A	XRC-SP/LS DBM	0.23	20.3	81
B	RC-SP DBM No MgO	0.36	8.42	173
C	XRC-SP BM (No MgO)	3.6	5.53	109
D	RC-SP DBM	0.38	9.33	148
E	CR-30	0.05	25	130
F	RC-SPF-DBM No MgO	0.38	8.52	177

* All powders (except E) were supplied by Malakoff Industries Inc. a division of Reynolds Metals Company. Alumina E was supplied by Baikowski International Corporation.

** As metal oxides. The major impurities were SiO_2, Na_2O, K_2O, CaO, and Fe_2O_3.

Table 2. Preparation of the suspension used for slurry coating.

First milling	
Alumina F	100 g
Toluene (solvent)	18 ml
Methyl Ethyl Ketone (solvent)	18 ml
Defloc Z-3 (dispersant)	3 g
Santicizer (Plasticizer)	4.3 g
Ball milled for	8 hr
Second milling	
Butvar B-79 (binder)	5 g
MEK	20 ml
Toluene	20 ml
Ball milled for	24 hr

Table 3. Electrical properties of alumina coatings made by EPD and slurry coating.

Temperature (°C)	EPD coated samples Resistivity (Ω-cm)	EPD coated samples Resistance (10^6 Ohm)	Slurry coated samples Resistivity (Ω-cm)	Slurry coated samples Resistance (10^6 Ohm)	Resistivity Al_2O_3 Xtal.* (Ω-cm)
800	-	-	337×10^6	9.6 (2.0)†	2.25×10^{22}
850	-	-	197×10^6	5.6 (1.4)	3.81×10^{21}
900	70.1×10^6	222	145×10^6	4.1 (1.3)	7.53×10^{20}
950	15.3×10^6	48.1	43.2×10^6	1.2 (0.4)	1.70×10^{20}
1000	5.53×10^6	17.5	38.3×10^6	1.1 (0.4)	4.30×10^{19}
1050	3.16×10^6	10.0	23.2×10^6	0.66 (0.3)	1.21×10^{19}
Radius of wire (r_o)		0.127mm	-	0.071mm	-
Thickness of coating (t)		0.55mm	-	0.022mm	-
Sample length (l)		6.84mm	-	15.0mm	-
Alumina Type		D		F	
Total Metal Oxide Impurity		148ppm	-	177ppm	-

*Data are for an alumina single crystal, reference 7.

† Numbers in the parentheses are the standard deviations, 200 measurements were made.

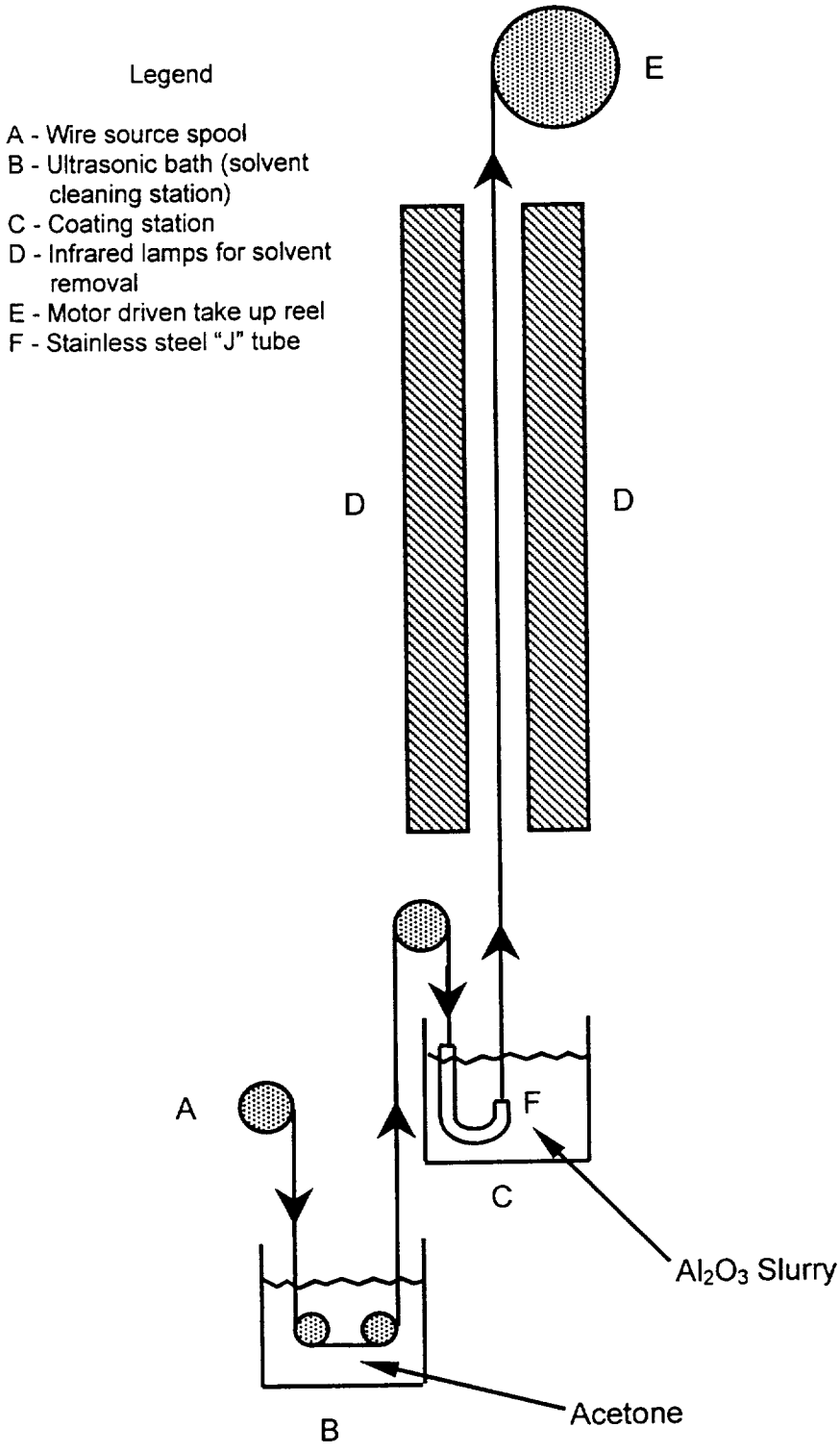

Figure 1. Laboratory scale wire coater.

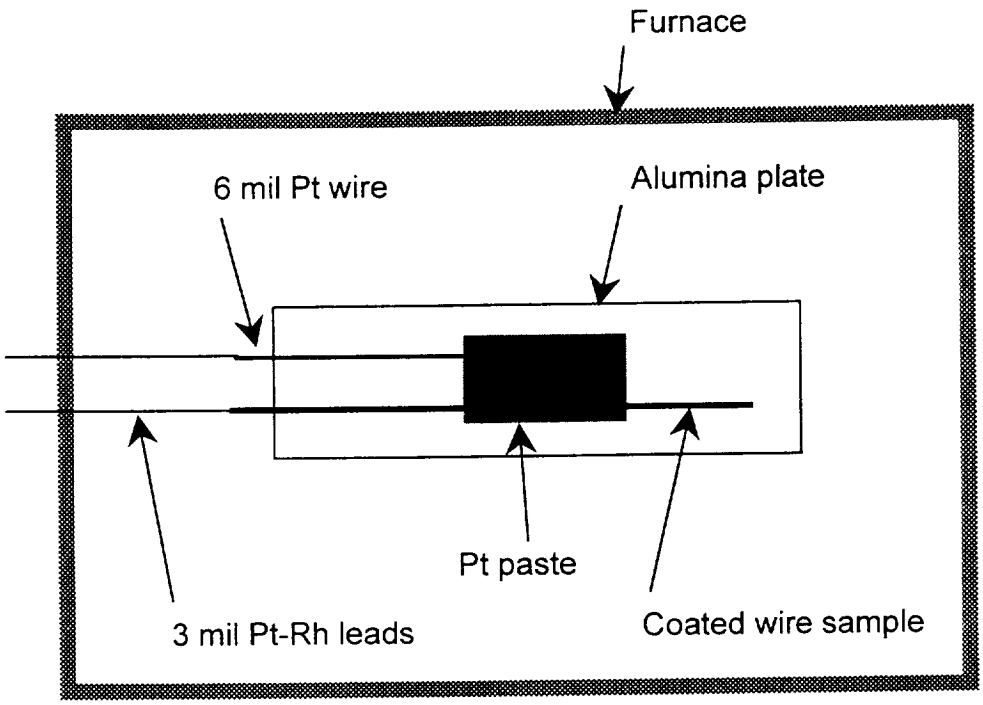

Figure 2. Sample configuration for measuring resistivity of slurry coated samples.

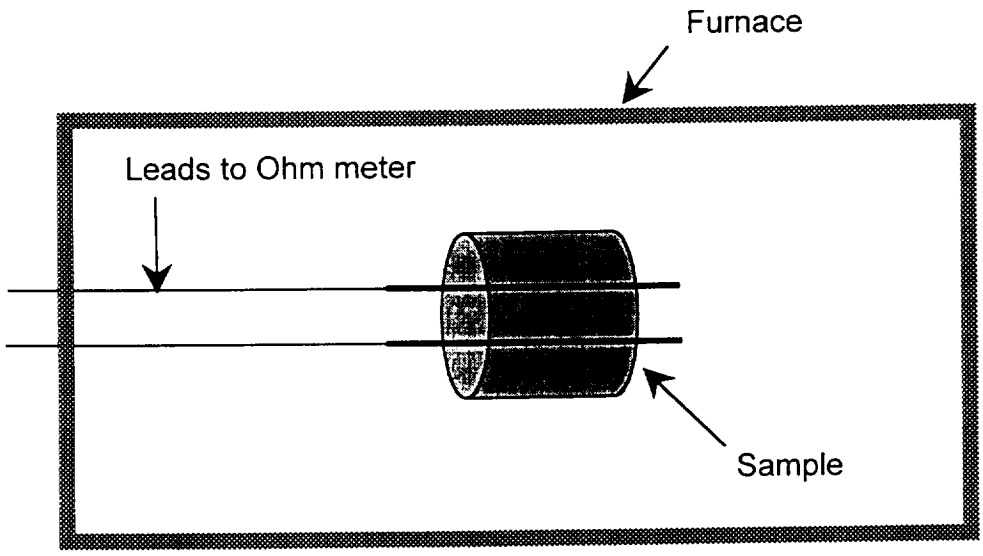

Figure 3. Sample configuration for resistivity measurements on EPD samples.

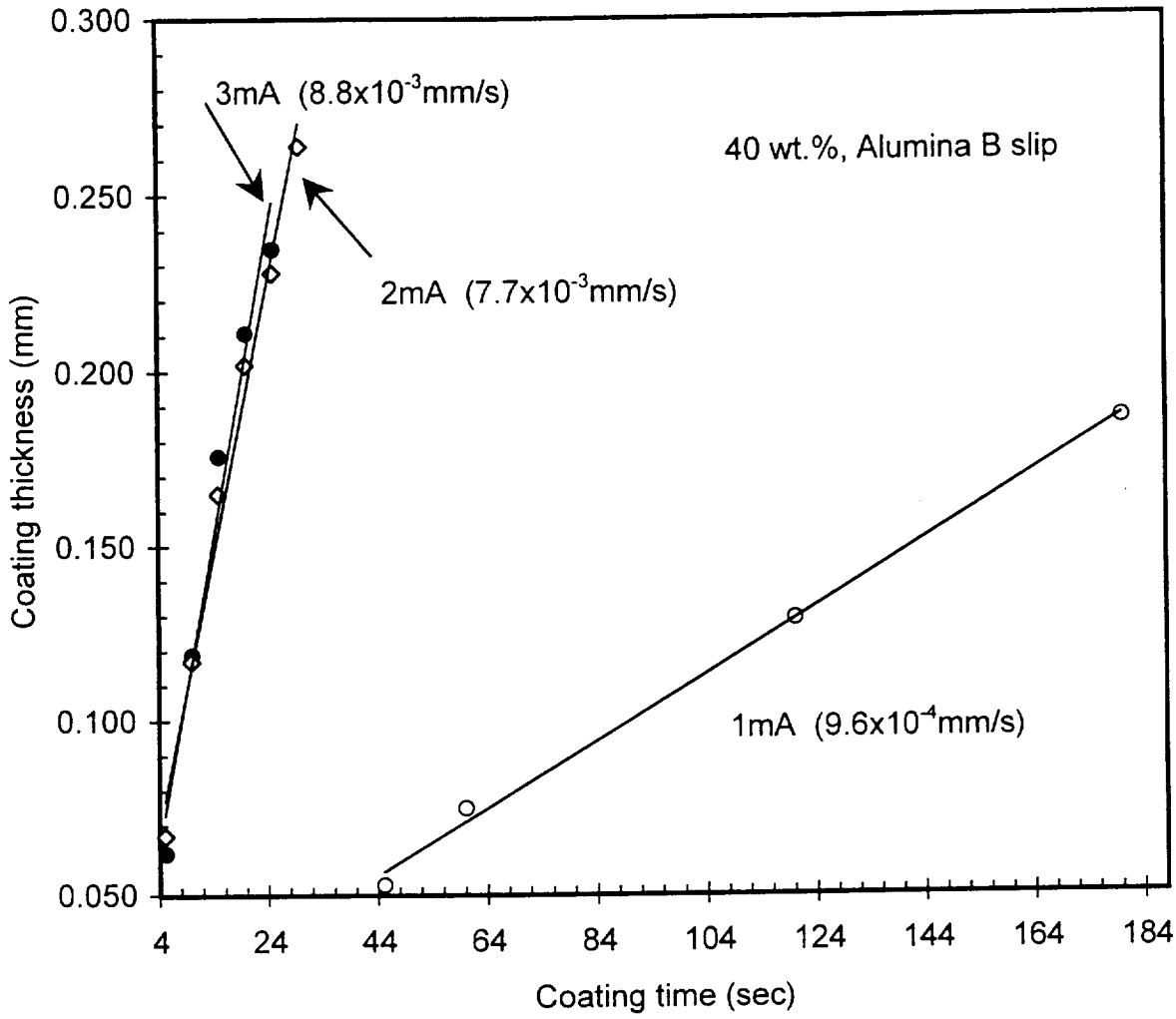

Figure 4. Coating thickness as a function of deposition time and current. Coating rates are given in parentheses.

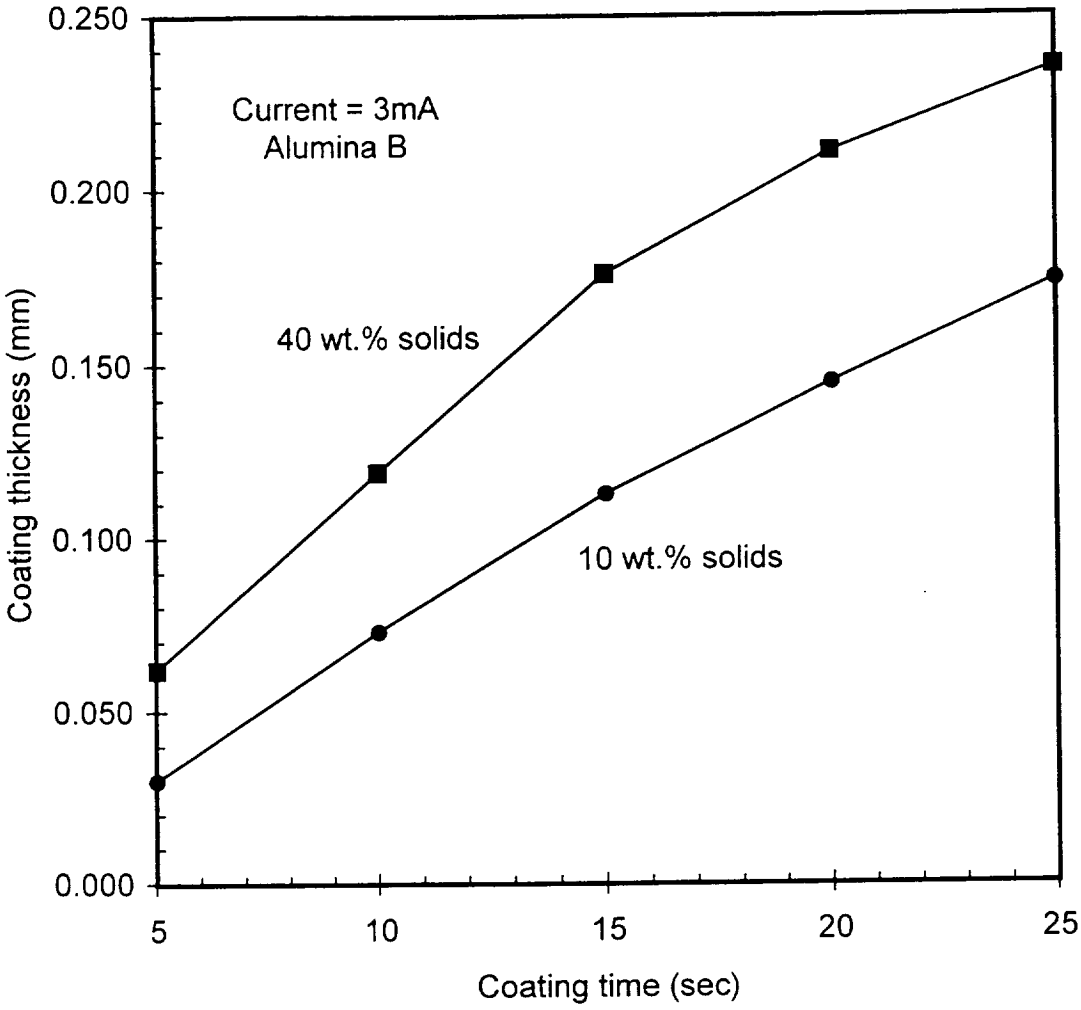

Figure 5. Effect of solids content on the evolution of coating thickness with time.

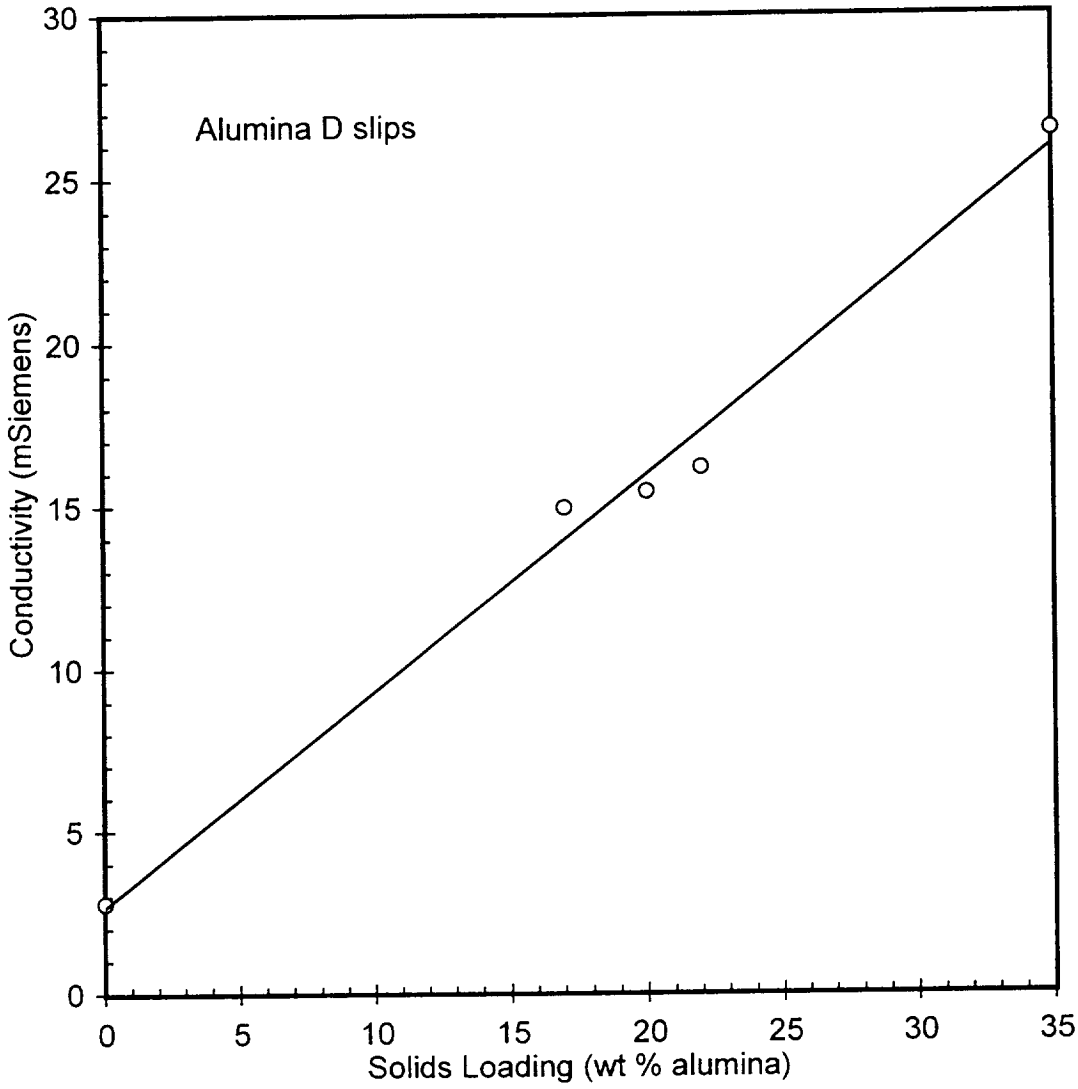

Figure 6. Conductivity of slips with various loadings of alumina dispersed in a mixed ethanol-acetone solvent.

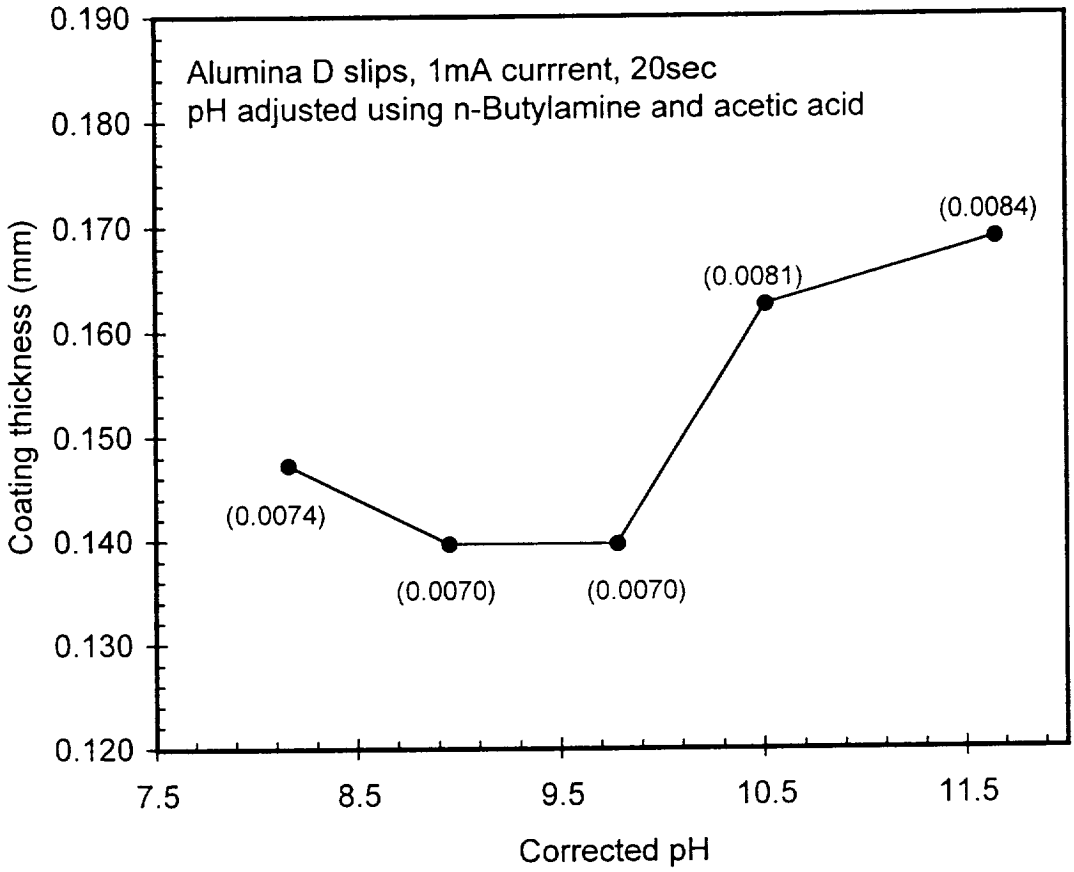

Figure 7. Effect of pH on non-aqueous EPD coating thickness. Coating rates (mm/s) are given in parentheses.

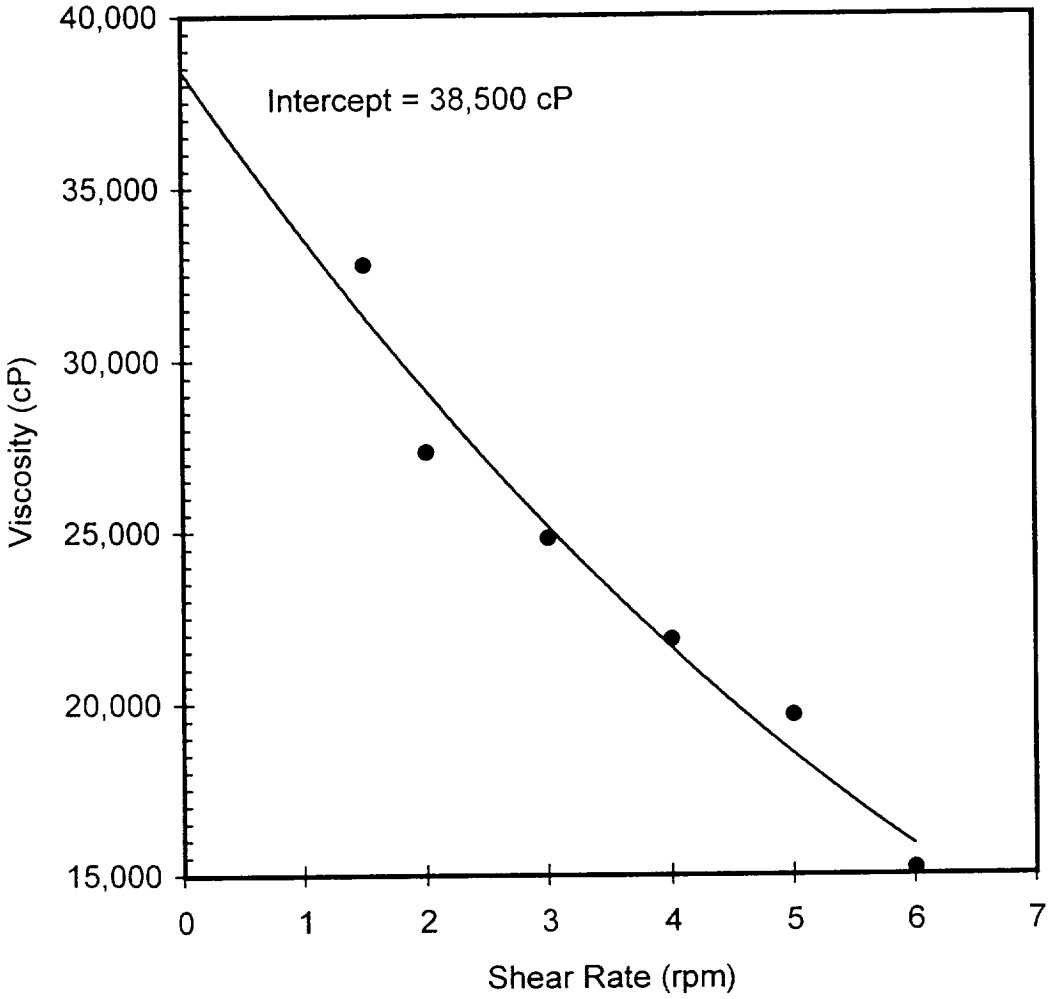

Figure 8. Viscosity of suspension used for slurry coating.

Figure 9. An EPD coating made from an aqueous slip. The large pores formed as the coating grew around oxygen bubbles attached to the electrode. The bubbles were formed by electrolysis of water.

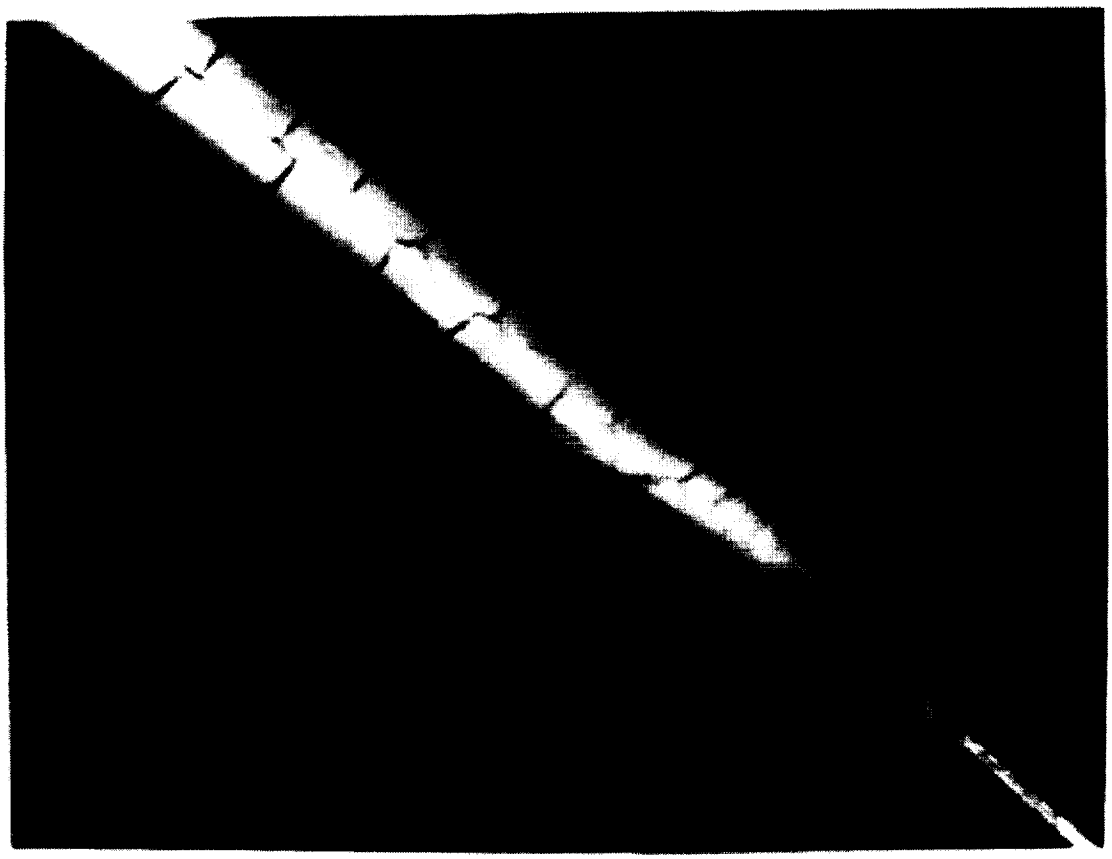

Figure 10. Optical micrograph of an aqueous EPD coating showing an undesirable interconnected cracking pattern.

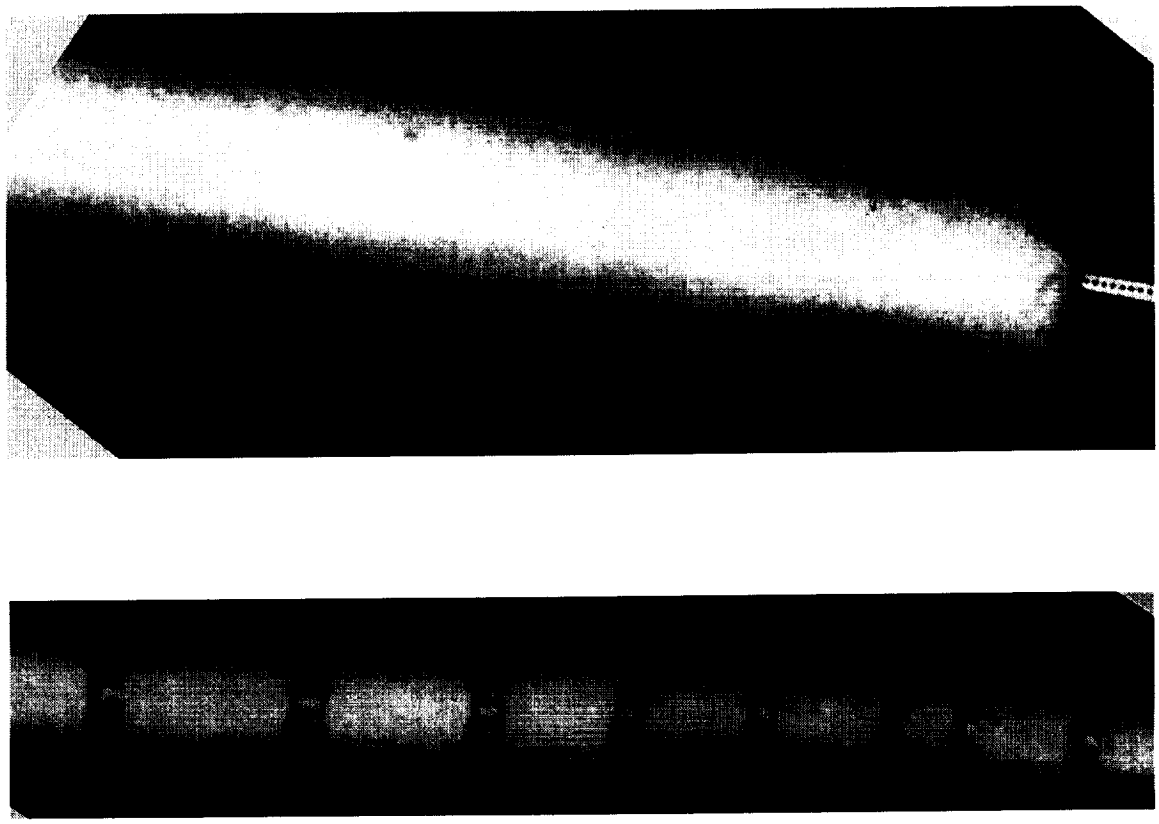

Figure 11. Coatings prepared by EPD from ethanol-based dispersions. No cracks were present after drying but transverse cracks developed during sintering. Wire diameter = 5.8mil.

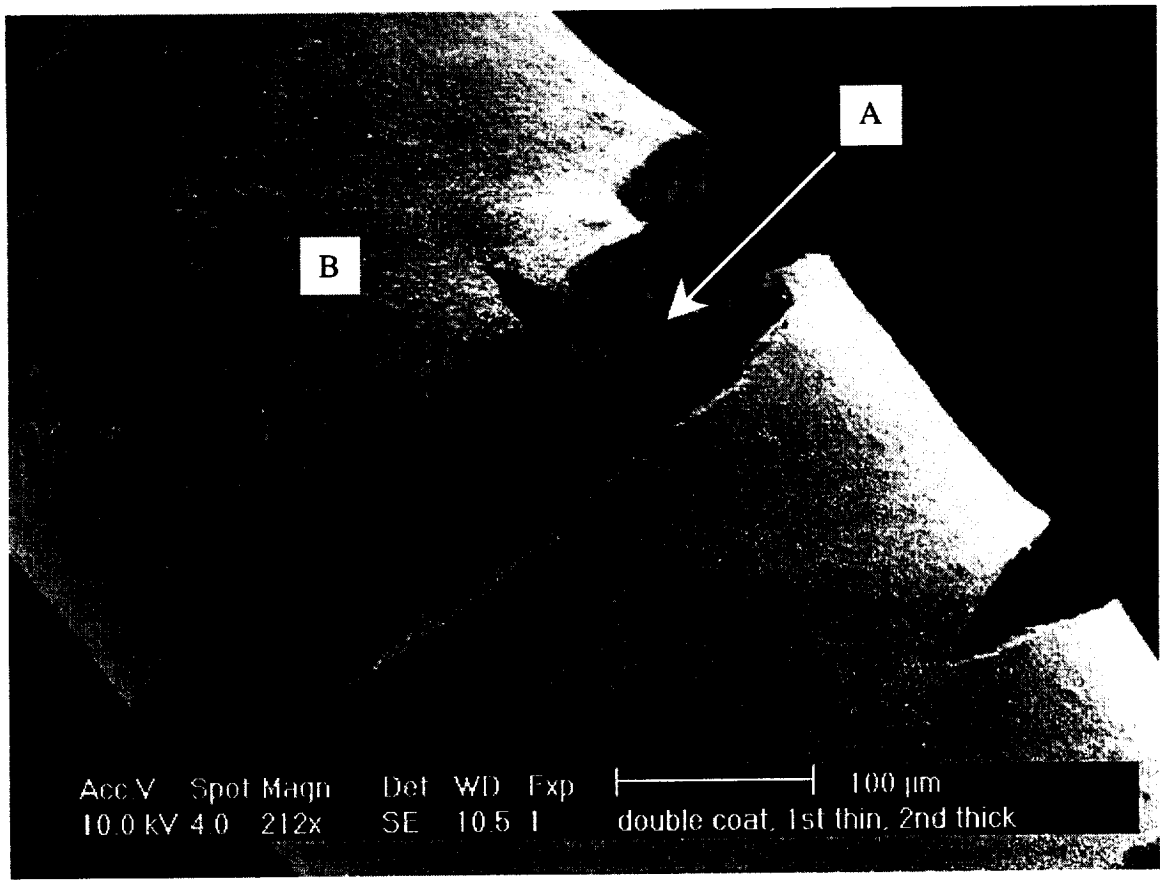

Figure 12. Scanning electron micrograph showing a second coating covering the cracks in the first coating in a double EPD-coated wire. A = first coating (thickness = 1.7 mil), B = second coating, (thickness = 2.8 mil).

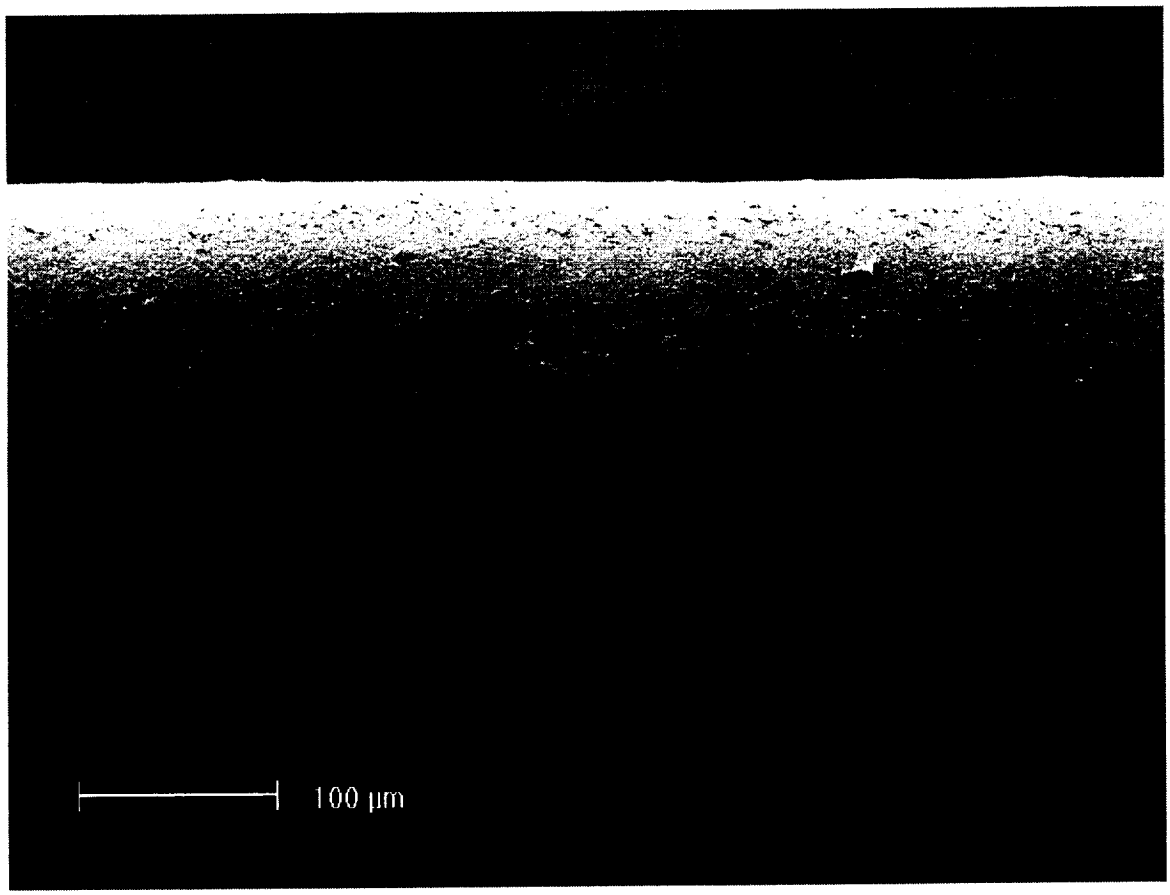

Figure 13. Scanning electron micrograph of a sintered slurry coated wire, showing a smooth crack free surface. Wire diameter = 5.8mil.

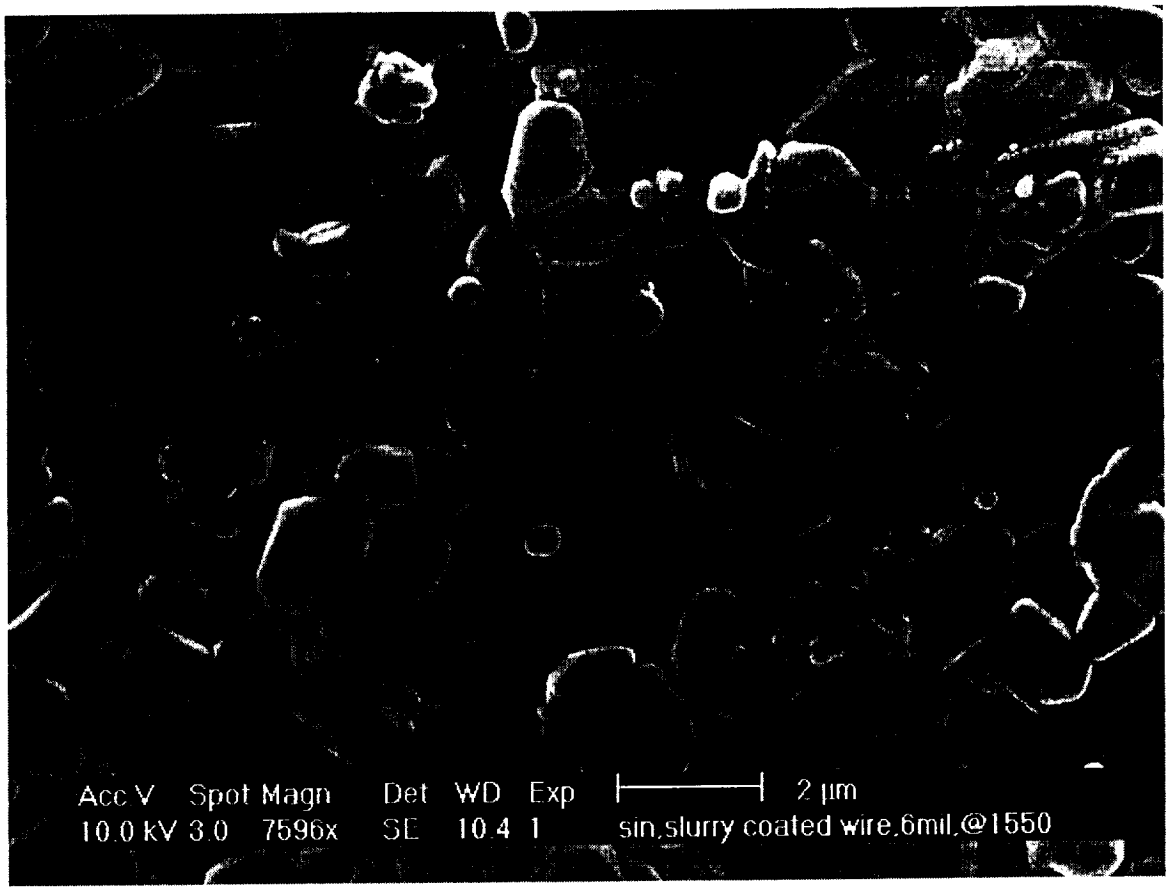

Figure 14. SEM micrograph of a sintered, slurry coated, sample showing that the alumina coatings were sintered to theoretical density.

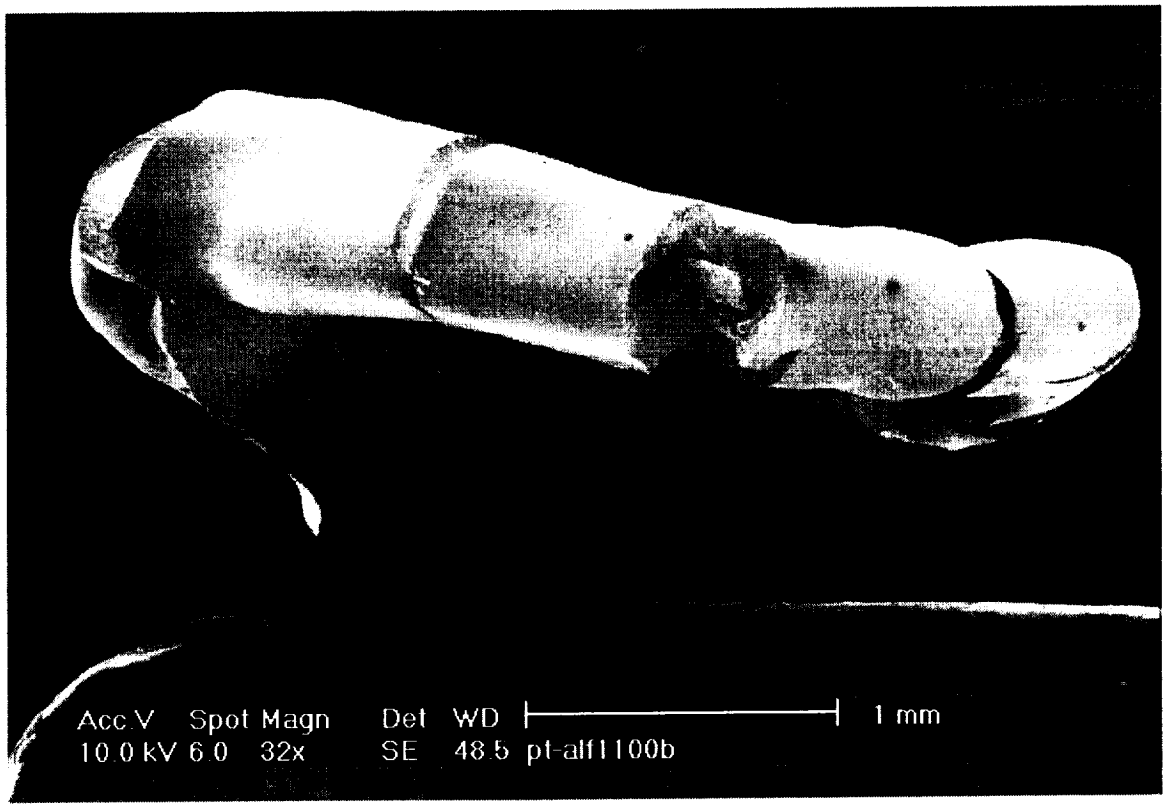

Figure 15. SEM micrograph of a thick, pre-cracked EPD coating showing that the coating remains in place when bent around a 1/16" rod.

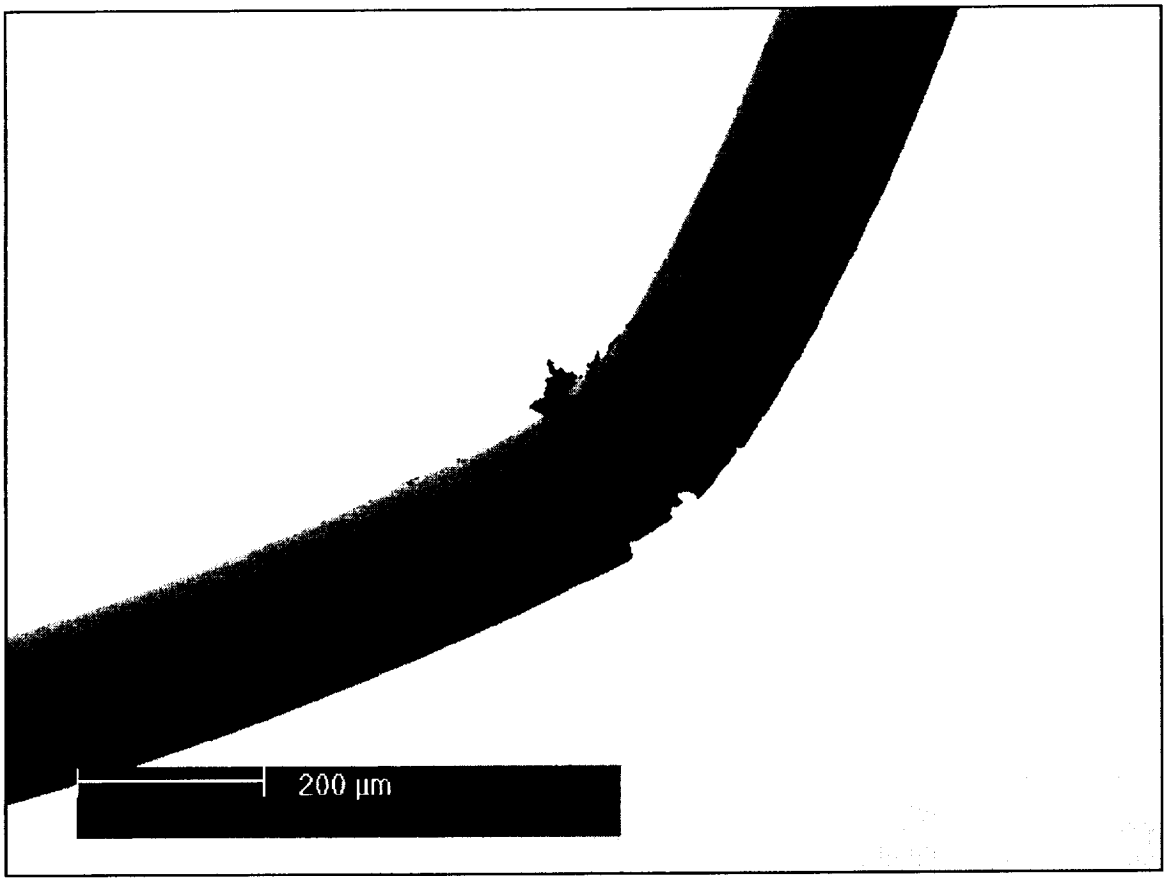

Figure 16. SEM micrograph of a slurry coated sample showing that only a small portion of the coating falls off even at sharp bends.

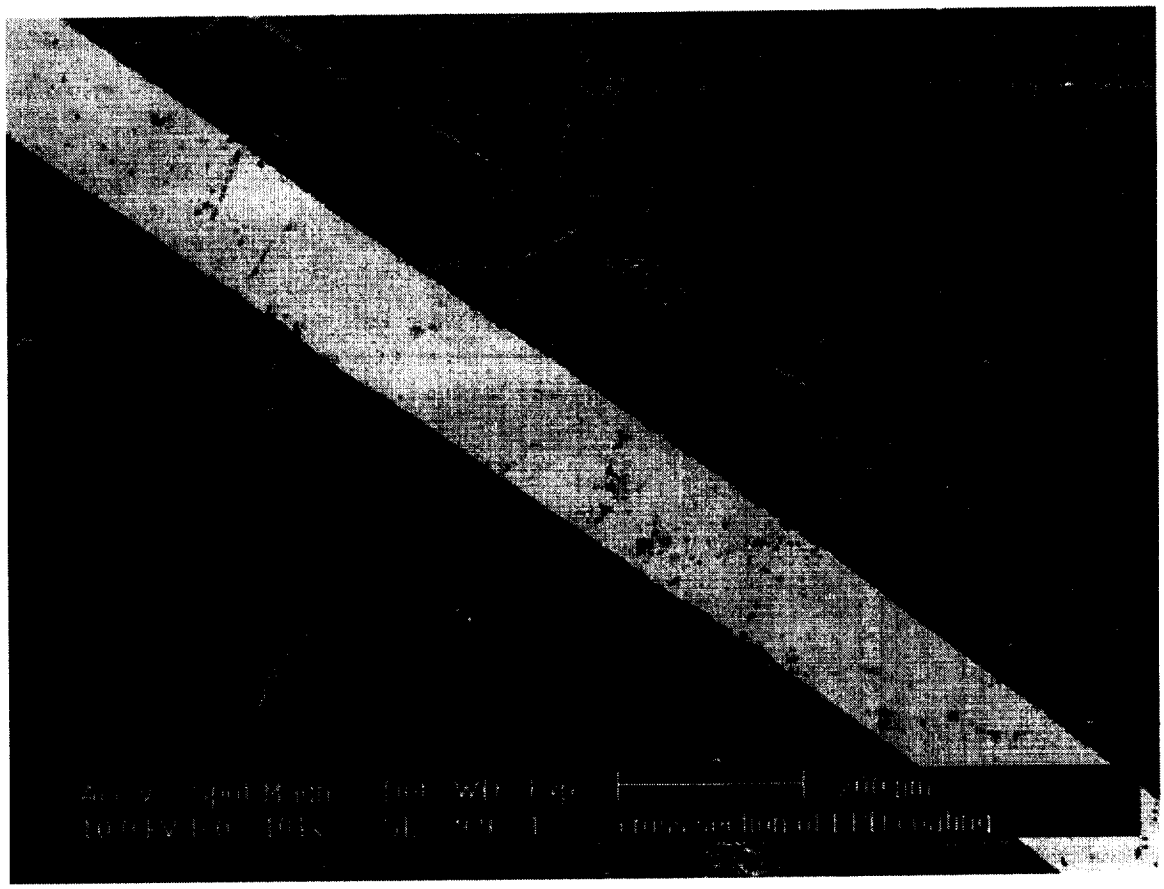

Figure 17. Cross section of a sintered coating made by non-aqueous EPD. The coating was made from a suspension of alumina D and was sintered at 1550°C for 2.5 hr.

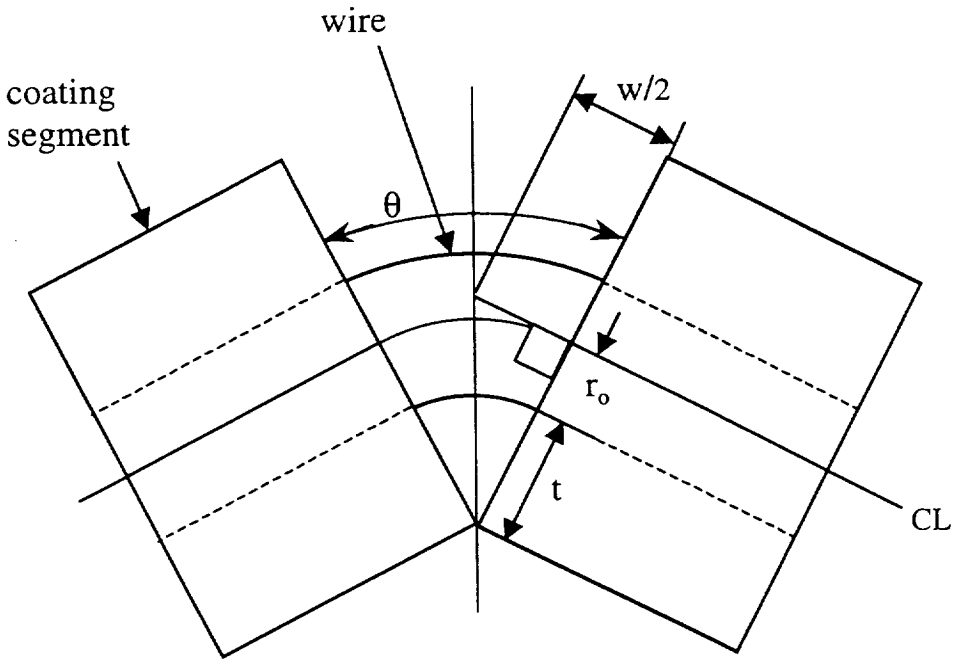

Figure 18. Geometry around a single bend in a pre-cracked wire. See text for meaning of symbols.

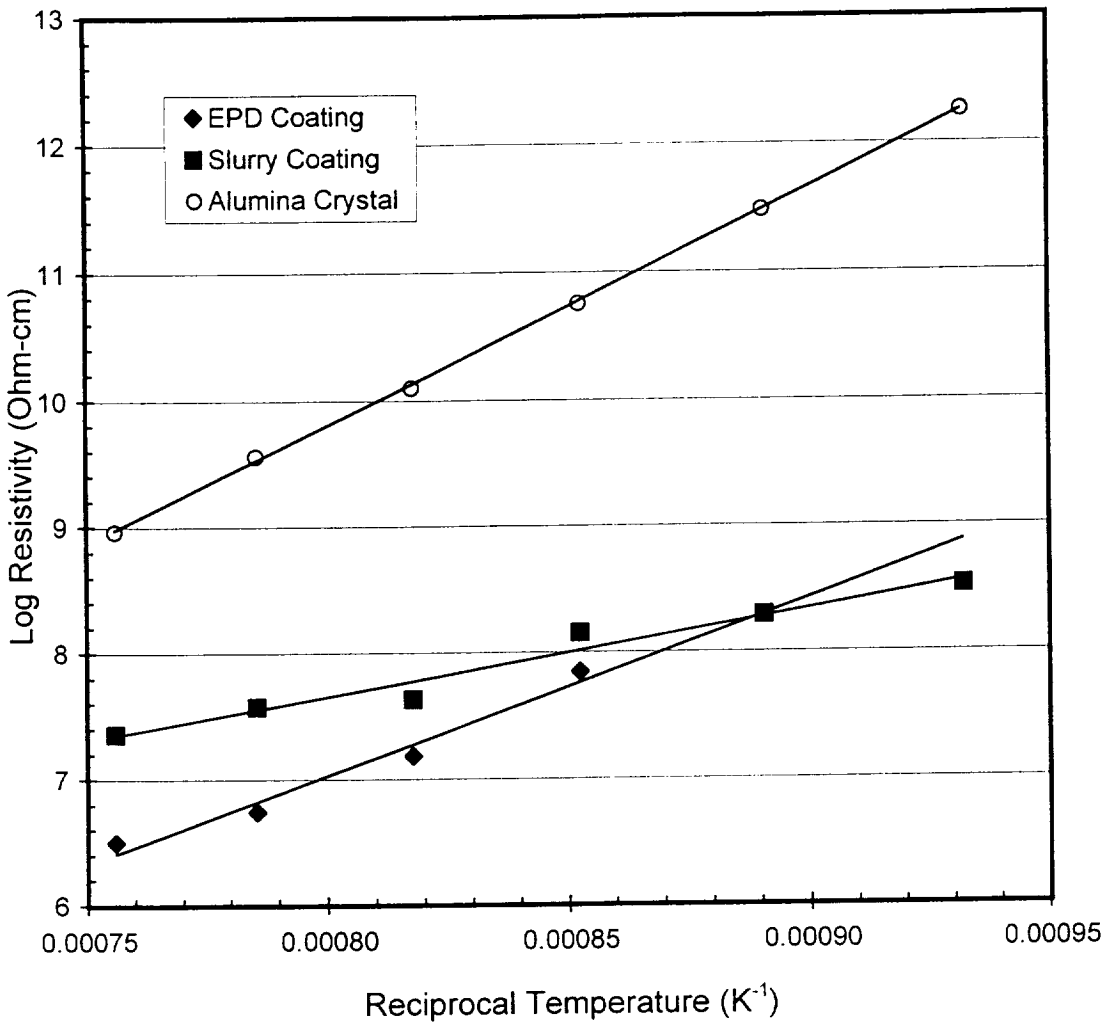

Figure 19. Comparison of the resistivity of an alumina single crystal with that of alumina coatings made by EPD and slurry coating.

Insulated Flexible Wires Useable to 1920°F (1050°C)*

Eric R. Kreidler and
Vidya Praveen Bhallamudi

Dept. of Materials Science and Engineering
The Ohio State University

* Poster presented at OAI Collaborations Workshop, May 31 to June 1, 2000.

Problem*

"Many, probably the majority, of sensor failures in turbine engines can be traced to the lead wire system."

Target Lead Wire Properties*	Targets Achieved
♦ Good Wire Flexibility	✓ "Flexible" Continuous & Discontinuous Insulation
♦ Insulation not Degraded at 1470°F	✓ Very High Purity Coatings
♦ Resistivity $1x10^{6}$ Ω-cm at 1470°F	✓ $2.2x10^{9}$ Ω-cm at 1740°F
♦ Small Diameter (< 63 mil for two)	✓ ≤ 15 mil for two
♦ Low Conductor Resistance	✓ Pure Platinum 10^{-5} Ω-cm (RT)
♦ Joining by Soft Soldering or Spot Welding	Probably (Remains to be shown)

*Adapted from PIWG Suggested Research Opportunity Form I-36, 1998

Insulated Flexible Wires Useable to 1920°F (1050°C)

by
Eric R. Kreidler and Vidya Praveen Bhallamudi

Department of Materials Science and Engineering
The Ohio State University

There is a need for new insulated wires to replace the metal clad mineral insulated wires traditionally used in the hot sections of advanced turbine engines. A process has been developed at the Ohio State University to coat platinum wires with pure aluminum oxide. The coatings were made by drawing the wire through a slurry, containing alumina, organic solvents, and binders. After solvent evaporation, the wire can be spooled without damage to the green ceramic coating. The wire is then fired in air at 1550°C (2822°F). The resulting coatings are free of pores and cracks. Our most successful coatings are about 0.5 mil thick and give a very flexible wire having overall diameter of 7 mils or less. When bent around sharp corners, the coatings fracture locally but most of the coating remains in place and bare wire is not exposed. The coatings strongly adhere to the wire and can not be easily removed by mechanical abrasion. It may, in fact, be necessary to develop a chemical etchant to strip the ends of the wire. Resistivity of the coatings at 1050°C (1922°F) was $1x10^8$ Ω-cm, at lower temperatures the resistivity is much higher. The large resistivity values are due to the high purity of the coating, and are well in excess of that presently needed for instrumentation lead wiring (i.e. ~$1x10^6$ Ω-cm at 800°C {1472°F}).

We have also made segmented coatings by electrophoretic deposition of alumina from both aqueous and non-aqueous suspensions. Both slurry coating and electrophoretic deposition are fast enough to coat wire at rates sufficient for commercial production.

Small samples of wire will be available for inspection.

The authors thank the NASA Glenn Research Center for financial support of this work. This material is based upon work supported by the NASA Glenn Research Center Award No. 3-2090. Any opinions, findings, conclusions, or recommendations expressed in this publication are those of the authors and do not necessarily reflect the views of the NASA Glenn research Center.

Professor Eric R. Kreidler
Department of Materials Science and Engineering
The Ohio State University
2041 College Road
Columbus, Ohio 43210

Tel. 614 292 6754
Fax 614 292 1537
e-mail Kreidler.1@osu.edu

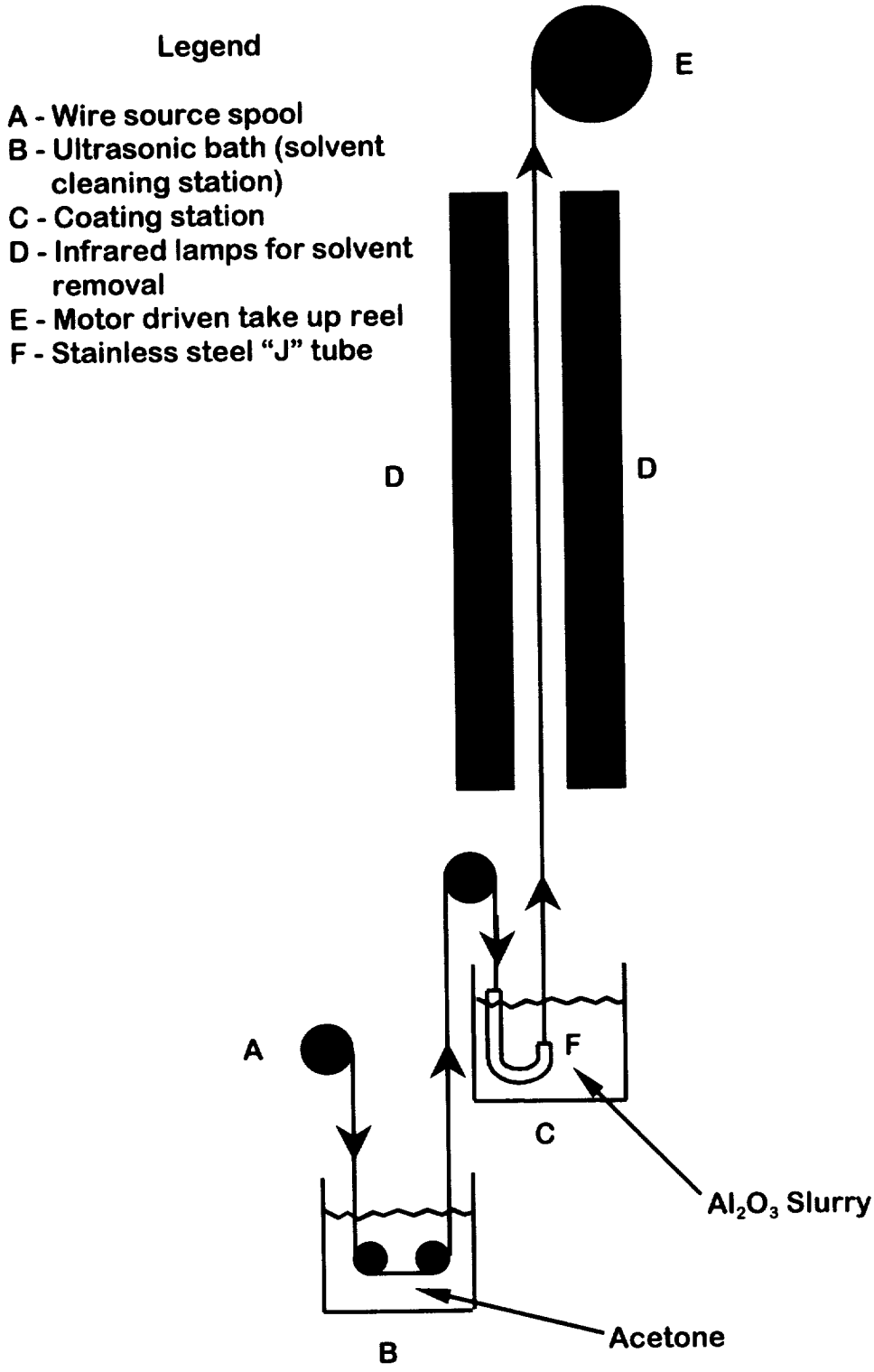

Figure 1. Laboratory scale wire coater.

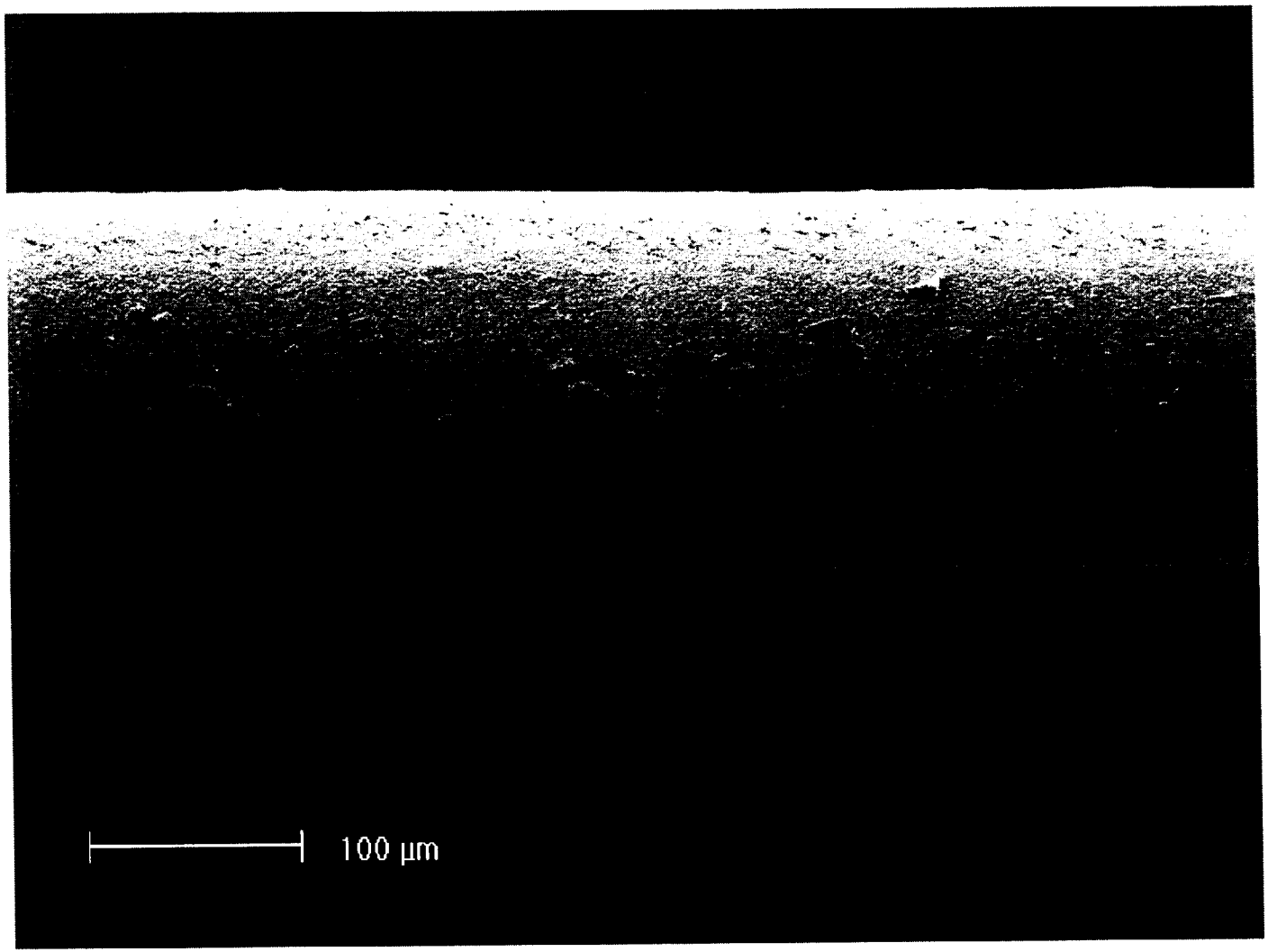

Slurry Coated Platinum Wire

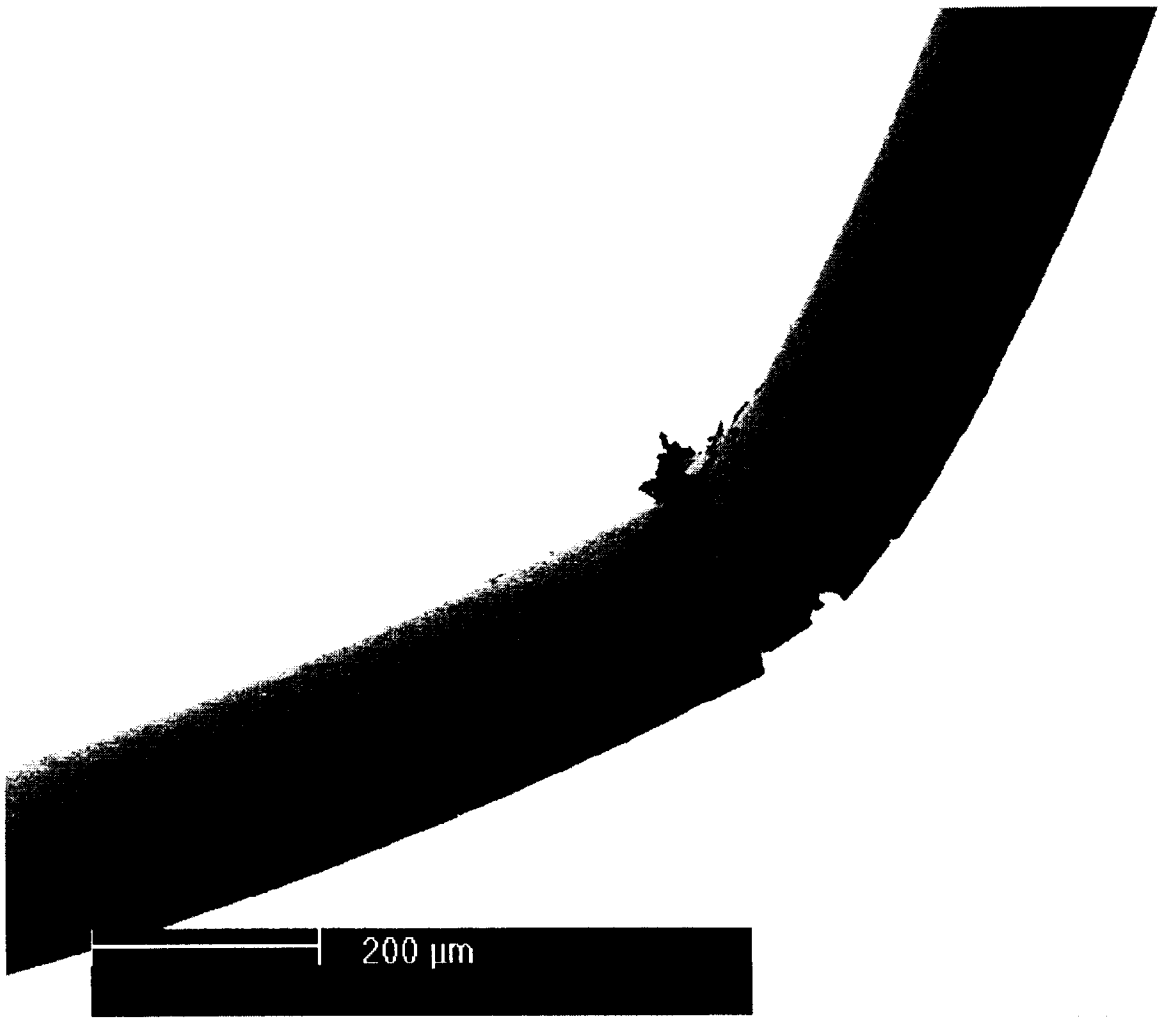

Slurry Coated Platinum Wire With Bend Showing Good Adherence of Coating

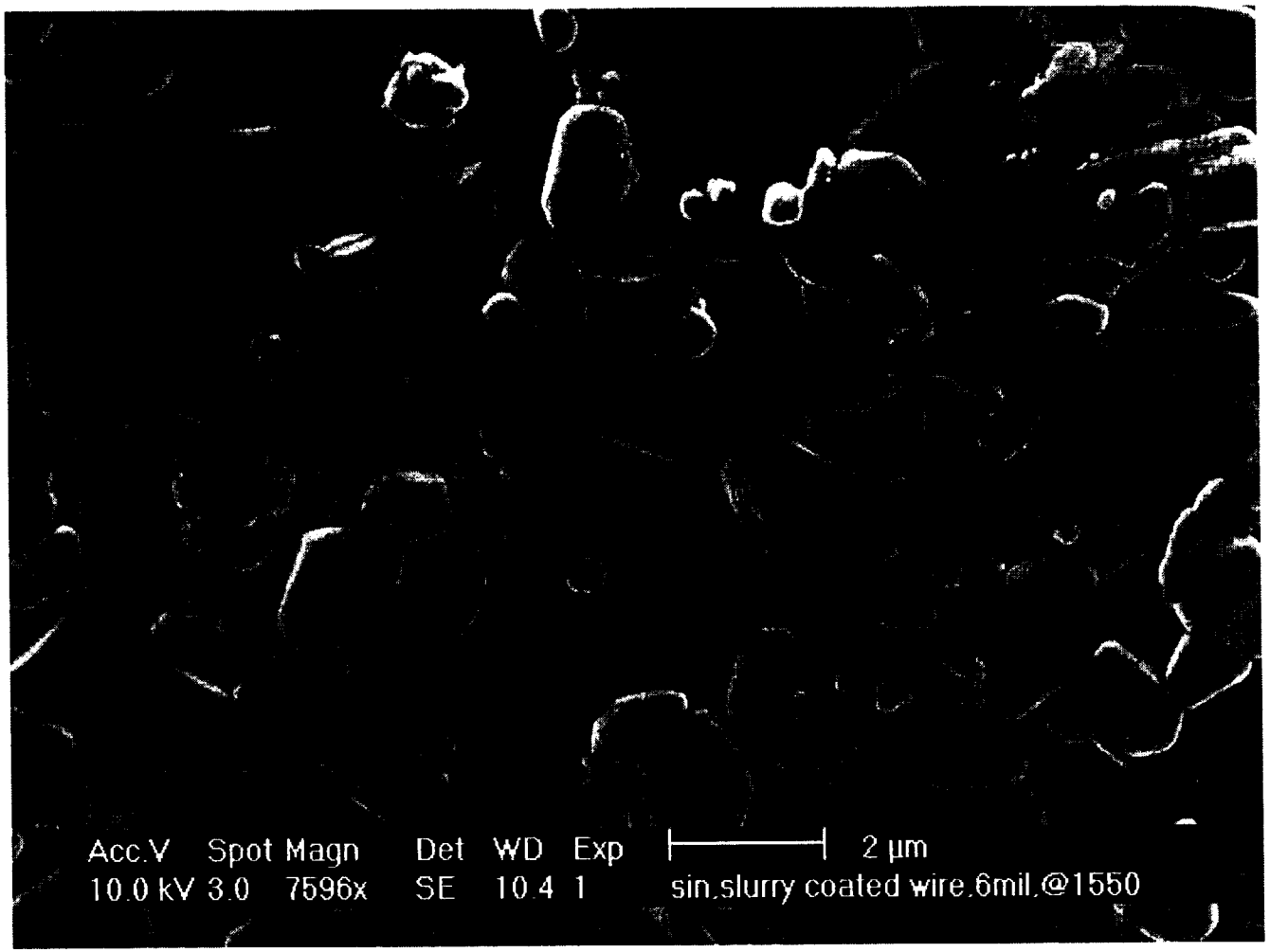

Slurry Coated Platinum Wire Close Up of Sintered Alumina Coating

Electrophoretic Deposition

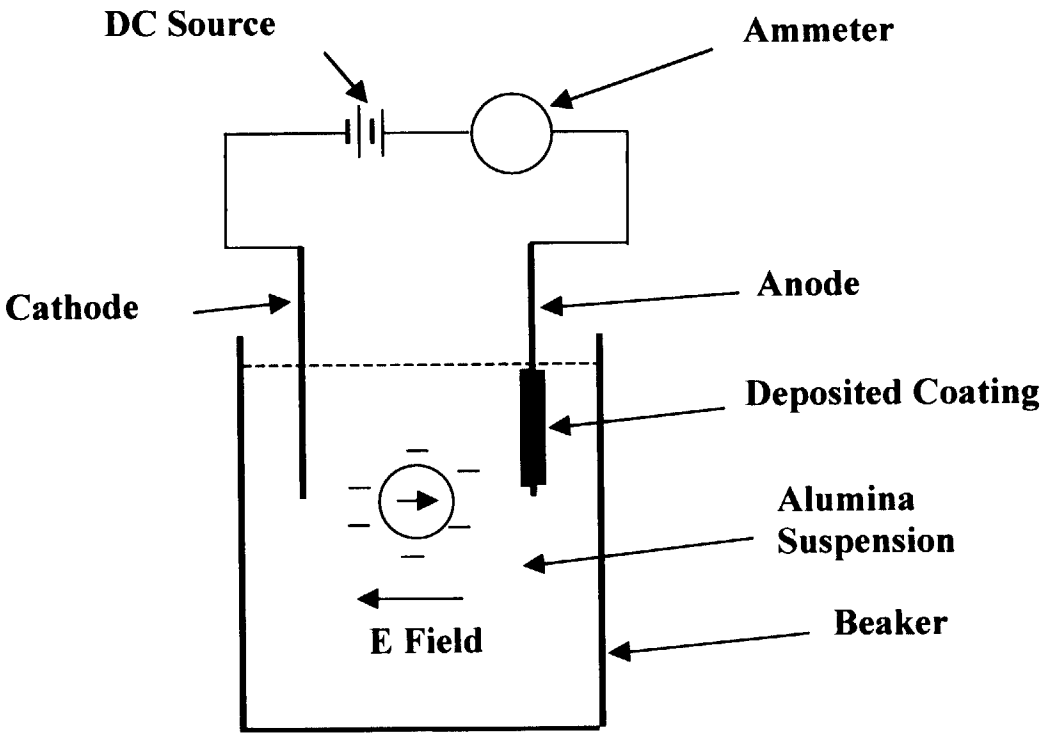

Schematic of the coating equipment

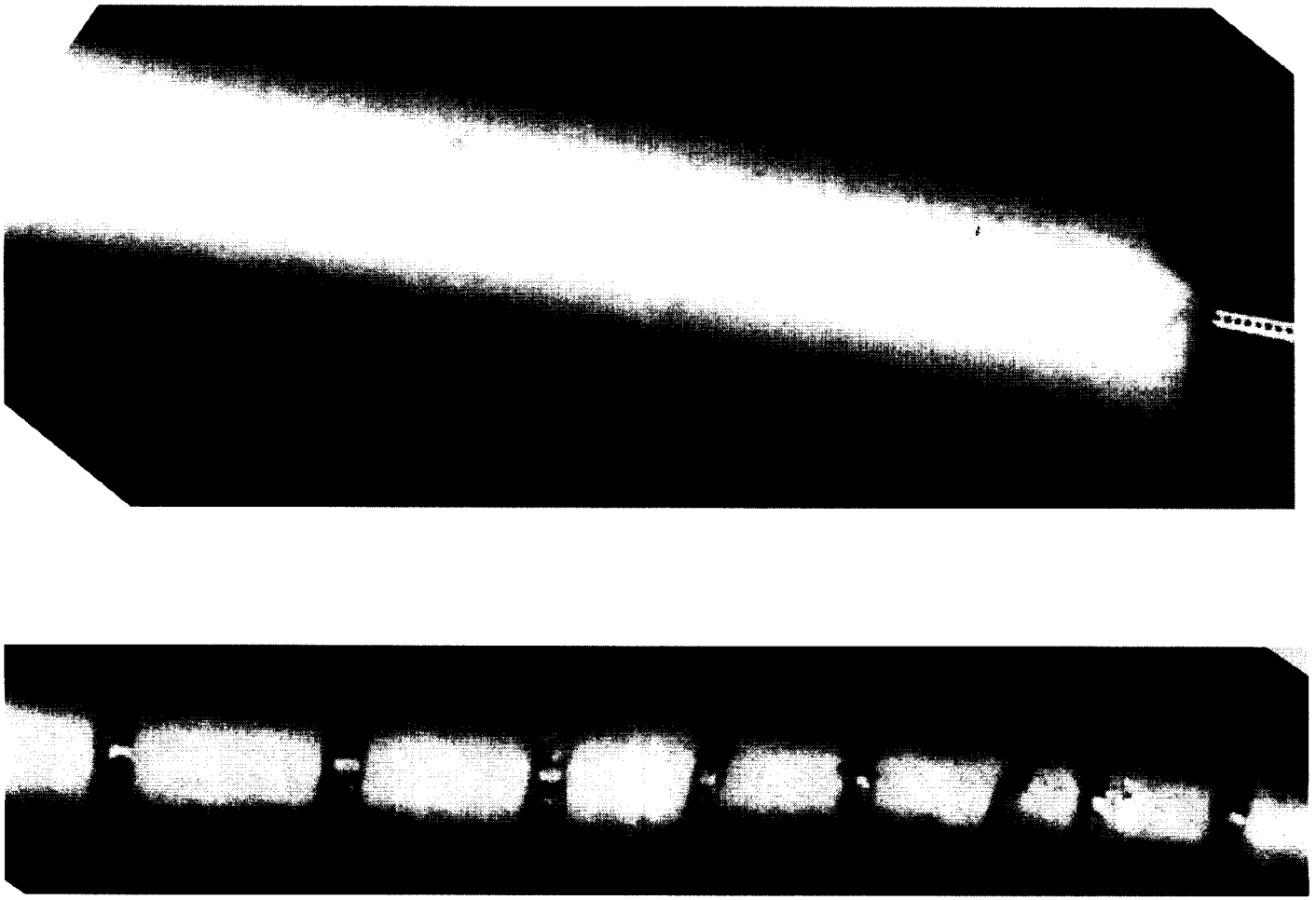

Electrophoretically Coated Platinum Wire Before (Top) and After (Bottom) Sintering

Bent Electrophoretic Coating Showing Good Adherence to Wire

COATING HIGH TEMPERATURE LEAD WIRES WITH ELECTRICALLY INSULATING ALUMINA BY ELCTROPHORETIC DEPOSITION AND SLURRY COATING

Thesis

Presented in the Partial Fulfillment of the Requirements for

the Degree Master of Science in the Graduate School of

The Ohio State University

By

Vidya Praveen Bhallamudi, B-Tech

****

The Ohio State University
2000

Dissertation Committee:

Dr. Eric R. Kreidler, Adviser

Dr. Charles H. Drummond

Approved by

_____
Adviser
Materials Science and Engineering Department

ABSTRACT

Flexible and electrically insulating alumina coatings, on metallic lead wires for high temperature applications, have been made using Electrophoretic Deposition (EPD) and Slurry coating techniques.

Experiments were done to study the effect of deposition current, solids content and alumina particle size on the EPD of alumina from aqueous suspensions. The alumina was dispersed using an ammonium salt of polyacrylic acid. A current of 1mA, solids content of 40 wt.%, 0.23 μm alumina particle size gave the best results for aqueous EPD. A pH of 8.17 and conductivity of 16280 μS/cm gave the highest rate of deposition. However the overall effect of the pH and conductivity is not completely understood. The effect of sintering temperature, coating thickness, wire thickness, wire material and its surface condition on adherence of the coating were also studied. The various parameters were qualitatively observed by studying the variation of "crack density" due to these parameters. Adherence was observed to be better for thinner coatings and for coatings made on thinner wires. Adherence also increased with sintering temperature. Heat treatments were done in air and vacuum to modify the surface condition. The heat treatments increased the surface roughness of the wires, which increased the crack density. Platinum showed the least effect due to the heat treatments, while chromel-p showed the maximum. Aqueous EPD samples showed extensive cracking and pores. Non-aqueous EPD was also studied. Coatings were made from suspensions in

mixture of ethanol and acetone. They did not have any drying cracks and showed only transverse cracks on sintering. The rate of coating is also much higher than in the case of aqueous EPD.

In the case of slurry coating, a machine was successfully built to continuously slurry coat metal wires. A slurry based on MEK and toluene, as dispersing liquids, and Butvar B-79 binder was used. An optimal slurry composition and rate of drawing were determined.

The resistivity of the coatings, made by both EPD and slurry coating was found to be of the order of 10^8 ohm-cm, even at 1050°C.

Dedicated to Dr. P.C.Salaria

ACKNOWLEDGMENTS

I am grateful to my adviser, Dr. Eric Kreidler, for being so supportive throughout the project and guiding me through the nuances of experimental research. A special mention must be made for his great help with the slurry coating experiments.

I wish to thank the entire staff at the Department of Materials Science and Engineering for their patient and valued support through out my Masters studies. Special thanks are due to Gary Dodge for helping with various aspects of the laboratory work and to Ken Kushner for his help in building the zeta-potential measuring equipment. Thanks are also due to Badri Narayanan and Ramchandra Rao for helping me with the resistance measurements.

Finally, I wish to thank NASA Glenn research center, Cleveland for funding this project. This material is based upon work supported by the NASA Glenn Research Center Award No. NAG 3-2090. Any opinions, findings, conclusions, or recommendations expressed in this thesis are those of the author and do not necessarily reflect the views of NASA Glenn Research Center.

VITA

June 12th, 1976.....Born- Parlakhemundi, India

June, 1997.....B-Tech, Institute of technology,
Benaras Hindu University, India

June 1997- May 1998..... Engineer trainee, BHEL-EPD,
Bangalore, India

June 1998-Present..... Graduate Research Assistant
The Ohio State University

PUBLICATIONS

Research Publications

1. Microwave-assisted preparation and sintering of the Mullite and Mullite-Zirconia composites from metal-organics – B.G.Ravi, V.Praveen, et.al, Materials Research Bulletin, 33[10], 257-1536.

FIELDS OF STUDY

Major Field: Materials Science and Engineering

TABLE OF CONTENTS

LIST OF FIGURES

LIST OF TABLES

LIST OF SYMBOLS AND UNITS

Symbols

ε_r	Relative permittivity / Dielectric constant
ε_0	Permittivity of free pace
Ψ	Potential
Ψ_0	Surface potential
ς	Zeta-potential
ρ	Deposit density
λ_0	Conductivity of the suspension
μ_e	Particle velocity
ρ_s	Density of the solid particles
ρ_l	Density of the suspending liquid media
ϕ	Weight fraction of the solids in the suspension
ΔW	Weight change in a mass transport cell
a	Particle radius
A	Hamaker's constant, area of the deposits (also given by S)
e	charge on an electron
c_i	local concentration of ions
C(t)	Concentration of the suspension at any time t

f	Deposition efficiency factor
$G_{R,a}(D)$	Gibbs free energy per unit of the surface at a distance D
h	Length of the deposits
I	current
k	Boltzman constant, kinetic parameter in the kinetic equations for EPD
L	Distance between the electrodes
r	Distance from the center, Radius of the wire with the deposit
r_0	radius of the wire
R_r	Ratio of the resistivity of the deposit to that of the suspension
S	Deposit area
t	Time
T	Temperature
U	Electrophoretic mobility
V	Volume of the suspension
Vapp	Applied voltage in constant voltage EPD
V_R	Repulsive energy between two approaching particles
V_A	Attractive energy between two approaching particles
w(t)	Weight of the deposit at any time t
w_0	Initial weight of the solid particles in the suspension
x	Packing efficiency of the deposits
z_i	valency

Units

mil	Thousandth of an inch, 25.4 microns
sec	Seconds
cm	Centimeter
micron	thousandth of a meter
cps	centipoise
V	volts

CHAPTER 1

Introduction: Problem Statement and approach

The performance and efficiency of aircraft improves as the operating temperature of their engines increases. So there is a trend towards increasing the operating temperatures of the modern engines. Thus, the lead wires used in airplane engines and other such places for connecting the various sensor and electronic monitoring systems are subject to very high temperature conditions (>800°C). Also, the acoustic vibrations are very severe in such environments. At such high temperatures the electrical insulation and mechanical properties of conventional insulator materials deteriorates rapidly and most of them fail. As such, insulation for these high temperature conductors is an issue of concern. Maintaining the adherence of the insulation to the conductor under such acoustic conditions and regular mechanical damage are another problem areas.

Currently metal-sheathed mineral insulated conductors (MIC's) are being used for these applications [1]. These wires consist of a conductor covered with particulate insulating material, typically MgO. The insulator is kept in its place by a metal sheath. For ease of applying the insulating coating, minerals of the insulating materials are used. As such, the insulating material does not have very have high purity. There is a two to three orders of

magnitude change in the resistivity and dielectric constant of such materials at high temperatures. This causes failure of insulation, leading to inaccuracy and instability of the instrumentation systems. Also, the insulating coating is not very rugged in the above mention configuration and tends to strip off easily.

As can be seen from the foregoing discussion, there is a need for flexible and adherent insulating coatings that can withstand high temperatures without significant change in their properties.

The problem may be divided into two parts - 1) identification of a suitable material and 2) identification of a suitable processing technique to apply the insulation coating on the conductors.

Ceramic materials are known for their high temperature properties. They are thermally stable and many of them have very high resistivities. Alumina, especially, has excellent characteristics (Table 1.1). Alumina was therefore chosen as the insulation material. However the purity of alumina is very important in determining its high temperature electrical properties. Alkali ions such as Na^+ are especially detrimental as they have very high mobilities at high temperatures. Hence very pure alumina was used throughout this work.

Melting Point (°C)	2013
Density (gm/cc)	3.95
Tensile Strength (psi)	37-37.8 X 10^3 at R.T 33.9 X 10^3 at 1050°C
Resistivity(ohm-cm)	> 10^{14} at RT 5 X 10^8 at 700°C
Co-efficient of thermal expansion($°K^{-1}$)	5.6 X 10^{-6} 0 to 27°C 8.18 X 10^{-6} 0 to 1027°C
Oxidation resistance	A temperature range above 1700°C needed in air to cause severe erosion in few hours

Table 1.1. Physical properties of α-Alumina [2].

Identification of a processing technique is the more difficult aspect. The conventional techniques use the ceramics in a MIC structure (described earlier) or as beads or tubes. However, all these techniques are cumbersome and not very reliable. It may however be better to bond the ceramic material directly to the metal conductor for better insulation and adherence. However, bonding ceramic material to a metal is difficult. Also, maintaining the flexibility of such wires is not easy. Additionally, commercial factors such as cost and rate of production should also be considered while selecting a suitable processing technique.

With this background, the present work was directed towards developing two processing techniques - Electrophoretic Deposition and Slurry Coating - for obtaining high temperature electrically insulating alumina coatings on metal wires.

The work can be logically divided into the following parts -

1. Electrophoretic Deposition
    a. Aqueous
    b. Non-Aqueous
2. Slurry Coating.

I shall deal with them individually for maintaining a coherent text. Chapter 2 explains the Electrophoretic Deposition (EPD) process in general. Chapter 3 discusses the experimental work done on aqueous EPD, and the results and discussion of the work. Chapter 4 focuses on the Non-Aqueous EPD- its advantages over the aqueous counterpart, the experimental

work, and the results and discussion. Chapter 5 deals with slurry coating. The resistivity measurements of the coatings are described chapter 6. In chapter 7, the conclusions and summary for the entire project will be presented and pointers for possible future work will be given.

CHAPTER 2

Electrophoretic deposition: Introduction and Theory

Electrophoretic deposition (EPD) is a process wherein ceramic particles are deposited on a substrate from a colloidal or nearly colloidal suspension under the influence of an electric field. Compared to many of the conventional processing techniques it is a fast and convenient way of applying both thin and thick coatings. It can be used to uniformly coat substrates of fairly complex shapes and almost any geometry. It has been used commercially in the production of clay tiles, plates and other such materials [3]. In these applications it was found to be 5-10 times faster than the conventional slip casting process. Other commercial applications include depositing glassy enamel frit on metal surfaces. It has been used to make laminated alumina-zirconia composites[4]. Insulating alumina films were obtained on tungsten wires, used in cathode ray tube heaters, by EPD[5]. It has also been used in the continuous fabrication of superconducting fibers of $REBa_2Cu_3O_{7-x}$ [6] (RE: rare earth elements)

A schematic of the EPD process is shown in Fig.2.1. EPD consists primarily of two processes, electrophoresis and deposition. When solid particles are dispersed in a liquid phase, the particles of the former can be induced to move by applying an electric field.

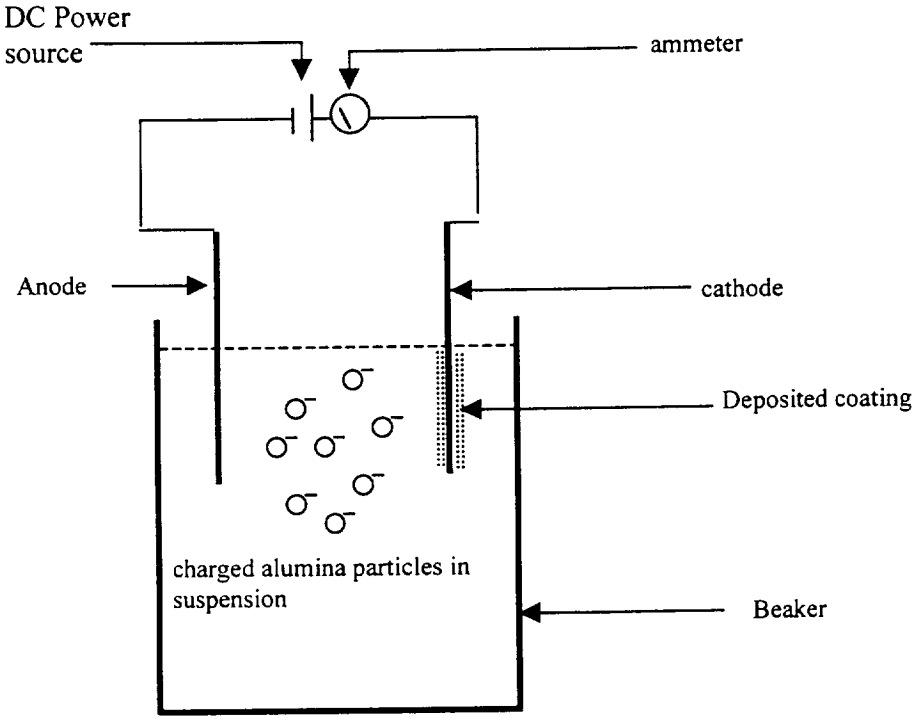

Fig.2.1. Schematic of the experimental set-up for electrophoretic deposition.

This is called electrophoresis. Deposition is a mechanical process, which is similar to sedimentation. These two will be dealt in greater detail in the following paragraphs.

Charge on a solid surface and the Electric double layer [7]:

The phenomena that make EPD possible are the surface charges on the solid particle and the electric double layer formed at the interface of two phases (we are primarily interested in solid liquid interfaces). There are several ways in which charges can be introduced on a solid surface and these will be discussed later. Even in vacuum there usually is a separation of opposite charges at the surface of a solid. In the most elementary form these can be electrons in metals protruding outwards from the surface, which are compensated by the positive charges just inside the surface. This also implies that when two phases are in contact, there is a tendency for charged species to reorient themselves with respect to the two phases. The resulting electric field will cause an electric potential to develop between the interiors of the two phases. This difference is called the "inner" or "Galvani" potential difference. In particular let us consider an example of a solid phase with a positively charged surface, in contact with a liquid with negatively charged surface. The potential decreases as one moves from solid to liquid and finally becomes constant in the bulk of the liquid, at a distance away from the solid surface. In aqueous systems this distance is of the order of 5-200nm. This arrangement of positive (or negative) charges on the solid surface and negative (or positive) charges at the liquid surface is called the *electric double layer at the interface*.

Causes and nature of charges at the interface [8]:

Since in this study solid suspensions are the main consideration, the discussion will be limited to solid-liquid interfaces. The various methods by which charge can be obtained at the interface are:

1. Dissociation or ionization of the surface groups on the particle surface: In this mechanism H^+ or the OH^- ions are the *potential determining ions*. The solid surfaces, such as those of the inorganic oxides, have basic sites resulting from broken bonds and other factors. The potential determining ions from the dispersing media then react with these sites to give a net charge on the surface. Given the nature of the potential determining ions pH of the suspension plays an important role.

   e.g: $(M\text{-}OH)^0_{surface} + H^+ \rightarrow (M\text{-}OH_2)^+_{surface}$ at low pH

   $(M\text{-}OH)^0_{surface} + OH^- \rightarrow (M\text{-}O)^-_{surface} + H_2O$ at high pH

2. Readsorption of potential determining ions: In this mechanism the solid is slightly soluble and becomes dissociated in the dispersing media. The resulting ions are then readsorbed on the solid surface to establish equilibrium. This readsorption of charged ions leads to a net charge on the surface. For example - in the AgI/water system, either Ag^+ or I^- ions are radsorbed on the AgI surface
3. Adsorption of ionized surfactants: Some ionic surfactants when added to the suspension get adsorbed on to the solid surface and give a charge on the surface. This is the mechanism used in this study and will be explained in greater detail.

1. Isomprphic substitution: This mechanism is especially applicable to clays. In such materials isomorphic substitutions based on size similarity is common. However, the substituting species may not have the same magnitude of charge as the previous species. This can lead to an net charge at the surface. Examples are Al^{3+} substituted by Mg^{2+} and Al^{3+} substituting for Si^{4+}.

The electric double layer:

In the earliest model the electric double layer was considered analogous to a molecular condenser with both layers of charge in fixed planes. However Gouy and Chapman developed the diffuse double layer theory. Acording to this theory, one of the charge layers is assumed to be uniformly distributed over the plane surface. The compensating charges are supposed to be point charges, immersed in a continuous dielectric media, whose strength gradually decreases as one moves away from the interface. The double layer is modeled by the Poisson-Boltzman equation:

$$\varepsilon_r \varepsilon_0 \nabla^2 \Psi = -e \sum_i z_i c_i \exp\left(\frac{z_i e \Psi}{kT}\right)$$

The solution to the above equaiton is derived using Debye-Huckel approximation. The approximation converts an exponential function into a linear function and holds good for any $Y << 1$. Mathematically, $\exp(Y) = 1+Y$

Using this approximation, the solution for a single particle, having an infinite and uniformly charged planar surface in one dimension is given by:

$$\Psi(x) = \Psi_0 \exp(-\kappa x)$$

And for a spherical particle of radius a, the Debye-Huckel approximation is

$$\Psi(x) = \Psi_0 \frac{a}{r} \exp[-\kappa(r-a)]$$

Where, κ is called the Debye screening length and is given by

$$\frac{1}{\kappa} = \left(\frac{\varepsilon_r \varepsilon_o kT}{\sum_i (z_i e)^2 c_o} \right)^{\frac{1}{2}}$$

A typical variation of the double layer potential is given in Fig2.2. The Debye screening length, also called the characteristic length of the double layer, determines how rapidly the potential falls in the diffuse layer. The characteristic length is inversely related to the electrolyte concentration of the solution (C_0) and to the ionic charge (Z_i).

The assumptions of an equipotential surface and uniform permittivity of the dispersing media were too simple. The ions could not be regarded as point charges and also permittivity of the media was affected by the potentials at the interface. So modifications were made by Stern. Stern assumed that a layer of adsorbed ions specifically interacted with surface of the solid. However, this has been further revised by specifying a distance of closest approach x_1 to the wall (Fig.2.3), called the Stern plane. So the region $0<x<x_1$ is depleted of charges. The region $x_1<x<x_2$ is assumed to be a chemically adsorbed layer, with the ion concentration

being specified by Langmuir's isotherm. The diffuse layer starts at x_2, (the surface of shear) and extends into the bulk liquid. The Poisson-Boltzmann equation satisfactorily represents the potential distribution only of the diffuse region. The potential in the region before the surface of shear is governed by short range interactions.

Surface of Shear and Zeta-Potential:

Another important concept in the double layer theory is the surface of shear. It is a hypothetical concept. It is supposed to lie close to the solid surface and within which the fluid is stationary. In the case of electrophoresis the surface of Shear forms an envelope and the material inside this envelope moves as a single kinetic unit called the lyosphere. As can be understood, under real situations this surface will be a constantly varying one and hence is a time-averaged quantity for mathematical treatments.

A related concept is that of zeta-potential, represented by the Greek letter "ς". It is the average potential on the surface of shear. It arises because the surface charges on the solid particle are not completely compensated by the counter-ions within the surface of shear. Since the surface of shear is not a well defined term, it is difficult to measure the zeta-potential. However with some assumptions, it can be reasonably determined from electrophoretic mobility measurements. The final surface of the kinetic unit is the shear surface and zeta-potential is the charge on it. Hence, the zeta-potential is the most important parameter characterizing the double layer.

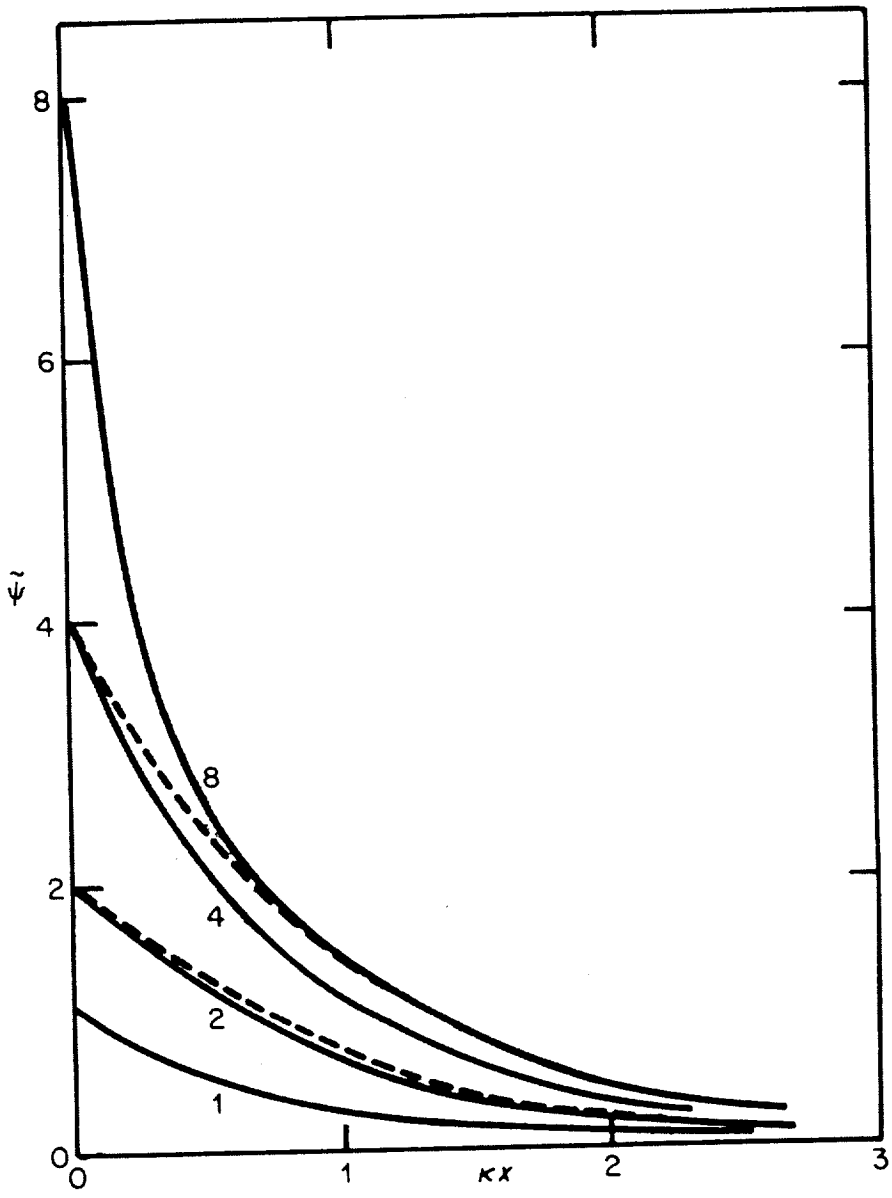

Fig.2.2. A typical variation of potential as one moves into the liquid phase from the interface [7].

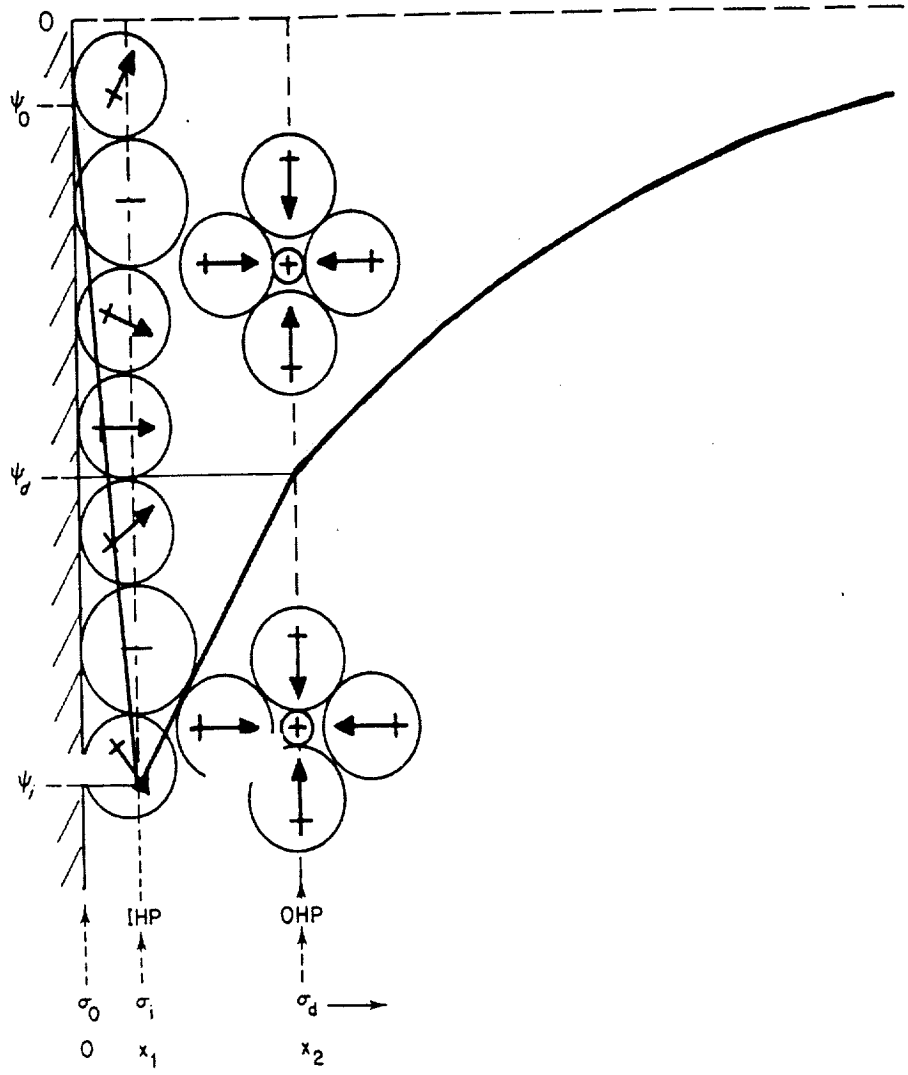

Fig.2.3. Schematic representation of the potential distribution of a double-layer given by the modified Stern theory. Note the stern layer (at x_1) and surface of shear (at x_2)[7].

Effect of Electrolytes on the double layer:

The electrolyte refers to what are called *indifferent ions*. These ions are not adsorbed on to the solid surface and hence do not directly contribute to the surface potential of the solid surface. However they do influence the double layer configuration.

The computation of the potential distribution as a funtion of the electrolyte concentration shows that the diffuse double layer is compressed towards the solid surface with increase in the indifferent electrolyte concentration. The effect on surface potential and surface charge depends on the type of double layer:

1. If the double layer potential is governed by potential determining ions, then the surface potential is not effected by the indifferent ions. This is under the assumption that the concentration (activity) of the potential determining ions is not effected by these ions. For these kind of double layers the surface charge however will increase with electrolyte concentration.
2. In double layers with surface charge primarily dependent on interior crystal imperfections, the surface charge remains constant, whereas the surface potential decreases with increasing electrolyte concentration.

An interesting example given in Fig.2.4, shows the variation of potential in three systems having the same ς-potential. Curve one with a high positive surface charge and small diffuse

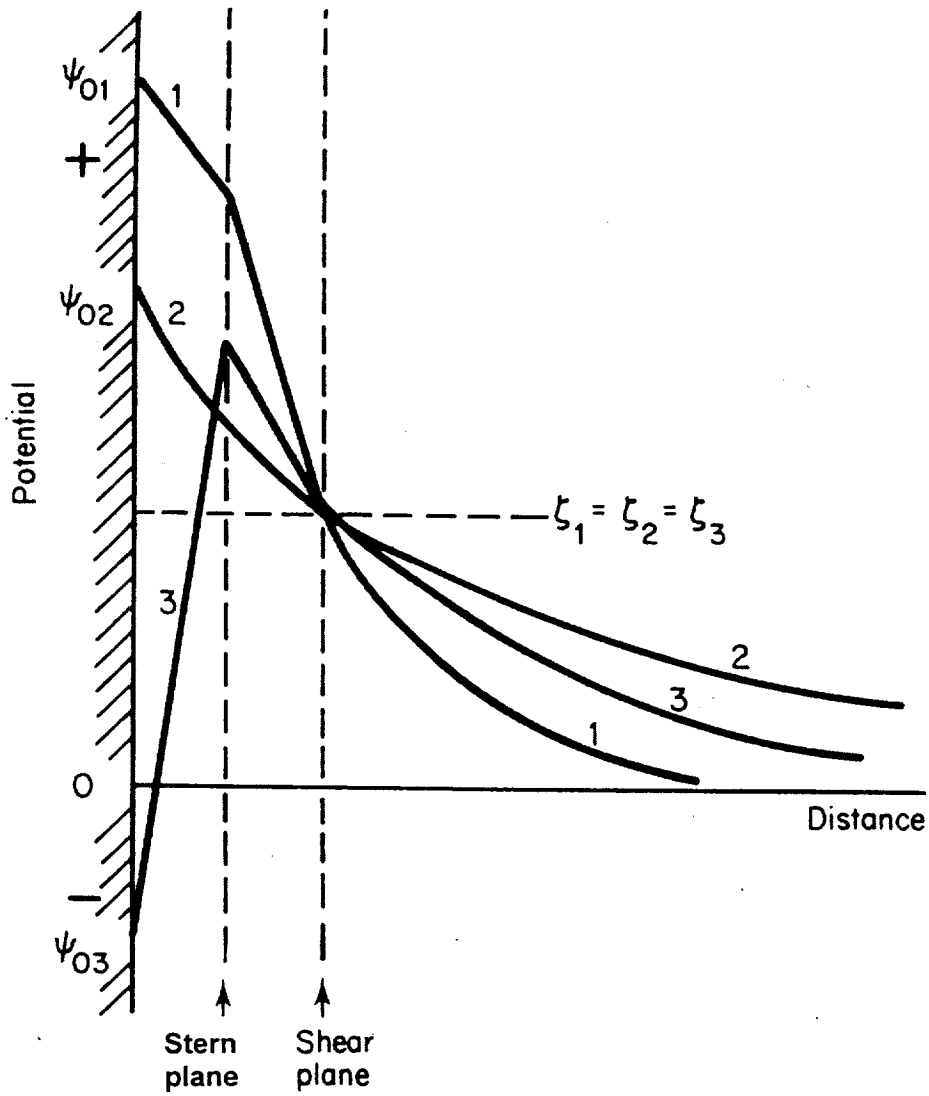

Fig.2.4. An example of three different double-layer potential distributions leading to the same zeta-potential due the different interactions between the adsorbed and the indifferent ions[7]

layer results from a combination of low to moderate adsorption of an anionic species and a supporting electrolyte concentration. The second curve has a low positive surface potential and highly extended difuse layer. This is due to little stern layer adsorption and low concentration of electrolytes. The third curve has a very strong adsorption at the stern layer and a moderate concentration of supporting electrolyte giving a moderate extension of the diffuse layer. The example also illustrates that one must be careful while correlating zeta-potential and surface charge.

Electrophoresis:

Electrophoresis occurs when a solid phase is suspended in a liquid . As described earlier, an electric double layer is created at the interface leading to the formation of a lyosphere around the solid particles. A lyosphere has a net charge on it. So, when an electric field is applied to these particles, they will move towards one of the electrodes. This motion of the solid particles is called electrophoresis.

Interaction between particles :

After the particles are transported to one of the electrodes by electrophoresis, they usually form a deposit at the electrode. The deposit is a thermodynamically more stable structure under the conditions existing at the electrode. Deposit formation is primarily governed by the interaction of the various forces as the particles come close to each other and to the electrode. The theory discussed below is applicable (to a large extent) to the formation of a deposit under many circumstances, not just electrophoresis. It essentially is the DLVO theory.

Two principal forces that always act on two particles approaching each other are, first the Vander Waal's force which is attractive in nature and second, an osmotic force which is repulsive in nature. It should be noted here that the repulsive force between the particles is osmotic rather than electrostatic. The osmotic pressure originates due to the difference in concentration of the ions in the bulk liquid and the liquid between closely spaced particles[8]. Since the particles have a sheath of counter-ions around them, the electrostatic forces are not dominant.

The potentials due to the two opposite forces are given by the following equations:

$$V_R = 2\pi a \int_D^{\infty} \left(G_{R,a}(D) - G_{R,a}(\infty) D \right)$$

and $$V_A = -\frac{A}{6D}\left(\frac{a_1 a_2}{a_1 + a_2}\right)$$

Where, V_R is the potential due to the repulsive forces,

$G_{R,a}$ is the Gibbs free energy per unit of surface (at a distance D and infinity).

V_A is the potential due to Vander waal's interaction

and, a_1 and a_2 are the radius of the two particles

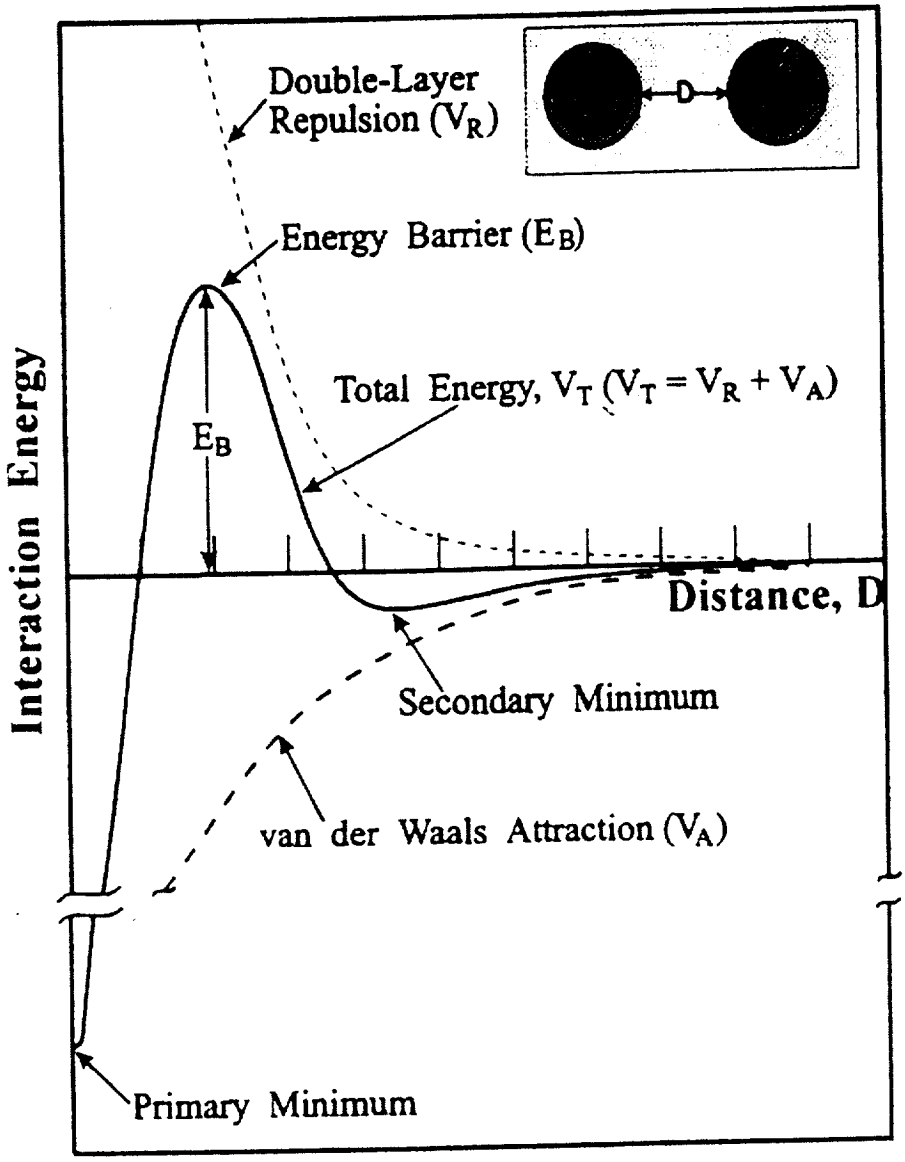

Fig.2.5. The variation of energy with distance between two particles due to the interaction of various forces between the two particles. interact[8].

Fig.2.5 shows the interaction energy versus distance curve for two particles as determined from the interaction of these forces. Particles in a structure with interparticle distances corresponding to the two minima will give thermodynamically stable deposits. However, a distinction must be made between the two minima on the curve. The particles in the primary minimum are very stable and adhere strongly to each other. On the other hand, although the secondary minimum can result in a deposit, it tends to result in a flocculated mass with large interparticle separation. Also the shallowness of the minimum implies that the particles can be removed from the deposit with little effort. So, the deposit resulting from the secondary minimum is not the most stable one.

Effect of electric force and deposition by EPD:

As shown in Fig.2.5, the particles need additional force to overcome the energy barrier and reach the primary minimum. Such a force is provided by gravity in a sedimentation process. It can also be provided by centifugal force. In electrophoretic deposition, the applied electric field is the driving force. The original theory, proposed by Hamaker and Verwey [9], was developed by analogy to sedimentation. According to this theory, the first particles arriving near the electrode do not at once reach the electrode due to the prevailing repulsive forces. This is graphically represented on an energy versus distance diagram in Fig.2.6 by curves M. The particles remain at a distance corressponding to the secondary minimum. But as more and more particles arrive, a pressure builds up, which is represented in the figure by the straight lines through the origin. Increasing slope of the pressure lines indicates increasing pressure because of the accumulation of large number of particles. The secondary minimum in the net energy curve vanishes as the pressure increases and finally the particles become trapped in the primary minimum. The primary mininum as explained earlier results in a deposit which is

mechanically more stable. This theory by Hamaker, however, is not quantitatively correct and a more recent explanation has been advanced by Sarkar and Nicholson [8].

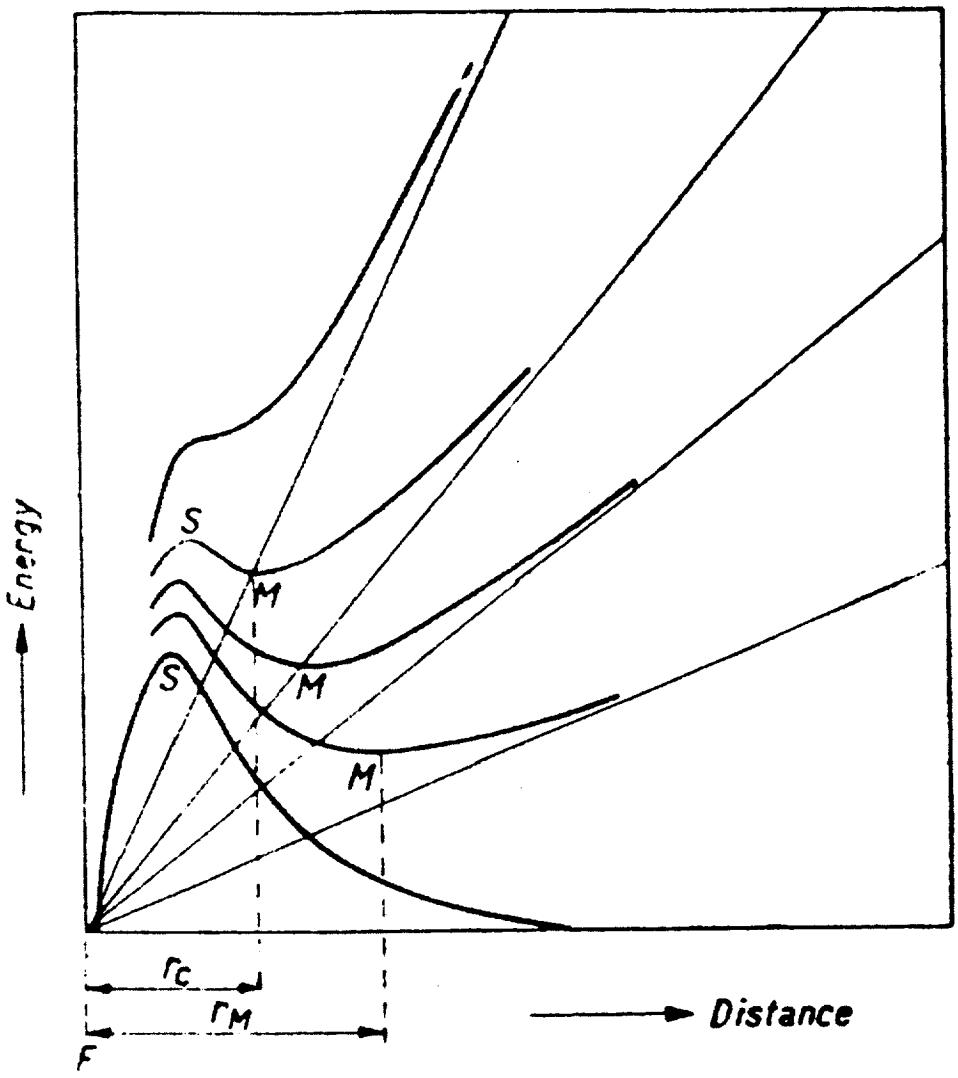

Fig.2.6. Gradual disappearance of secondary minima as the pressure due to the accumulating particles near the electrodes increases [9]

The deposition mechanism, according to Sarkar and Nicholson, is shown in Fig.2.7. The lyosphere moving towards the electrode in an EPD cell is distorted by fluid mechanics and the applied field. It becomes thinner ahead of the particle and wider behind the particle. To maintain constant charge density in this non-uniform shape, the zeta-potential has to correspondingly vary, with the leading edge having the greatest value and the trailing edge having the smallest value. The counter-ions in the tail region tend to react with ions of opposite charge (and same charge as that of the solid surface) in the dispersing media. They tend to establish an equilibrium governed by thermodynamics. When two lyospheres tend to approach each other, the concentration of the counter-ions increases locally, resulting in an osmotic repulsion between the lyospheres. Hence, the lyospheres cannot approach too close to each other. However, due to the high concentration of ions near the electrode, the counter-ions in the tail are neutralized. This thins the tail of the lyosphere. Now another approaching lyosphere, with thin leading edge can come close enough for the two solid particles within the lyospheres to coagulate togather due to Vander Waal's forces. This entire process is called coagulation/deposition by lyosphere distortion and thinning.

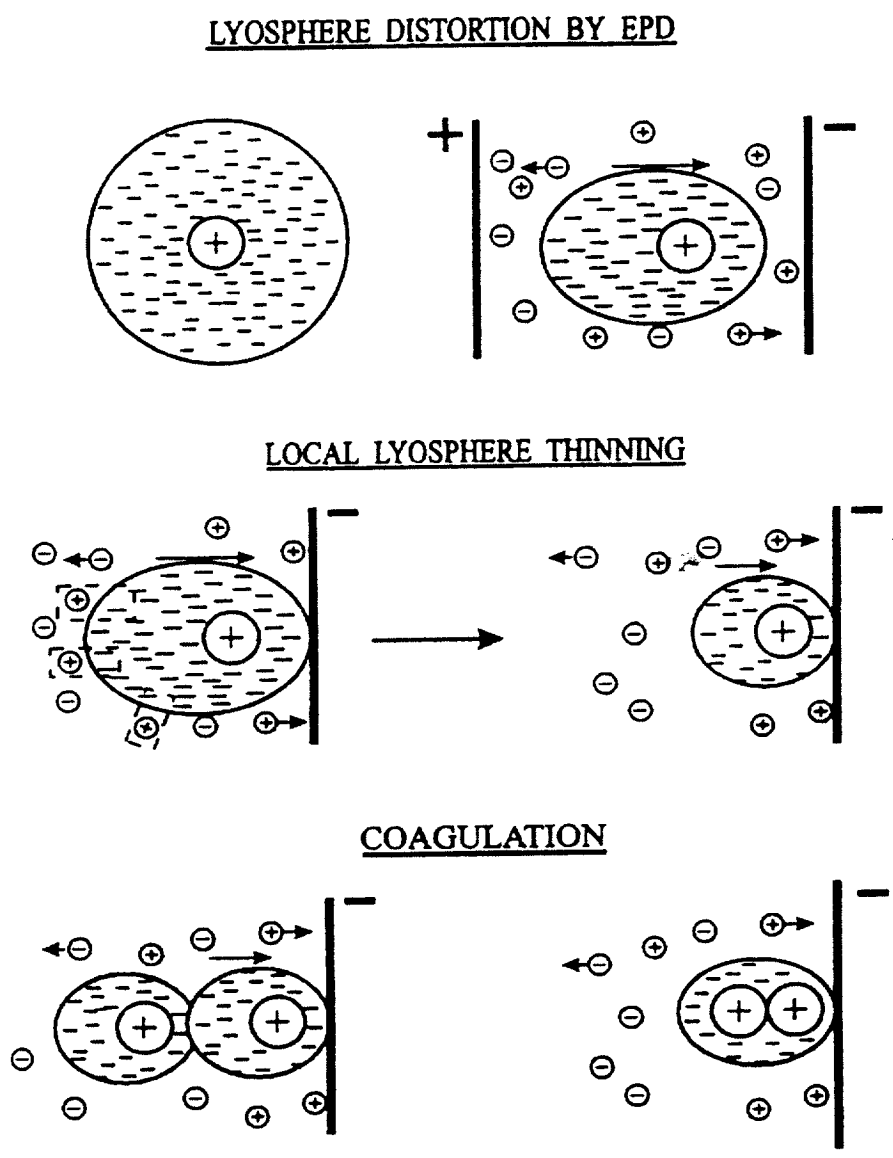

Fig.2.7. Formation of a deposit by lysoshere thinning and coagulation [8].

Kinetics of deposition:

For proper control of the amount of material deposited and its thickness, it is esential to understand the kinetics of the process. Especially from a commercial point of view it is important to know whether it is possible to achieve high rates of production without loss of quality. EPD can be carried out under two different conditions, constant current and constant voltage:

In constant current EPD, the current between the two electrodes is kept constant. While depositing non-conducting materials, such as inorganic oxides, the resistance between the electrodes increases as the deposit is formed. This implies that to keep the current constant, we will need to increase the deposition voltage.

In constant voltage EPD, the voltage of the deposition is kept constant. The net electric force acting on the particles in the suspension is due to the potential after the voltage drop across the deposit. For resistive deposits this force rapidly decreases which is a serious disadvantage.

As might be understood the kinetics in these two cases will be different. The change in suspension concentration, as the deposition process continues, is another factor influencing the deposition kinetics. However, it is significant only when a large fraction of the material has been removed and deposited from the suspension. This changes the basic suspension properties such as conductivity and solids loadings. Each of these factors influences the depostion kinetics in its own way. Sarkar and Nicholson reviewed [8] the mathematical models for four cases of deposition:

1. Constant current and constant concentration

2. Constant current and varying concentration
3. Constant voltage and constant concentration
4. Constant voltage and varying concentration

In early experiments it was observed that the deposit weight depended on the suspension concentration. This showed that EPD is a non-Faradic process. Understanbly, it was also seen to depend on the electric field , time of deposition, and the area of deposition. Hence a basic equation for the kinetics of EPD process can be written as:

$$\int dw = \iint fu\, C(t)\, (dS)\, dt$$

where, dw is the weight of the material deposited per surface area dS of the substrate, in infinitesimaly small time dt, C(t) is the concentration of the suspension at any time t, f is the deposition efficiency factor, and u is the electrophoretic mobility of the particles.

The model assumes a steady-state condition . The limits on the voltage range are the minimum voltage required for deposition and the maximum voltage up to which Ohm's law is obeyed. Further the suspension is assumed to be homogeneous and stable. Any decrease in concentration is supposed to be due to EPD, and not due to sedimentation or any other factor. Also, the equations are worked out for planar substrates. The kinetics for the above mentioned four cases are given by;

1. $w(t) = kw_0t$
2. $w(t) = w_0(1- e^{-kt})$
3. $R'(w(t))^2 + Lw(t) - k'V_{app}t = 0$

4. $R'(w(t))^2 + (R'w_0 + L)\ln(1 - w(t)/w_0) + k'V_{app}t = 0$

where, $k=Sfu/V$, $k'=\mu_e k$, $R'=(R_r-1)/S\rho$, w is the weight of the deposit, w_0 is the initial weight of the solids in the suspension, S is the surface area of the substrate, L is the distance between the electrodes, V_{app} is the applied voltage, R_r is the ratio of the resistivities of the deposit to that of the suspension, t is the time of deposition, μ_e is the particle mobility (not electrophoretic mobility), and ρ is the density of the deposit.

However, not much is said in the literature about EPD in non-planar geometry. It is not clear how the field effects the particles which are not between the electrodes and how far the effects of the field extend. One can expect the particles directly between the two electrodes to have a greater tendency for electrophoresis and deposition. If true, it may effect the w_0 and 'f' factors in the equations above. The efficiency factor might also be effected by the current, especially around the critical minimum current required for deposition.

The suspension:

Till now we have discussed the basic EPD process separated from the suspension itself. The suspension is a near colloidal suspension of micron or sub-micron sized particles. Its properties effect the EPD process enormously.

The most important aspect of the suspension is its stability. Most of the theory on EPD assumes a well suspended stable sol or suspension. A stable suspension refers to how well deflocculated are the solid particles in the suspension and how resistant they are to settling. A good stable suspension should not have agglomorated particles and particles should not settle easily under the influence of gravity. Also, when they do eventually settle, they should form a

hard deposit which can not be easily redispersed by mechanical agitation. A soft deposit which is easily redispersed is an indication of agglomorated particles. Vice versa a stable suspension will give a hard deposit during EPD. The stability also effects the kinetics of deposition through the efficiency factor. A maximum efficiency of unity is assumed for well dispersed slips.

Theory of stability of suspension:

Much of the treatment of stability of suspensions derives from that of interactions of double layers within a suspension, minus the effect of electric field. For a suspension to be stable and well dispersed, the particles (with their double layers) should be repel each other as much as possible. This will imply a high zeta-potential on the particles. This is the basic requirement for a stable and well dispersed suspension. To ensure a high zeta potential various methods might be used. The most common one is to add a surfactant / deflocculent to the suspension. The deflocculent contributes species that are adsorbed on to the solid surface and raise its zeta-potential.

The other factors that influence the stability of the suspension are the pH and electrolyte concentration. In many cases H^+ or OH^- are the potential-determining ions. In such and other cases where ions get adsorped, they directly effect the surface potential and hence the zeta-potential. In the case of indifferent electrolytes, mentioned before, the electrolytes compress the double layer. This implies that the particles can come closer to each other. This in turn means that there is a greater tendency for the particles to coagulate. The effect of pH and zeta-potential may be better understood by looking at Fig.2.8 and Fig.2.9 . These figures show the variation of zeta-potential with pH and electrolyte concentation for alumina suspensions. By having such plots one can suitably adjust the suspension. However, one must be careful in

using these graphs, as they are unique for a specific solid/ dispersing media/ dispersing agent (if any) system. The important thing to note in the zeta-potential Versus pH graphs is the *Isoelectric point (IEP),* the point at which the zeta-potential is zero.

The suspension has the greatest tendency to settle out and coagulate near this pH. Another related concept is the *Point of Zero charge (PZC).* It is the point at which surface charge is zero. It is coincident with IEP in quite a few cases, but need not be so. This fact is evident from the previous discussion on the correlation of the two parameters.

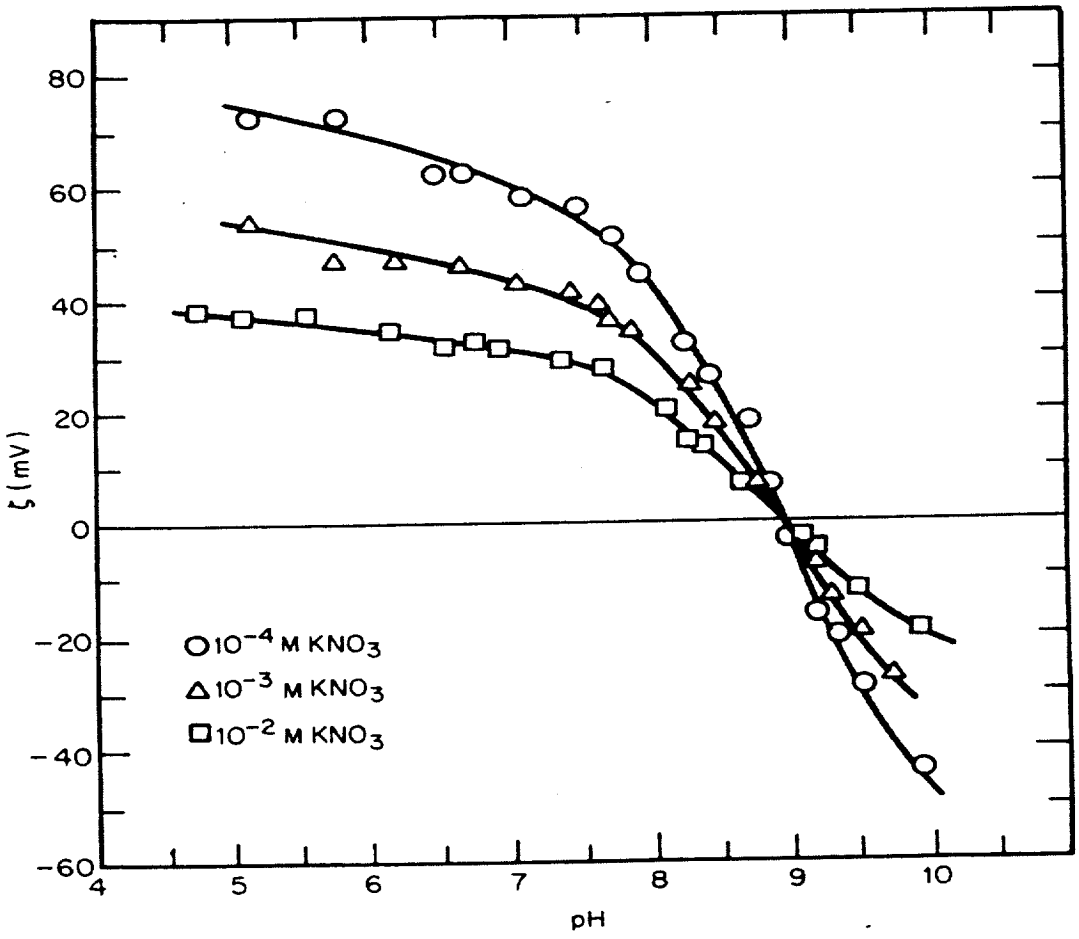

Fig.2.8 Variation of the zeta-potential of alumina with pH. The conductivity was maintained constant by using excess of an indifferent ion. γ-alumina of 0.01 microns particle size and $80m^2/gm$ specific surface area was used in these studies[7,11].

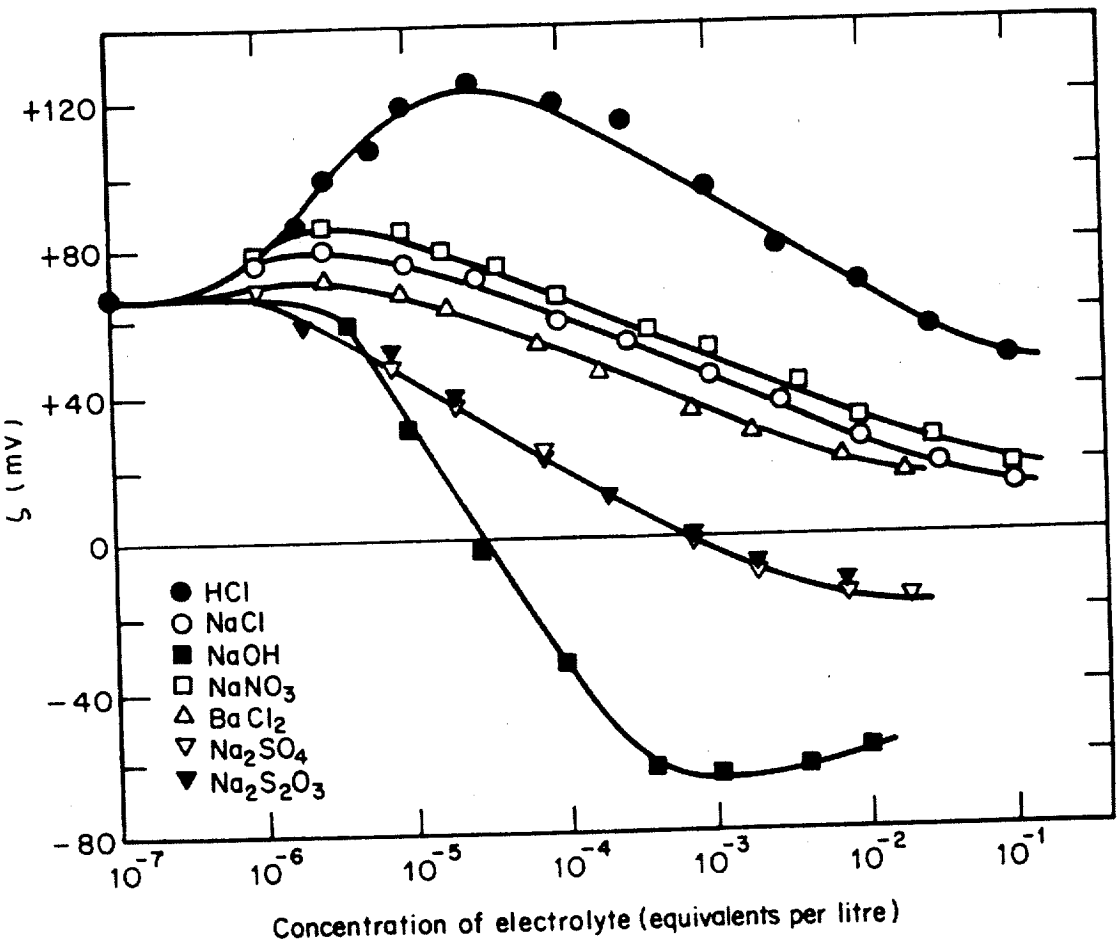

Fig.2.9. Variation of the zeta-potential of alumina with electrolyte concentration[7]

Measurement of Zeta-Potential:

While there are a number of ways of measuring electrokinetic parameters, each of which can be correlated to the zeta-potential, only two will be discussed here.

1. Direct measurement of electrophoric mobility: This method is used in commercial instruments. In this method, a sample of the suspension is put into a transperent electrophoresis cell and electric field is applied. A microscope enables us to see the particles as they move under the influence of the electric field. As the particles move towards one of the electrodes, they are traced through the microscope and their velocity measured directly. The electrophoretic mobility and zeta-potential are then calculated from these measurements.
2. Mass transport method: In this method by Olivier and Sennett[12], the quantity of material deposited during EPD is correlated to the electrophoretic mobility. A schematic of the apparatus used in this method is shown in Fig.2.10. While making the measurements, the reservoir is filled with the suspension as is the test cell. Then the electric field is applied. The EPD is carried out under constant current conditions. Deposition weight can be calculated by noting the weight change of the test cell before and after the deposition. The electrophoretic mobility, u, then is given by:

   $u = (\Delta W.\lambda_0)/ (\phi(1- \phi)(\rho_s - \rho_l)It)$

   where, ΔW is the change in weight of the test cell, λ_0 is the conductivity of the suspension, is the weight fraction of the solids in the suspension, ρ_s is the density of the solid particles, ρ_l is the density of the suspending liquid, I is the deposition current, and t is the time of deposition.

It should be mentioned here that since the particles need not be deposited on the electrode to observe the weight change, the measurements made here are not affected by deposition kinetics. They are governed primarily by electrophoresis.

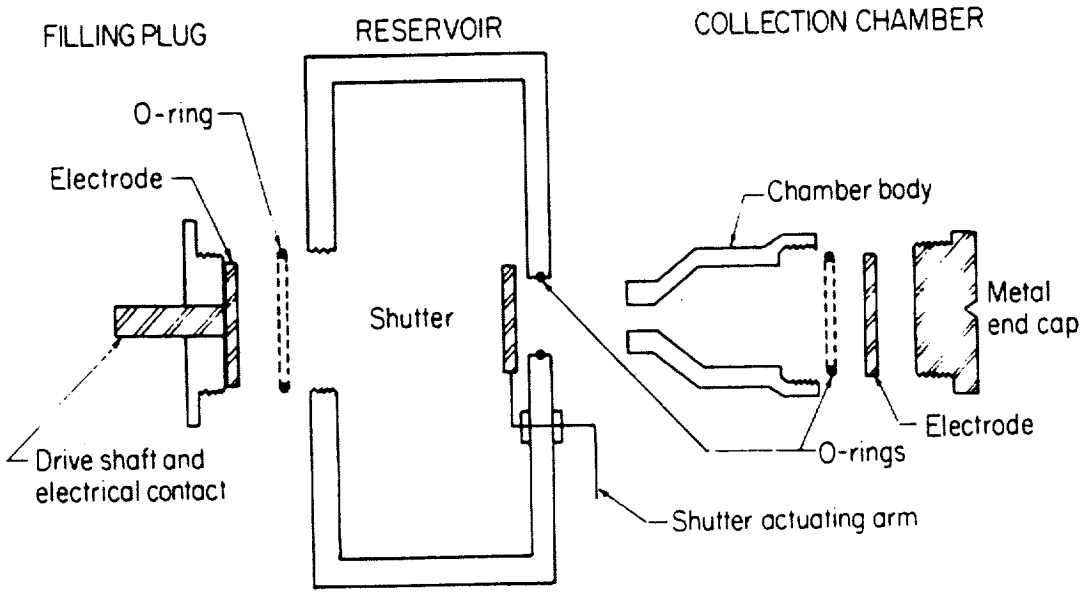

Fig.2.10 Schematic of the apparatus for measuring zeta-potential by mass-transport method[7]

Ideal conditions for EPD:

There is a discrepency in the literature about what investigators consider as the ideal zeta potential for EPD. Although high zeta potential means a stable suspension, it also implies a higher potential barrier for deposition and hence a slow deposition rate. Thus, depending on what deposition rates are required, an optimum zeta-potential must be derived.

As the electrolyte concentration, C_i, increases, the conductivity, σ, of the suspension increases:

$\sigma \propto C_i \Rightarrow$ Resistance, $R \propto 1/C_i$

Also, current, $I = V/R$, where V is the voltage drop acorss the suspension

As can be seen from these relationships, as the concentration of the ions increases, the resistance decreases. Under constant current conditions, this results in a lower voltage drop across the suspension to maintain a constant current, and hence a lower force on particles for electrophoresis and deposition. The overall effect of an increase in the concentration of indifferent ions is to reduce the electrophoresis rate and deposition rate.

Aqueous EPD:

The EPD process can be classified based on the type of suspending liquid being used. As evident from the name, aqueous EPD refers to EPD from aqueous suspensions. Aqueous EPD has the advantage of having a very inexpensive dispersing media. However, very pure water should be used, as the presence of ions in water can severly affect the EPD process. Another important advantage of aqueous EPD is of being environment friendly. However the greatest disadvantage of aqueous EPD is that of gas evolution at the elctrodes. Water easily dissociates under moderate electric fields. This leads to the evolution of gases at the electrodes. These gases escape through the deposits leaving pores behind. Thus, they deteriorate the quality of the coatings. This puts a limitation on the magnitude of current that can be used and hence the rate of deposition.

The other kind of EPD, non-aqueous EPD will be discussed later.

CHAPTER 3

Aqueous EPD: Experimental Procedures and Results

Experimental

The Alumina suspension:

As mentioned before suspensions made by dispersing alumina in water were used for the aqueous EPD. Various grades of Reynolds alumina were used. The specifications of the various alumina powders supplied are given in Table 3.1. The important consideration in selecting the alumina powders was low alkali, especially soda, content. As explained before, mobile ionic species can affect electrophoresis and deposition. More importantly, since the final application of the alumina coatings is as high temperature insulating coatings, the presence of conducting impurities like sodium can severely deteriorate their performance. Ten to forty percent by weight alumina was used in preparing the suspensions. Double distilled water was used throughout. Again, the motivation was to reduce the amount of mobile ionic impurities. Since it was found that the alumina particles are not sufficiently charged, Duramax D-3021 dispersant from Rohm and Hass Company was used. It is an ammonium salt of polyacrylic acid. In solution it dissociates to give $R\text{-}COO^-$ ions. These are then adsorbed onto the alumina particles and yield negatively charged surfaces, 0.5mgs of dispersant was added per square meter of specific surface area of the alumina powder.

Referred to as	Product Code	Particle Size (μm)	Specific Surface Area (m^2/gm)	Composition (ppm) Na_2O, CaO, MgO, Fe_2O_3
A	XRC-SP/LS DBM	0.23	20.3	11, 10, 3, 11
B	RC-SP DBM No MgO	0.36	8.42	79, 10, 5, 7
C	XRC-SP BM (No MgO)	3.6	5.53	31, 5, 5, 11
D	RC-SP DBM	0.38	9.33	65, 2, 2, 7
E	CR-30	0.05	25	20, 5, >5, 10
F	RC-SPF-DBM No MgO	0.38	8.52	64, 13, 7, 8

Table 3.1. Specifications for the various Alumina Powders. All powders (except E) were supplied by Reynolds company. Alumina E was supplied by Baikowski

After mixing all the ingredients the slip ball milled in a polyethelene bottle using alumina balls for 24-48 hrs for proper mixing and dispersion.

EPD:

A voltage source, EC250-90 of E-C Apparatus Corporation, was used for applying the electric field. The source was capable of acting either as a constant current or as a constant voltage source. All the depositions in this study were carried out under constant current conditions. As explained earlier, constant current deposition has advantages with respect to controlling the deposition rate of the coatings. One of the two electrodes was the wire sample to be coated. Different wires were used as substrates for coating. Since the wires should be able to withstand high temperatures, platinum and its alloys were used. The specifications of the wires are provided in Table 3.2. A 20mil platinum wire was used as the second electrode.

Preparation of the samples:

The experimental set-up for the EPD process is shown in fig.2.1. The suspension was contained in a beaker. The electrodes were cleaned with acetone. The electrodes, held in place by a stand, were then dipped into the suspension and the electric field was applied. The current and time of deposition were noted. Once the samples were coated, they were removed and dried in air by hanging them from a wire. This was done to ensure uniform drying. The dried samples were then sintered as required.

Composition	Diameter (mils)	Melting point (°C)	Oxidation behavior
nickel	15	1455	Oxidizes below 500°C
platinum(90%)-nickel 10%)	5	1540	Susceptible to oxidation
platinum	5 and 10	1768	Can be sintered in air without oxidation
platinum-Rhodium (3%)	3	1840	Can be sintered in air without oxidation
chromel-p	10mil	< 1250	Susceptible to oxidation

Table 3.2. Specifications of the various wires used in this study[13]

The above mentioned experimental procedures were used in general in all the experiments. Exceptions and other specifications will be provided for individual experiments. The literature suggests that most of the voltage drop occurs across the coatings and very little across the suspension. This was verified during an EPD experiment by measuring the voltage drop at various points between the electrodes using a Radio Shack 24-range LCD Digital multimeter. This implies that the potential varies very gradually across the suspension between the electrodes. Hence the distance between the electrodes was assumed not to be a critical factor for deposition or electrophoresis. Also, the size of the beaker used for deposition was not considered critical.

Experiments to study the effect of various parameters on EPD:

Initial experiments were done to determine optimal coating conditions with respect to deposition current, solid loading, pH, and alumina particle size. No quantitative estimation of the porosity and surface finish of the coatings could be made because of the fragile nature of green coatings. However, the coatings were examined using optical microscope to qualitatively study these factors and the observations were considered in evaluating the effect of the parameters. Each of the above mentioned factors were varied individually and the effect of each on the rate of deposition was studied.

Coatings were made on 0.381mm (15mil) nickel wires under varying conditions. Coatings were obtained using 1, 2 and 3mA constant currents to study the effect of deposition current. To study the effect of solid loading, coatings were made from suspensions having 10, 20 and 40 weight percent of alumina B. Three different types of alumina powders- types A, B, and C, were used for characterizing the effect of particle size.

The results will be discussed in detail in the next section. Briefly, it was found that higher solid contents and finer particles give better coatings. The choice of deposition current depends on whether, the rate of deposition or the porosity of the coatings is important. Though the rate of deposition increases substantially between 1mA to 2mA, the electrolysis of water also increases. This leads to increased evolution of gases at the electrodes and hence more porous deposits. The choice of deposition time depends on the required coating thickness.

An instrument was built for measuring electrophoretic mobility of the suspensions. It was based on the principle of the mass transport analyzer explained in the second chapter. It is also similar to a commercial model by Micromeretics. The details of our instrument are provided in Appendix A. Variation of zeta-potential with pH of the slip was measured using this instrument. This was done in addition to experiments done to study the variation of deposit weight with pH.

As explained earlier, the zeta-potential was measured by measuring the weight change of a test cell due to electrophoresis for a specified period of time at a constant current. All the measurements were done using 1mA current, the time though varied between different measurements. The principle has been explained in chapter 2. The polarity of the electrodes was so adjusted that material was deposited into the test cell. This was done to ensure that the weight change being seen was due to electrophoresis an not due to accidental weight loss of the slip from the test cell. The following formula was used to convert the observed weight loss to electrophoretic mobility (also given in chapter 2):

$$u = (\Delta W.\lambda_0)/ (\phi(1- \phi)(\rho_s - \rho_l)It)$$

Where, ΔW is the change in weight of the test cell, λ_0 is the conductivity of the suspension, ϕ is the weight fraction of the solids in the suspension, ρ_s is the density of the solid particles, ρ_l is the density of the suspending liquid, I is the deposition current and t is the time of deposition.

Coatings were made from a slip containing forty weight percent alumina A, to study the effect of pH. Then the slip was divided into different portions. The pH of each portion was adjusted using diluted HNO_3 and NH_4OH or butylamine. The deposits were obtained at 1mA and a deposition time of 180secs. They were dried and then their weight was measured. Their thickness was also measured using a graduated optical microscope. The conductivity was also measured after changing the pH. The variation of viscosity with pH was also studied. All the pH and conductivity measurements were made using an Accumet ARO model, pH and conductivity meter from Fisher Scientific. The viscosity measurements were done using a Brookfield DE-V model viscometer.

Experiments to study the effect of various parameters on adherence:

The effects of coating thickness and the type of substrate on the adherence of sintered coatings were studied. Coatings were made on two different wires [0.381mm (15mil) nickel and 0.127mm (5mil) Pt-Ni (10%) wires] for different times to obtain coatings of different thickness. All the coatings were deposited using a current of 2mA. The adherence was tested by coiling the sintered coated wires around 1/4", 1/8", and 1/16" diameter rods. The coiled coatings were studied for loss of coatings using optical and electron microscopes. Coatings were made on 0.254mm (10mil) platinum wires to study the effect of sintering temperature. The coatings were made from a forty weight percent alumina A slip of pH 9.19 (as dispersed).

A current of 1.0mA current was used. The coatings were of comparable thickness. Different samples were then sintered at 1600, 1500, 1400 and 1300°C. The samples were then bent and studied as mentioned above. Some coatings made on nickel and platinum-nickel wires during earlier experiments were also subjected to bend tests. These samples had been sintered at 1100°C and 1300°C respectively. To study the effect of particle size, the coatings were made using three different kinds of alumina. The coatings were sintered and their adherence tested by coiling around mandrels.

The results of the bend tests (provided in detail in next section) did not show any effect of substrate or its surface condition on the adhesion of the coatings. The influence of the substrate on coating adhesion has been reported in the literature for other coating methods[14-16]. The following set of experiments was done to determine if effects existed for EPD alumina coatings.

It was observed that the coatings developed cracks during drying and sintering. These were examined with the following assumptions:

a. The "crack density" (number of cracks/unit length), their size, and spacing can be qualitatively related to the adhesion of the coatings to the substrate during drying or firing. (Note that this "adhesion" is different from the one mentioned previously).
b. The adhesion of the coatings is dependent on the surface condition of the wires.

It was further assumed that the parameters affecting the crack density and the crack spacing are the coating thickness, wire material, wire diameter, and surface condition of the wire. The wires listed in Table 3.3 were given three different kinds of pre-treatment prior to coating to

study the effect of each of these factors. The first set was vacuum fired, the second was fired in air, and the third was used without any pre-treatment. The details of the pre-treatments are also given in Table 3.3. The coatings were made using alumina B slips and 1mA current. In each set, coatings of different thickness were obtained by varying the deposition time. The coatings were then sintered as shown in Table 3.3. Then the cracks were studied using optical and electron microscopes. The number of cracks per unit length was plotted against the coating thickness for each set of wires. Also the surface condition of the bare wires with each kind of pre-treatment was studied using Scanning Electron Microscope (scanning electron micrograph) and Energy Dispersive X-ray analysis (Philips XL-30 FEG) to understand the effect of the pre-treatments on the wire surface and ultimately on the coatings.

wire	Diameter (mils)	Atmos phere	Pre-treatment Time (hrs)	Pre-treatment Temp (°C)	Sintering Time (hrs)	Sintering Temp (°C)
nickel	15	UT	N.A	N.A	6	1200
nickel	15	VF	1.5	800	6	1200
nickel	15	AF	500	2	6	1200
Pt-Ni(10)	5	UT	N.A	N.A	2	1400
Pt-Ni(10	5	VF	1.5	800	2	1400
Pt-Ni(10	5	AF	500	2	2	1400
platinum	5	UT	N.A	N.A	2	1500
platinum	5	VF	1.5	800	2	1500
platinum	5	AF	1.5	1000	2	1500
Pt-Rh(6)	3	UT	N.A	N.A	2	1550
Pt-Rh(6)	3	VF	1.5	800	2	1500
Pt-Rh(6)	3	AF	1.5	800	2	1500
Pt-Rh(10)	10	UT	N.A	N.A	2	1550
Pt-Rh(10)	10	VF	1.5	800	2	1550
Pt-Rh(10)	10	AF	1.5	800	2	1550
chromel-p	10	UT	N.A	N.A	8	1150
chromel-p	10	VF	1.5	800	8	1150
chromel-p	10	AF	1.5	800	8	1150

UT- untreated, VF- Vacuum-fired,
AF- Air-fired

Table 3.3 Details of the pre-treatments and sintering for different wires used to study crack density.

Results and Discussion

Effect of various parameters on EPD:

The rate of the deposition was determined by plotting the weight or the thickness of the deposited coatings against coating time. For Fig.3.1 the thickness of the coatings was calculated from the coating weight by assuming 60% packing density for the coatings. As seen in Fig.3.1 the rate of deposition increases with depositing current. This effect is most prominently seen between 1mA and 2mA currents, but was barely evident between 2mA and 3mA (Fig.3.1). When we increase the deposition current the ohmic potential drop across the suspension will increase. Since the electrophoretic mobility is directly related to this potential drop, an increase in the deposition rate with current might be expected. However, the difference of rates at 1mA and 2mA may not be entirely due to this. As mentioned by Hamaker et.al [9,10], a potential barrier must be crossed for particles to get deposited on the substrate. So even though the particles do move electrophoretically, they may not be deposited if sufficient electric force is not acting on them. If such a barrier was crossed by the particles just after 1mA, then a sudden change in the deposition rate between 1mA and 2mA, as seen in the Fig.3.1, might be expected. Also the magnitude of the deposition current has a significant effect on the quality of coatings as evaluated from the optical micrographs. As stated earlier, there is evolution of gas at the electrodes because of electrolysis of water. The electrolysis rate increases with current. The gases lead to porosity in the coatings and poor surface finish. So even though the deposition rate increases with current, the quality of the coatings goes down.

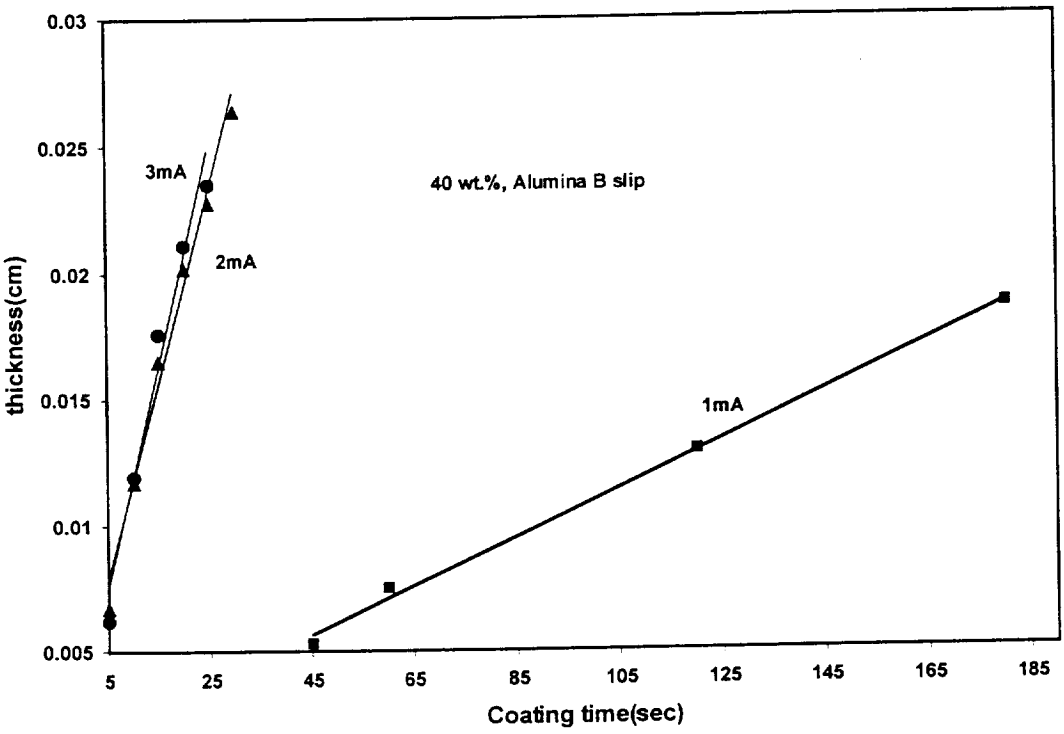

Fig.3.1. The evolution of thickness with coating time for different deposition currents

Since the weight fraction of material deposited during the present experiments is very low, the kinetics of the process was modeled by assuming constant current and constant weight conditions. The equations in the literature were derived assuming a planar substrate and require modifications before being applied to cylindrical substrates and deposits. The important consequence of the cylindrical shape of the coatings is that the area of the coatings increases as the deposition takes place and is a function of time. Taking this account, the equation for constant current, constant concentration kinetics becomes:

$$w(t) = \left(\frac{fuw_o}{V}\right)A(t)t$$

where, w is the weight of the deposit, f is the deposition eficiency factor, w_0 is the initial weight of the solids in the suspension, and A is the area of the deposits

$$\text{or, } \frac{dw}{dt} = \left(\frac{fuw_o}{V}\right)A(t)$$

However, the volume of the coating, $V_d = \frac{w}{\rho_s x} = \pi(r^2 - r_0^{\,2})h$

where, r_0 is the radius of the bare wire and r, the radius of the wire with the coating on it, ρ_s is the density of the solid, h is the length of the deposit, and x is the packing effciency of the deposits.

Hence area of the deposits, $A = 2\pi h\left(\sqrt{r_o^2 + \frac{w}{\rho_s hx}}\right)$

Substituting this in the differential equation above and solving, the thickness is

$d = \left(\frac{2fuw_o}{V\rho_s x}\right)t = kt$, where $k = \left(\frac{2fuw_o}{V\rho_s x}\right)$ is a constant at a fixed current

For a constant current, but varying concentration the thickness is given by

$$d = y_0(1 - \exp kt)^{1/2}$$

where, $y_0 = \sqrt{r_0^2 + \frac{w_0^2}{\rho_s x h \pi}}$ and $k = \frac{1}{2} y_0 \left(\frac{\pi h f u}{V} \right)$

The equations show that the thickness of cylindrical coatings will be a linear function of time for the constant current and constant concentration conditions. Fig.3.1 does show a linear relationship between the two, thus verifying that the experiments were conducted under constant current and constant concentration conditions. Fig.3.2 shows that rate of deposition decreases with increase in particle size.

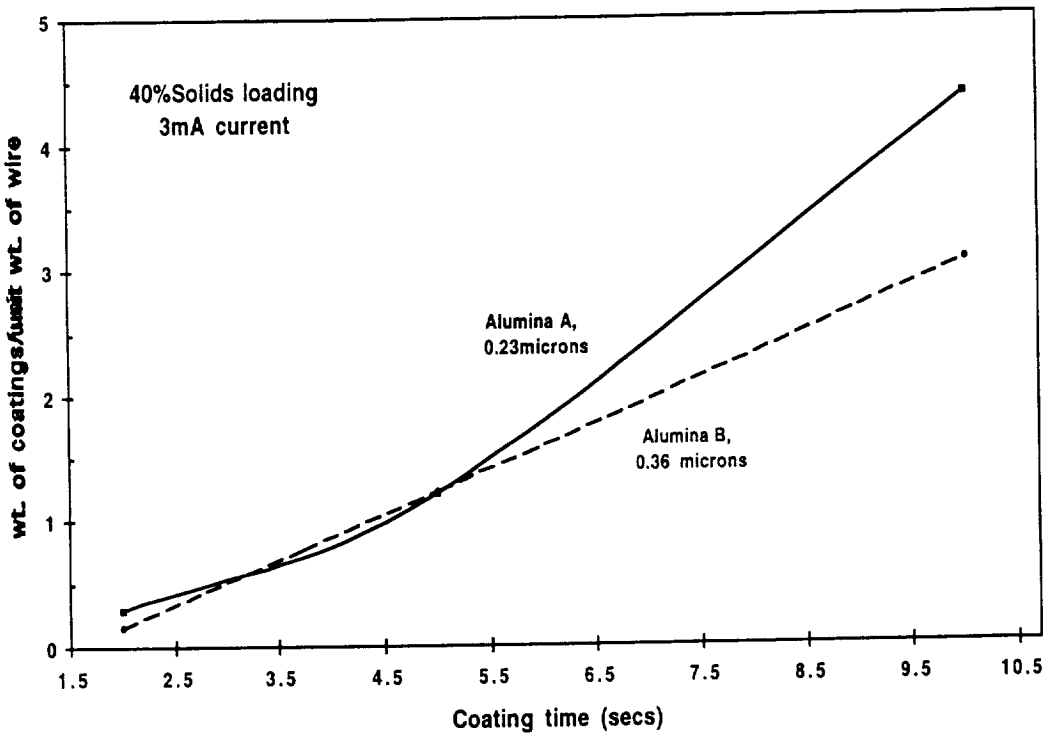

Fig.3.2 The variation of the weight of the deposits with time for different aluminas.

The effect of solids loading is shown in fig3.3. As can be seen, the rate of deposition increases with increase in solids loading. Hence the increase in rate of deposition by EPD is due to a larger number of alumina particles undergoing electrophoresis and deposition. Mathematically this increases the initial weight, "w_o", factor in the rate equation.

The pH has a direct effect on the surface charge and hence the zeta-potential. The conductivity on the other hand has an indirect effect on electrophoresis. The potential drop across the suspension is inversely related to the conductivity. Hence the electric force acting on the particles is related to the conductivity of the slip. Fig.3.4 shows the variation of deposit thickness with pH and conductivity. Since both the parameters are varying in these experiments it is difficult to make any judgement on the absolute effect of the individual parameters. It is important to again emphasize the distinction between electrophoresis and deposition kinetics. Not all the particles being transported to the electrode will be deposited. In the equations derived earlier, the deposition kinetics were assumed to be constant and modeled as a probability or efficiency factor. This assumption is valid so long as the conductivity or the zeta-potential does not vary much. There are no equations correlating zeta-potential, conductivity and deposition efficiency, and the deposition. However, the barrier height for deposition increases with zeta-potential, while the electrical force driving the deposition decreases with increase in conductivity. Hence the deposition efficiency is expected to be related inversely to both zeta-potential and conductivity.

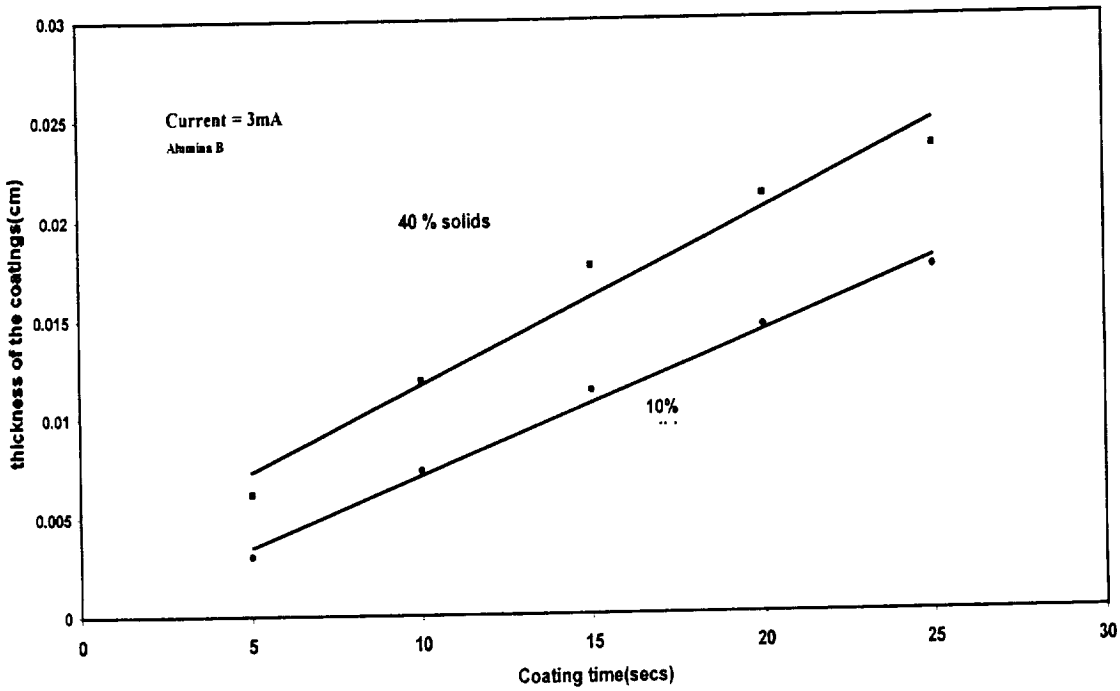

Fig.3.3. Effect of solids content on the evolution of coating thickness with time.

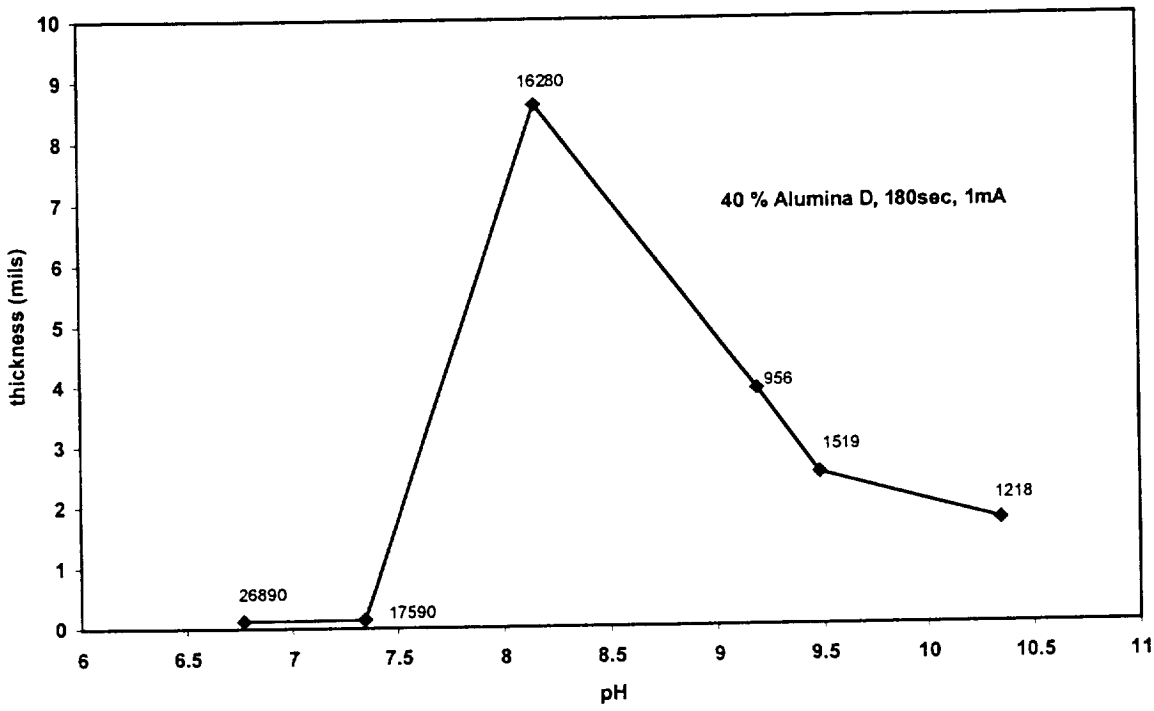

Fig.3.4. Variation of coating thickness with pH. The conductivity values are given next to each data-point. They are in 10^{-6} $(ohm.cm)^{-1}$.

The foregoing discussion is intended as a caution while interpreting this kind of data. However, the results can be interpreted in the following manner.

Fig.3.5 shows the variation of electrophoretic mobility with pH. The zeta-potential is lower at higher pHs. This explains the lower deposition rates at these pH values. However, at pH values below 8, both the zeta-potential and conductivity are very high . This will drastically reduce the deposition efficiency and hence the deposition rate. This may explain behavior seen in Fig.3.4. However, the raw data for the zeta-potential measurements shows a large standard deviation. Hence they have to be verified with some other standard measurements.

Also, Fig.3.6 shows the variation of viscosity with pH. Zeta-potential and viscosity should be inversely related, but the results in Fig3.5 and Fig.3.6 seem to contradict. However, no suitable explanation could be found for this. Since the reliability of the zeta-potential measurements is questionable, the matter was not pursued further.

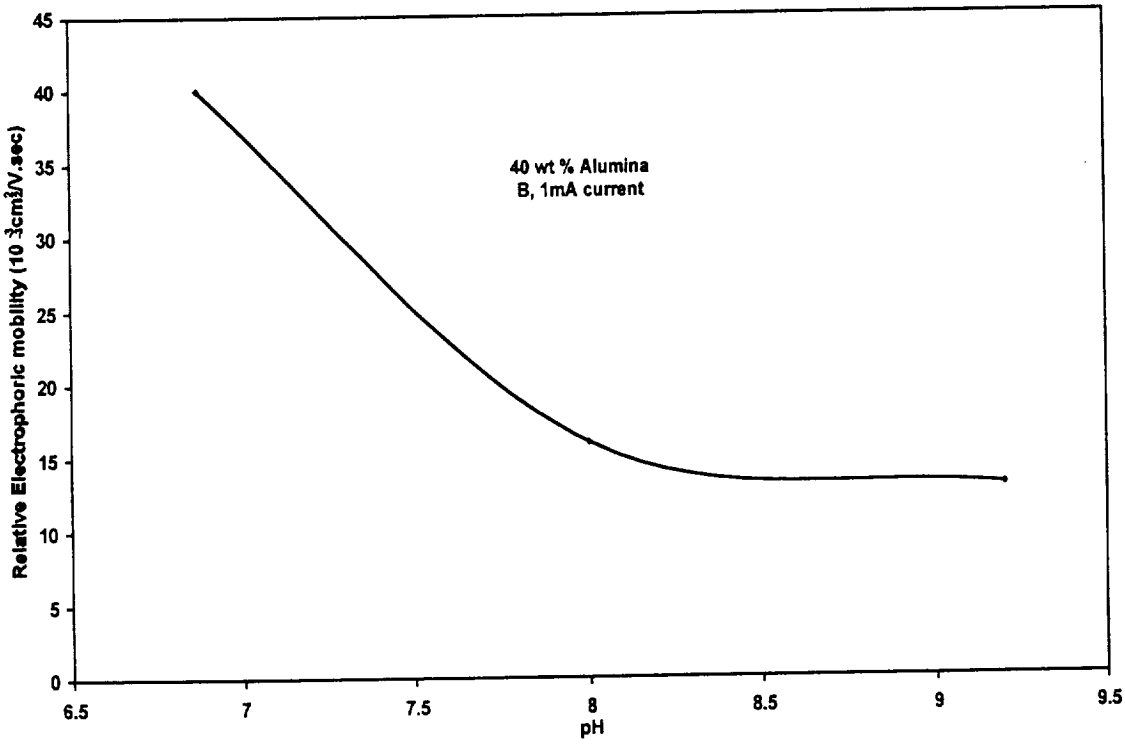

Fig.3.5. Variation of electrophoretic mobility with pH in aqueous alumina slips. All the measurements were done using 1mA current. More details of the measurements are provided in Appendix A.

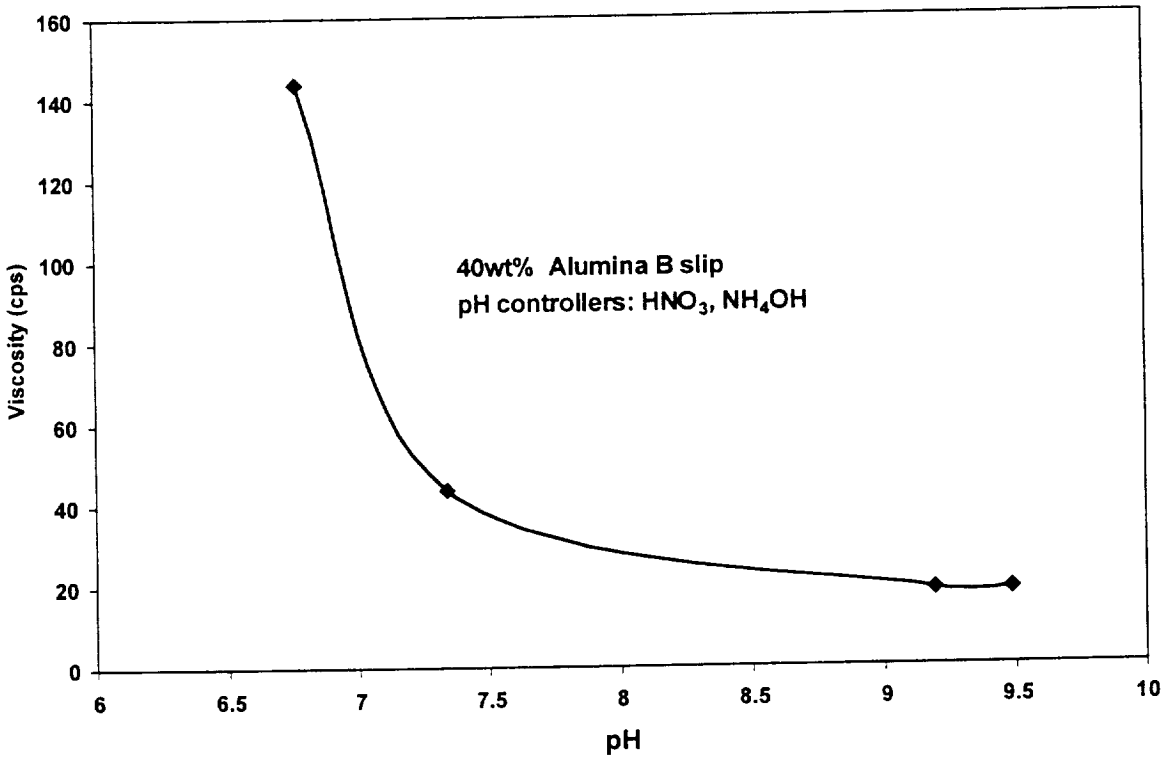

Fig.3.6. Variation of viscosity with pH in aqueous alumina slips

The cracks:

The coatings showed cracks on drying and sintering. Classically the drying cracks have been explained by a differential drying rate of moisture from the surface and the interior. The moisture gradient leads to differential shrinkage across the thickness and hence a stress in the coatings. This stress is supposed to be responsible for the development of the cracks. However, more recent studies have suggested an alternate theory [17,18] for the drying of thick-films on a substrate. According to the theory, the tensile stress responsible for the cracks results from the capillary forces of the liquid within the pores of the film. The capillary forces lead to a collapse of the double-layer between the particles, causing the film to shrink and develop an in-plane strain. In the presence of a substrate a dimensional constraint is imposed for particle rearrangement. Hence, the strain is not relieved. Consequently a tensile stress develops in the entire film and causes it to crack. The compaction during sintering leads to shrinkage. However, the substrate and the frictional forces at the interface, again, do not facilitate the relaxation of the strain. Hence, the coating cracks.

Adherence:

When a coated wire is coiled, the coating and the wire have different bending radius because of the geometry. Hence there is a differential strain between the wire and the coating. The coating develops cracks to relax this strain. Depending on the adherence between the wire and the coating, the coating may chip off on cracking or just remain cracked. Hence the loss in weight on bending can give a qualitative estimate of the adherence of the coating to the wire.

The adherence, as measured by the weight loss, (Fig.3.7) is better for thinner coatings, then decreases and is again good for the thicker coatings. If a coated wire is allowed to bend at the cracks, then the differential strain does not develop and the coating remains attached to the

wire. This will happen if the spacing between the cracks is much smaller than the bend curvature. The crack density is inversely proportional to the spacing between the cracks. It can be seen from Fig.3.8 that crack density is greater for thin coatings. Hence from the discussion above, they will be expected to have better adherence. In thicker coatings the wire bends primarily at cracks in the coatings and not around the rod. The coating itself does not bend. The scanning electron micrograph in Fig.3.9 shows that the coating is separated from the wire. However, it does not fall off. Hence the adherence, as measured by weight loss, is less in the case of thicker wires. The adherence is better for coatings made on thinner wires. Again Fig.3.8 indicates a higher crack density for coatings made on thinner wires. Hence they will be expected to have better adherence.

There is not much difference in weight loss of coated platinum wire samples sintered at various temperatures between 1300-1600°C on bending. Scanning electron micrographs (Fig.3.10) shows that the samples are well sintered. However, the scanning electron micrographs also do not show a significant difference in the adherence of the coatings sintered at these temperatures. However, there is a significant difference in the samples sintered at 1100°C and 1300°C. The adherence of the samples sintered at 1100°C is poor and most of the coating chips off on bending 360° around a $1/16^{th}$ inch mandrel.

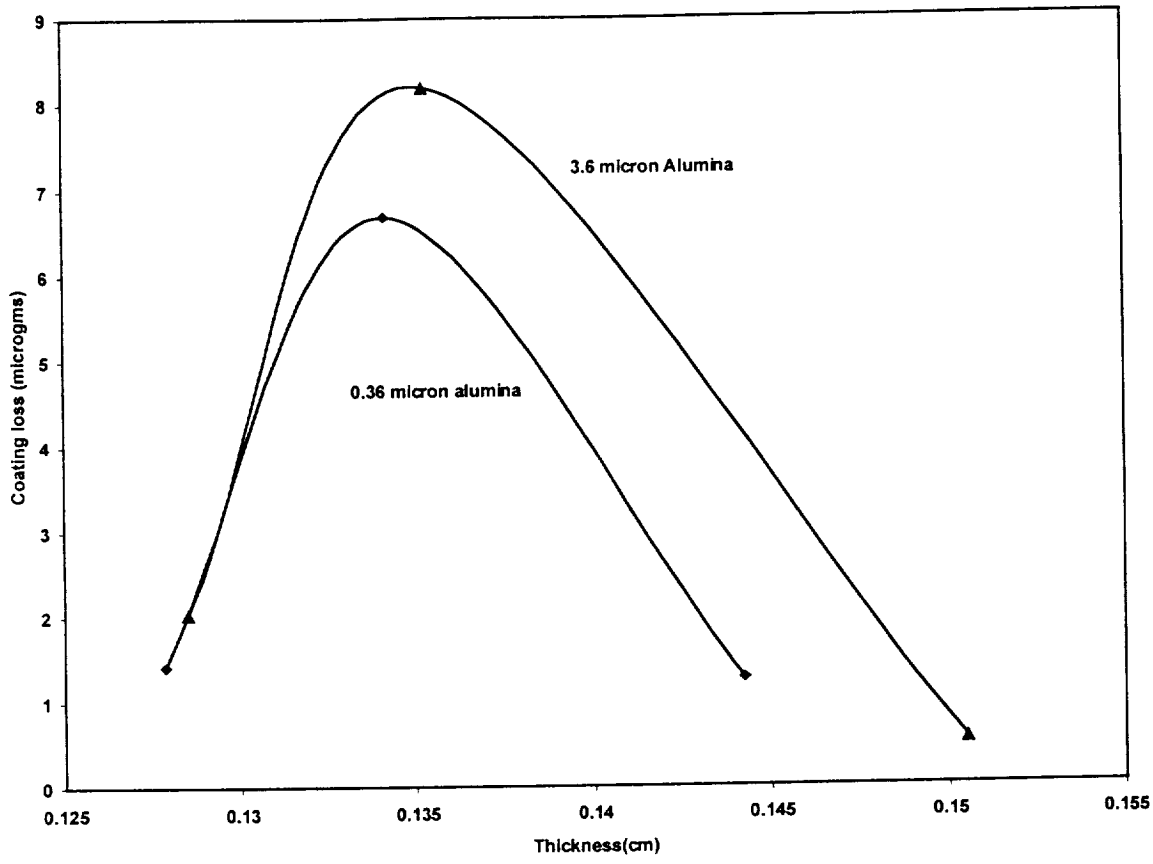

Fig.3.7. Variation of weight loss, on bending around a 1/16" inch mandrel, with coating thickness.

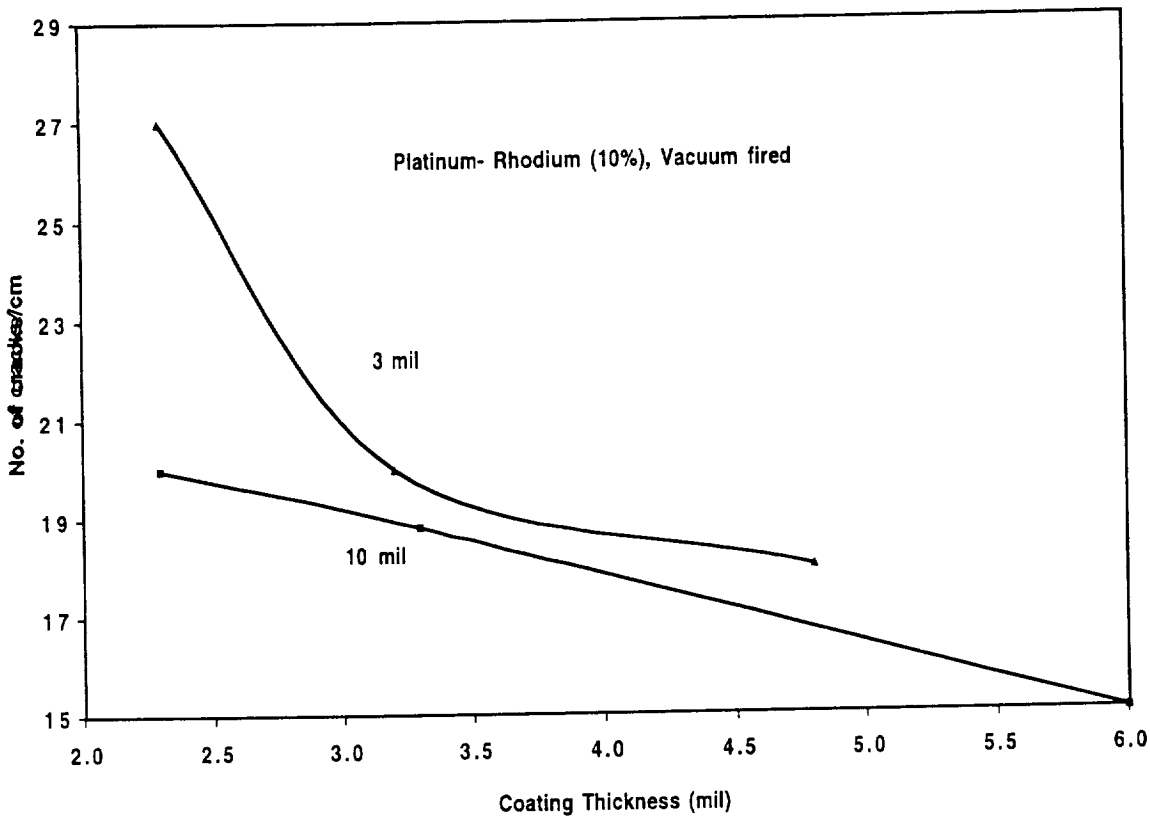

Fig.3.8. The effect of wire thickness on crack density. The experiments were done on vacuum fired Pt-Rh wires.

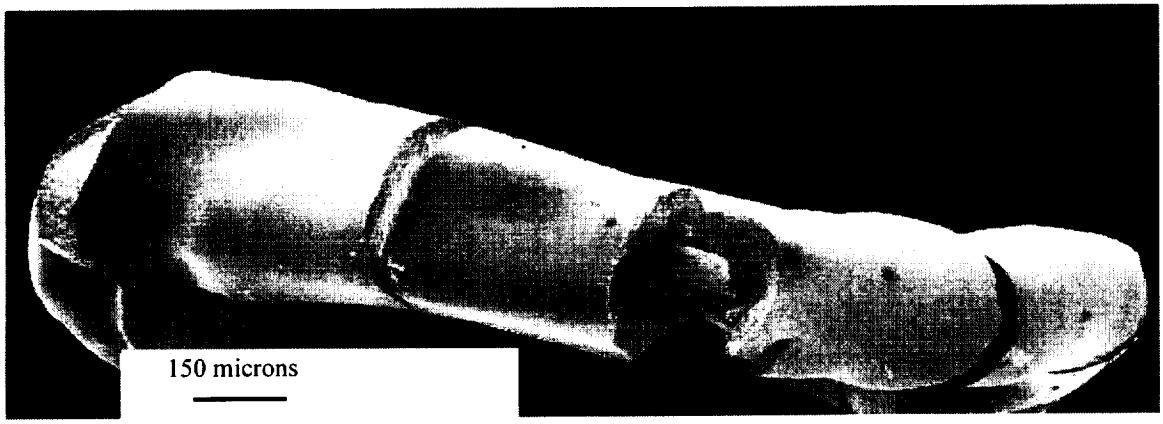

Fig.3.9. Scanning electron micrograph of a curled thick coating showing that the coating remains in place on bending.

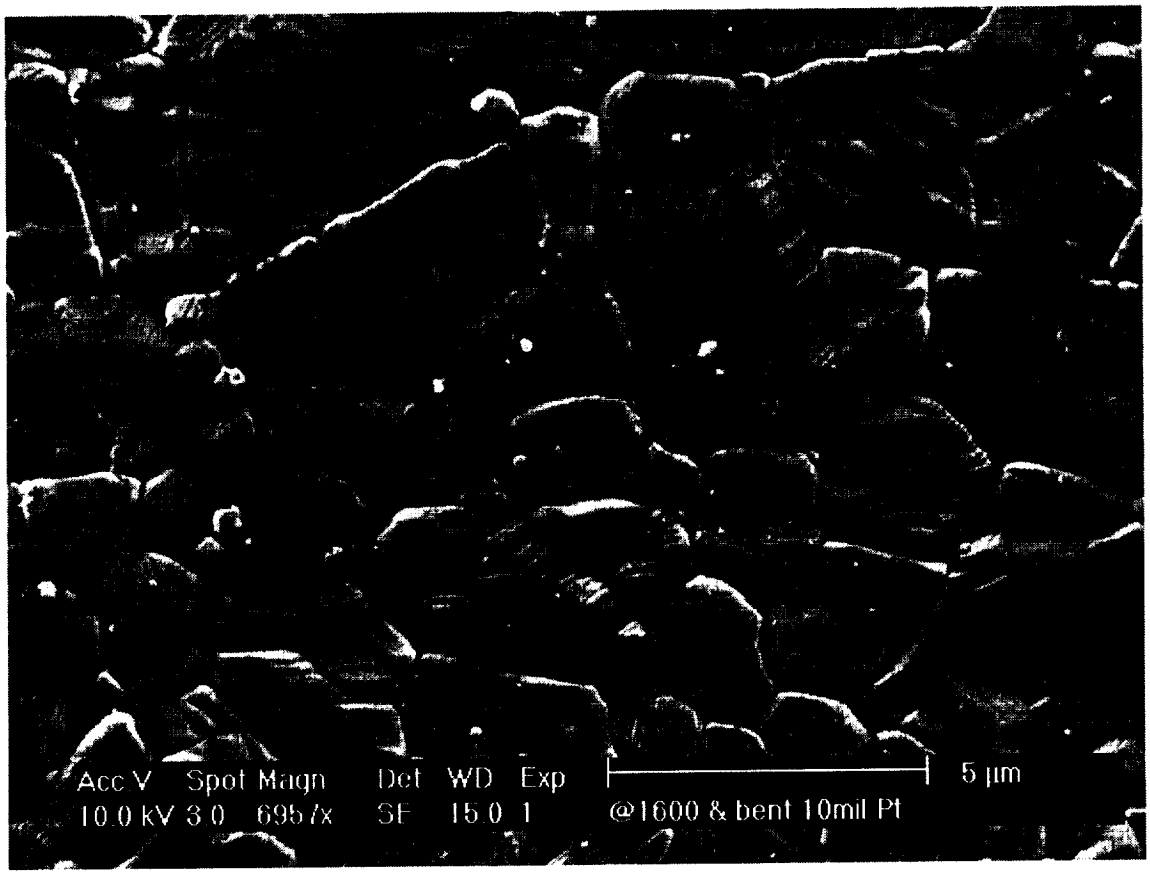

Fig.3.10. Scanning electron micrograph of a EPD coating sintered at 1600°C indicating that the coatings are well sintered.

The adhesion between the metal wire and the ceramic coating is primarily due to interdiffusional bonding. Since both sintering and interface bonding are diffusional process, based on similar parameters under these conditions, a better sintering should imply a better adherence. The samples fired at 1100°C are not well sintered and hence will be expected to have poor adherence. In general the sintering of the samples may be considered as a guide for the adhesion between the metal and the coating.

Effect of wire substrate on coating cracks:

The origin of the drying cracks has been explained. The sintering cracks are due to the shrinkage of the ceramic coating on densification and the friction at the wire (metal)-coating (ceramic) interface. Scanning electron micrographs of bare metal wires show thermal grooving in the vacuum fired samples (Fig.3.11a-c). Although in some cases the oxidation temperature was higher than the vacuum firing temperature, significant grooving was not seen in air-fired samples. The maximum change in the surface morphology, due to the heat treatments, was noticed in chromel-p. It showed a fair amount of oxidation, which made the surface extremely rough (Fig.3.11d). Even on vacuum firing its surface became extremely rough (Fig3.11e). Nickel wire did not show any significant effect of firing in vacuum. However, it did show extensive oxidation. A very finely cracked oxide layer was deposited over it (Fig.3.11f). Also, some carbon contamination was noticed on the bare wires, specially, in the case of vacuum fired samples. This is suspected to be from the graphite slab used to cover the samples in the furnace. Its effect on the electrophoretic deposition is not known.

a.

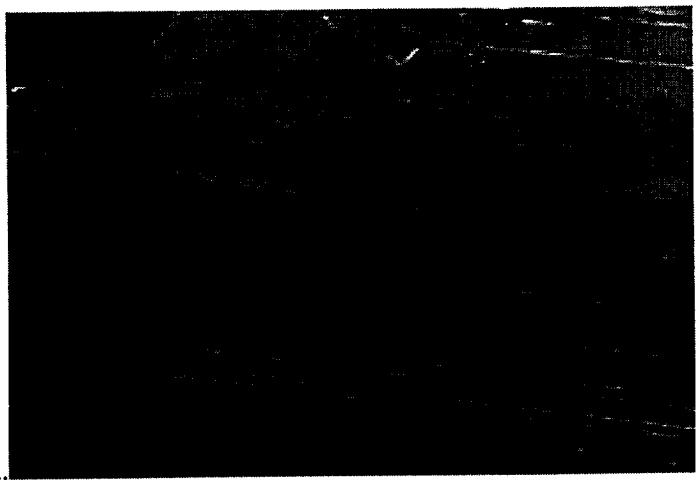

b.

c.

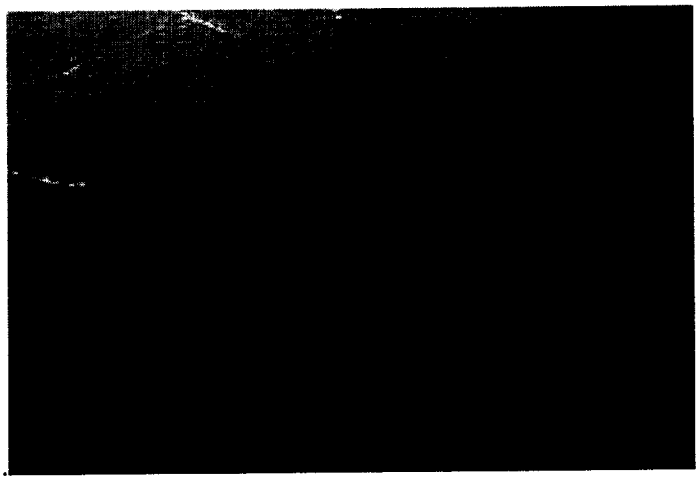

Fig.3.11. Scanning electron micrographs of a) Air fired platinum wire, b)Untreated platinum wire and c) Vacuum fired platinum wire d) Oxidized chromel-p wire, e) Vacuum fired chromel-p wire and f) oxidized nickel wire.

(continued next page)

d.

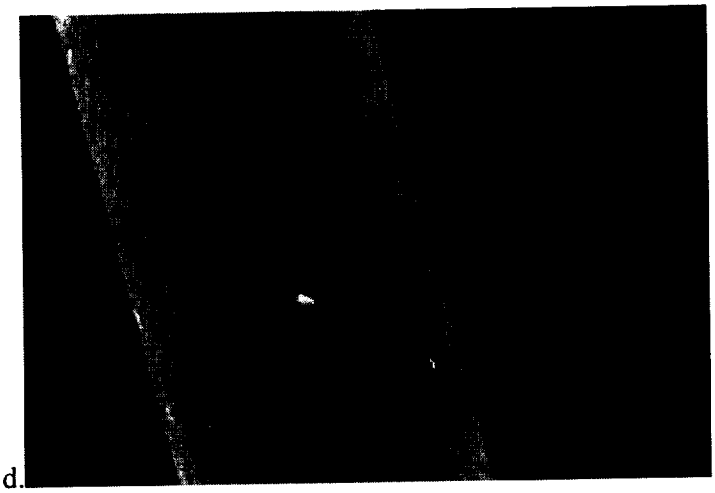

e.

f.

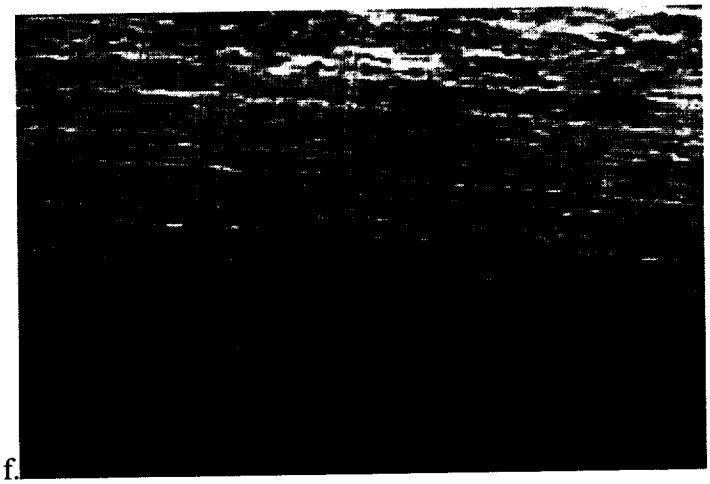

Also, it is seen from Fig.3.12 that on platinum wire, the vacuum fired samples have the largest crack density and untreated wires have the least. As mentioned above, vacuum firing results in thermal grooving of the wire, which roughens the surface. The co-efficient of friction increases with the roughness of the surface. This increases the constraint on the coating as it shrinks during sintering. Hence the crack density increases. The untreated wire also shows some roughness due to the drawing process used for making the wire. However, the drawing marks are in only in the longitudinal direction and hence do not offer resistance to the shrinkage of the coatings. In the case of chromel-p the oxidized wire showed the maximum crack density. This may be, again, due to the oxide layer formed on it, which roughened the surface. In the case of oxidized nickel, the effect of the oxide layer was to impede the deposition. In general, "surface roughening" seems to increase the cracking of the coatings.

Two kinds of cracking patterns were seen (Fig.3.13a,b)- (1) the cracks only run perpendicular to the wire axis, (2) a combination of interconnected normal and perpendicular cracks. The latter cracking pattern, undesirable as it reduces the adherence, is seen when the number of cracks is large. So, as expected, this kind of cracking is seen in thicker wires and thinner coatings. Also, coatings on chromel-P wire showed a significant amount of the latter type of cracking.

Although the coatings made from aqueous EPD are adherent and fairly flexible, they suffer from of cracks and pores. To overcome these problems non-aqueous EPD was tried.

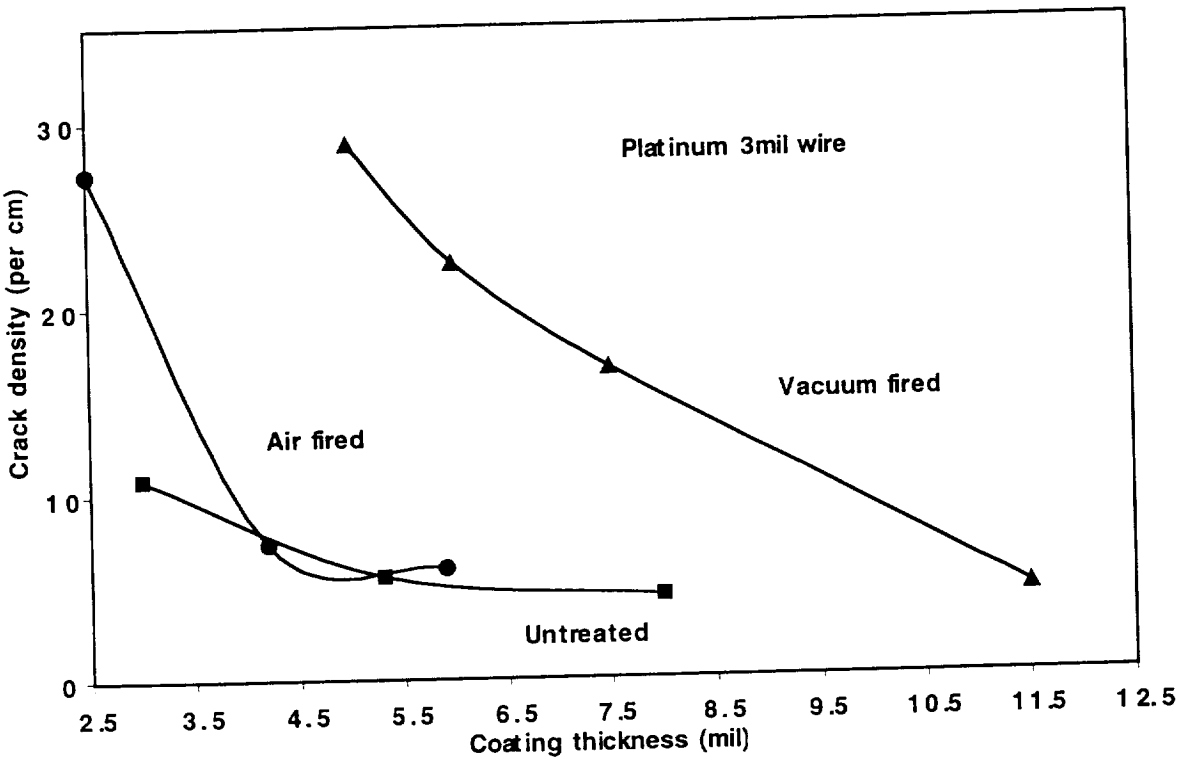

Fig.3.12. Variation of crack density with coating thickness in 3 mil Pt wire samples with different kinds of pre-treatments.

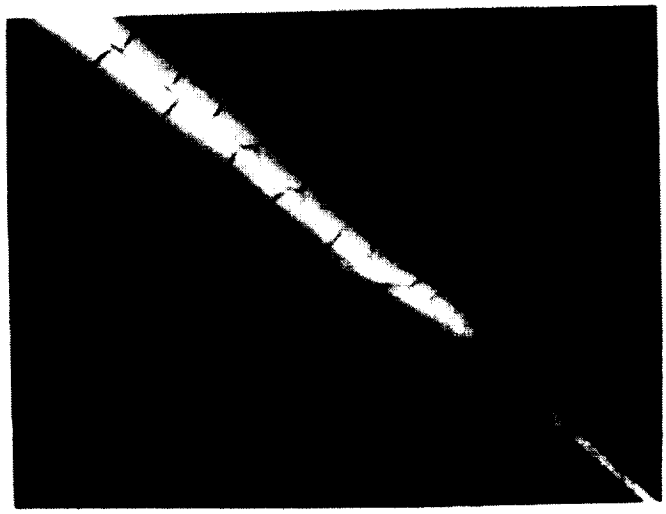

a.

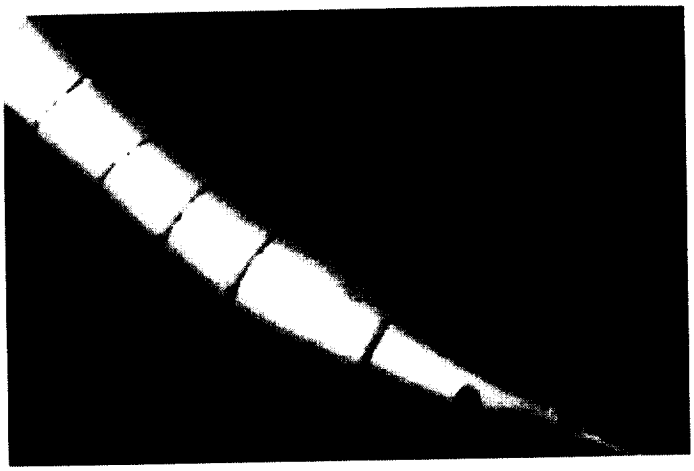

b.

Fig.3.13. Optical micrfographs of aqueous EPD coatings showing

a) an undesirable interconnected cracking pattern and b) a desirable cracking pattern

CHAPTER4

Non-Aqueous EPD : Experimental Procedures and Results

Non-Aqueous EPD

Non-aqueous EPD, as the name implies uses organic solvents which usually are less polar than water, as shown by the dielectric constants given in Table.4.1. Hence the solvent does not contribute many ions towards the surface charge of the solid particles. Therefore, the surface charge of as dispersed solid particles is very low. This in turn implies a low conductivity and hence low zeta-potential for as dispersed non-aqueous suspensions. As described earlier, a low zeta-potential and low conductivity result in high rates of deposition.

The gas evolution at the electrodes in aqueous EPD leads to porous deposits as shown in Fig.4.1. The other problem with aqueous EPD is of controlling cracks. The cracks in the coatings are desirable for the flexibility of the wires, but they have to be controlled. A crack pattern such as the one shown in Fig.3.11a is undesirable while the one shown in Fig.3.11b may be helpful. As mentioned before the cracking problem is two-fold- due to the existance of both drying cracks and the sintering cracks. The drying cracks are non-uniform.

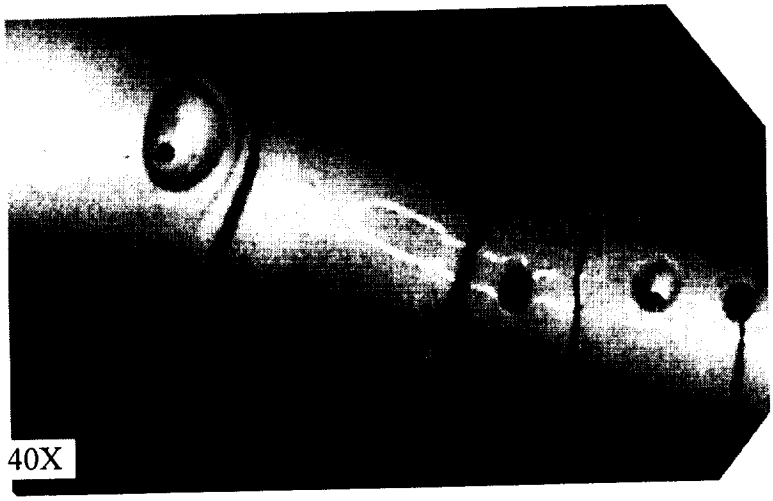

Fig.4.1. Pores formed in the coatings made from aqueous slips due to the gas evolution at the electrodes. The gas evolution is the result of dissociation of water under the influence of electric field.

Liquid	Dielectric constant (at 25°C)	Surface tension (mN/m)
Water	78.5	71.96 (value interpolated from data for 20°C and 30°C)
Ethanol	24.3	21.97
Acetone	20.7	27.10

Table.4.1 A comparison of surface tension of water and organic solvents. The data is for 25°C [19]

The non-aqueous dispersing liquids offer a better alternative. The drying cracks originate due to the capillary forces within the pores of the coating. The non- aqueous liquids usually have lower surface tension than water (Table 4.1). Hence the capillary force acting on the coating is lower for non-aqueous dispersing liquid, and cracking is less likely to occur on drying.

EXPERIMENTAL

The dispersion:

In the present study absolute ethanol was chosen as the dispersing media. However, voltages in excess of 250 volts were required for EPD when only ethanol was used. The power supply used in these experiments did not have such high voltage capabilities. Hence mixtures of ethyl alcohol and acetone were tried. These mixtures do require lesser voltages for EPD. However, keeping in view the high vapor pressure of acetone its proportion was limited to 25 volume percent

The as dispersed suspensions were found to be highly unstable. They had a strong tendency to settle but could be easily redispersed. Also, deposits obtained by EPD were observed to be thicker at the bottom. These observations indicated very low charge and zeta-potential on the particles and hence flocculation and settling. Various dispersants were tried for charging the particles.

Polyacrylic acid has previously been reported as a dispersant for ethanol based systems. However, the commercially available polyacrylic acids are mostly available as water-based solutions. Even though the dispersant is used in little quantities, it still has enough water to

give significant gas evolution at the electrodes. Hence polyacrylic acid was not used as a dispersant. Ionic dispersants such as acetic acid and n-butylamine were also tried as dispersant. The suspensions still had a tendency to settle rapidly and form soft agglomerates. Defloc Z-3 (oxidized manhadden fish oil), which is extensively used as a dispersant for tape casting systems, was also studied. The dispersions formed hard sediments on settling indicating that Defloc Z-3 does work well as a dispersant. However no deposits could be obtaied from these suspensions. It has been reported in the literature[20] that Defloc Z-3 works by steric hindrance rather than by electrostatic repulsion. Hence the Defloc Z-3 may not be imparting the necessary charge needed for EPD to the alumina particles. Since none of the dispersants seemed to work satisfactorily, the suspensions were used without any added dispersants.

Given the unstable nature of the slips the solid contents was restricted to 35 weight percent. The slips themselves were prepared by dispersing 35 wt% of alumina in mixtures of ethanol and acetone (75 vol%+25vol%). They were then ball milled for 24hrs. A magnetic stirrer was used during EPD to prevent the alumina from settling. Three mil and 10 mil platinum wires, and 15 mil nickel wires were used as substrates. Only the Pt wires were sintered. They were sintered in air at 1500°C for 2hrs. The sintered samples were studied under optical and scanning electron microscopes.

Due to lower polarity (table.4.1) of the dispersing media, very high voltages were required for deposition compared to aqueous deposition. A current of 1mA was used for deposition in most of the experiments due to system limitations. While using 2mA current the maximum possible voltage of the power supply (250V) was reached in about 20secs. Three milliamperes current could not be achieved.

The effects of current, solids contents, and particle size on the deposition rate are not dependent on the dispersing liquid. Hence they were assumed to be similar to those in the aqueous EPD. However, the effects of pH and conductivity on the deposition process were studied. Dilute solutions of acetic acid and n-butylamine in ethanol were used to vary the pH and conductivity of suspensions with 35% alumina D. Wire samples were coated at different pH values. The conductivity and the viscosity of the suspensions were also measured. The thickness and the weight of the coatings were measured and plotted against the pH and the conductivity.

Experiments on cracks:

As will be discussed in the Results section the deposits from non-aqueous suspensions did not show any drying cracks. This was a significant improvement over the aqueous EPD. However, further experiments were done to control the sintering cracks. The various experiments done are discussed in the following paragraphs.

Coatings containing mixtures of aluminas with different particle sizes, were made in an attempt to obtain higher packing densities in the coatings and consequently less shrinkage on subsequent sintering. Mixtures of slips of alumina E and D, and slips of alumina D and C were used in these experiments. Experiments were conducted beforehand to determine the deposition rates of these alumina powders. The proportions of the various alumina slips in the mixtures were adjusted to theoretically obtain a 60:40 ratio of coarse to fine particles in the final deposits, provided the rates of deposition of the particles in the mixture and single particle size slips were the same. Coatings were made on platinum wires and were sintered. The crack density of these coatings was then calculated and compared with those for single particle size particles.

Some "double coatings" were also made. A sintered coating was coated a second time to make the double coated wires. It was then sintered again. The coatings were studied using optical and electron microscopes.

Results and Discussion

In the absence of any specific dispersing agents, the charging mechanism of the alumina particles is not very clear. Although the absolute alcohol used throughout these experiments does not contain water, it does have a tendency to absorb moisture from air. It was initially thought that the absorbed water might be charging the alumina particles. However, it was seen that the conductivity of the suspensions almost linearly increased with solids content (Fig.4.2). This result suggests that the charging might be due to some other factor. It has been earlier reported[8] that alumina can be charged by ethanol in the following manner- 1) adsorption of ethanol molecules in undissociated form onto the basic surface sites,

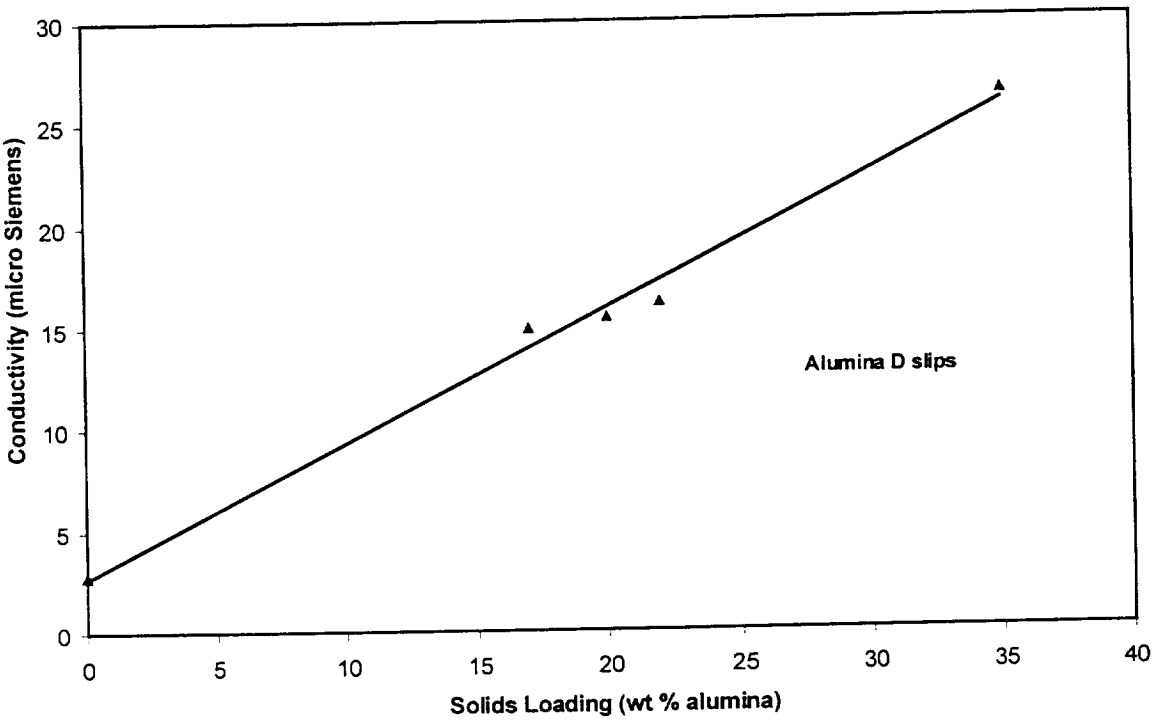

Fig.4.2. Variation of conductivity with solids contents in slips with alumina dispersed in ethanol and acetone mixtures

2) dissociation of the adsorbed ethanol molecules with $C_2H_5O^-$ ions dissolving back into the solution and the proton remaining adsorbed on the alumina surface. This mechanism will leave the alumina particles positively charged. On electrophoretically depositing, the alumina particles were deposited at the cathode, thus supporting the theory. The deposition rate generally is much higher than that of aqueous EPD. The electrophoretic mobility and the conductivity of the as dispersed slips are $25x10^{-6}cm^2/V.sec$ and 22 μs/cm respectively. Both are 2-3 orders orders of magnitude lower than those for aqueous slips. The very low electrophoretic mobility and low conductivity conditions are expected to result in the observed high deposition rates. The effect of pH and conductivity on non- aqueous EPD of alumina is provided in Fig.4.3. The viscosity data was not very reliable, as the viscosity of the slips is very small and significant changes were not noticed in viscosity with pH. Hence it is not presented here.

It should be mentioned here that the commercial instruments used for measuring pH are calibrated to a pH scale of 14, which is valid only for water. This pH, however, can be converted to a scale valid for any other media. The details for this conversion are provided elsewhere[8]. Fig.4.4 shows the correlation between pH scales in ethanol and water. This plot was used to convert the pH data obtained in these experiments. The decrease in deposition rates at higher pH values may be explained by the increase in conductivity. The increase in conductivity of the suspension decreases the voltage drop across the suspension. Since this voltage drop is the driving force for electrophoresis, a lower voltage drop reduces the driving force. Hence, the deposition rate also decreases.

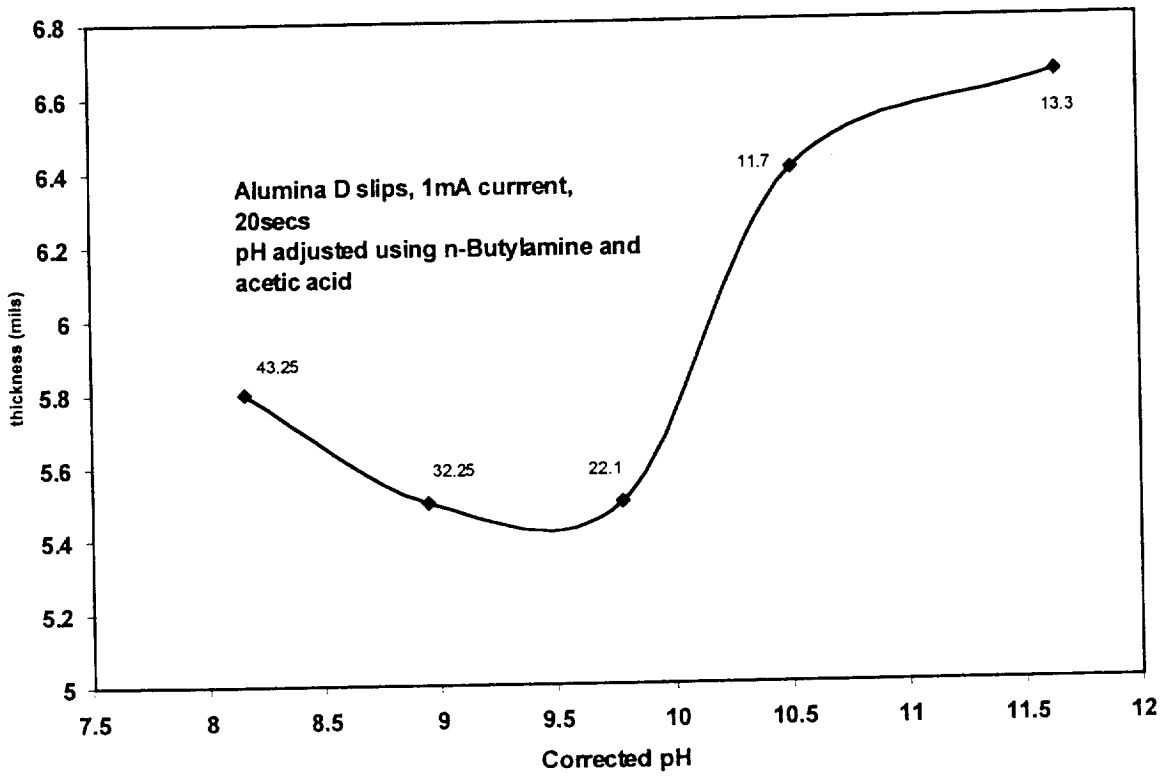

Fig.4.3. Effect of pH on deposited coating thickness in non-aqueous slips. The corresponding conductivity values are indicated on the curve. They are in $10^{-6}(ohm.cm)^{-1}$

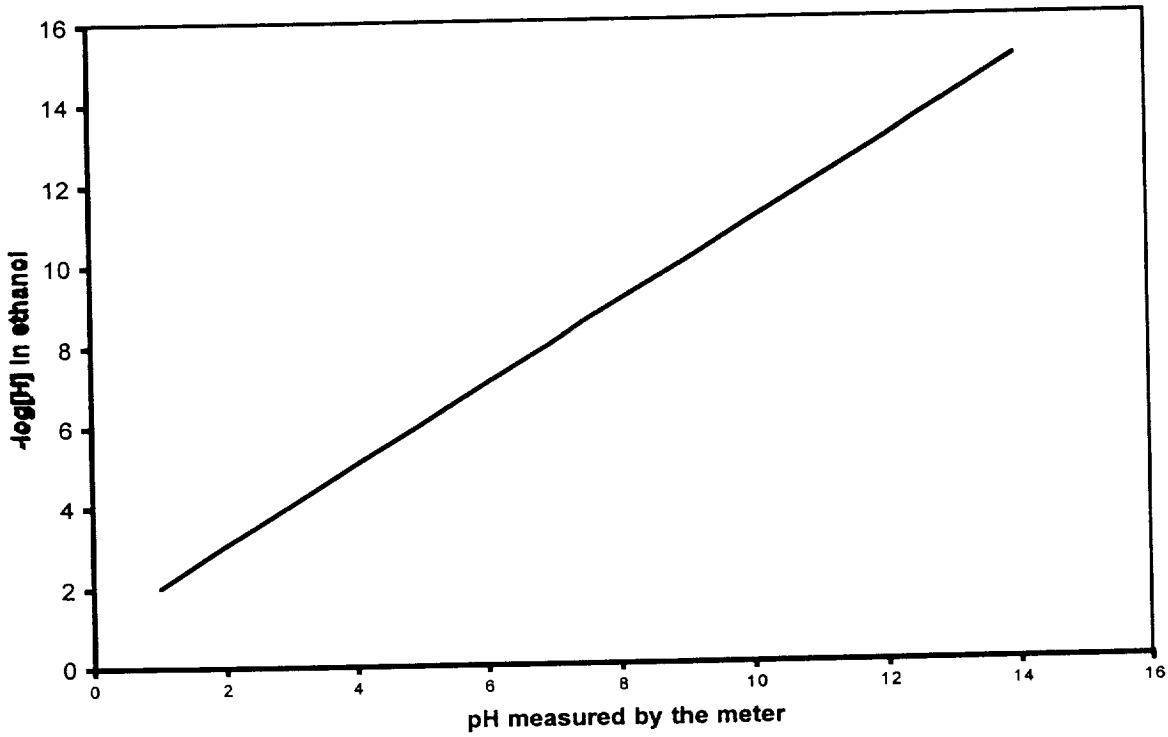

Fig.4.4. The correlation between the pH measured by a commercial instrument and the actual hydrogen ion activity in ethanol based systems[8]

As mentioned before the non-aqueous coatings did not show any drying cracks (Fig.4.5). They showed only transverse cracks on sintering. A 25-30% linear shrinkage in thickness of the coatings was measured on sintering. Most of the alumina powders have sub-micron size particle size and hence are expected to have high shrinkage. Assuming the shrinkage to be isotropic in all directions, a similar shrinkage is expected along the axis. Such shrinkage will result in transverse cracks as those observed in the samples. The crack width was measured using optical microscope. It typically ranged between 2-3 mil, which is small, compared to coated wire dimension. A cross-section of a sintered coated wire is shown in Fig.4.6. The cracks, as explained earlier, develop during the high temperature sintering process. It is also seen that the individual coating pieces have a curvature and are not bonded to the wire at the edges. Such a structure indicates a compressive force on the coating at the interface with the wire. As the coating densifies and shrinks during sintering, the coating at the interface has more constraint for shrinkage than the free suface because of the friction due to the substrate. However, the observed structure will develop only if the coating is very strongly bonded to the wire and the only way to release the stress is by "de-bonding" at the edges, and then bending. Hence, one can conclude from the structure of the coating that it strongly adheres to the wire at the time of sintering.

The rates of deposition of different particle size aluminas are provided in Table 4.2. As expected the finer alumina particles have higher deposition rates. The proportions of the different suspensions used to prepare mixed particle size suspensions are also given in the table. An interesting observation was made during these experiments. It was seen that the

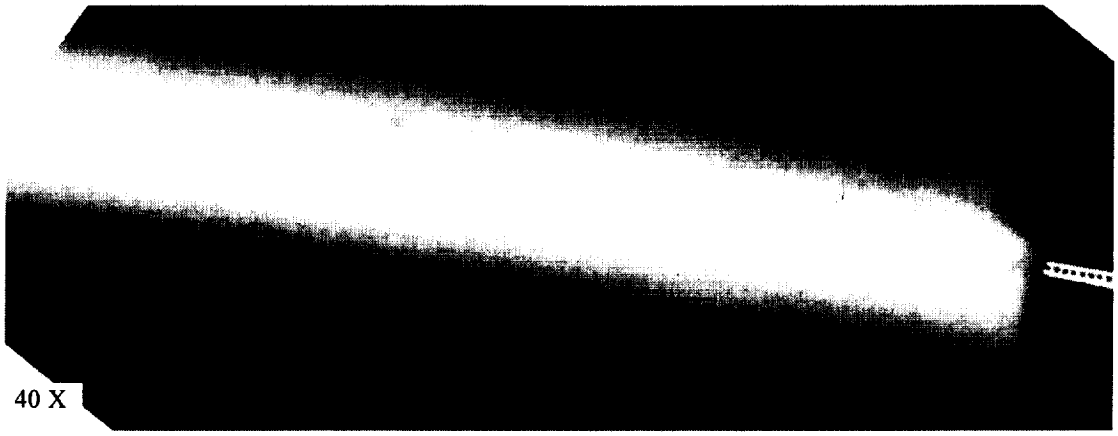

Fig.4.5. Coating prepared from non-aqueous dispersions after drying does not show any cracks. They showed only transverse cracks after sintering.

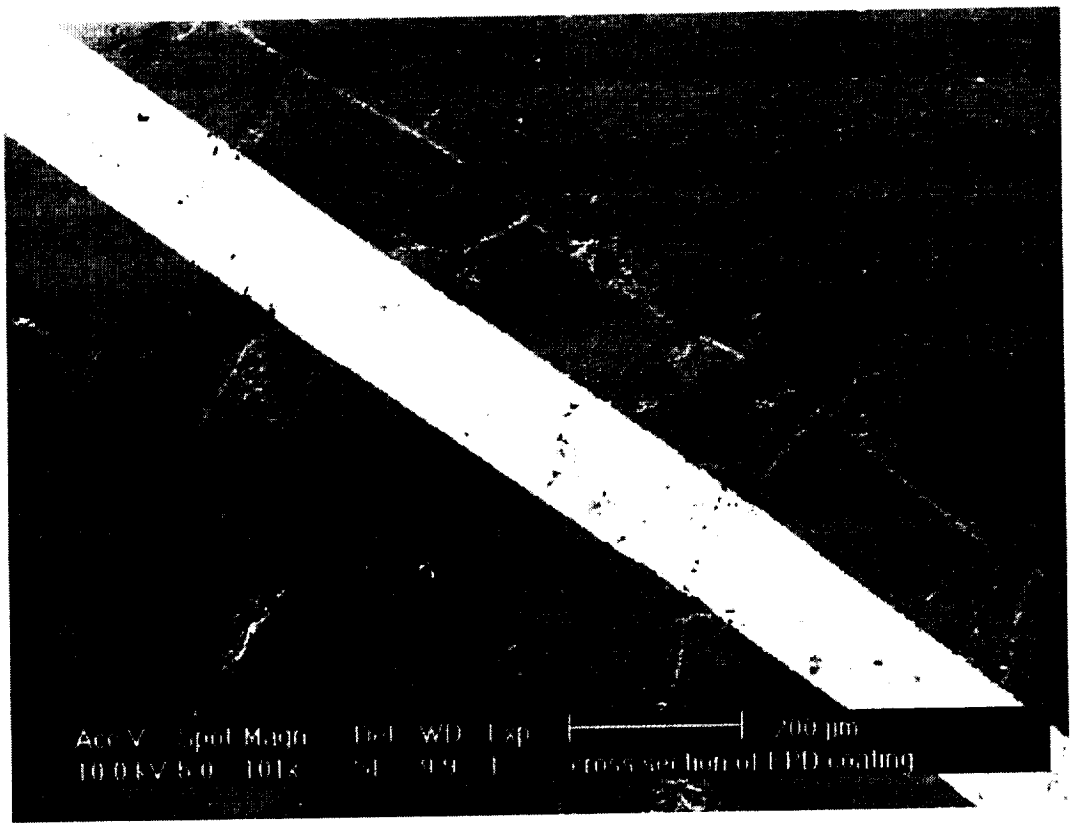

Fig.4.6. Cross section of a sintered coating made by non-aqueous EPD. The coating was made from a suspension of alumina D and was sintered at 1550°C for 2hrs and 30mins. The contamination seen in the micrograph most probably occurred during sample preparation for the scanning electron micrograph.

Alu-mina	Particle Size (microns)	Solids content (weight %)	Current (mA)	Time (secs)	Deposit weight / cm of the wire	Proportion used
D	0.36	35	1	20	3.79×10^{-3}	0.035
C	0.05	35	1	20	2.05×10^{-4}	0.965
D	0.36	20	2	5	0.78×10^{-3}	0.82
E	3.6	20	2	5	2.49×10^{-3}	0.18

Table.4.2. Details of slips used for preparation of mixed particle size coating. He experiments were done on 15mil Ni wires. The slips in rows D and C were used to prepare one slip, while those in rows D and E were used to prepare another.

coarse alumina, C (particle size: 3.6 microns), could not be deposited on 3 mil wires while it could be deposited on 10 mil wires. It is pointed out that the ratio of the wire to the particle diameter is 21:1, which may be small for the particles to be packed efficiently around the 3 mil wire.

The crack density (Fig.4.7) itself does not show significant effect of having mixed particle in the coatings. Scanning electron micrographs could not be obtained to study the packing of alumina particles in the as deposited material due to the fragile nature of the green coatings.

The scanning electron micrographs of the sintered coating are not expected to show the true ratio of particles in the deposits as larger particles grow at the expense of smaller particles during sintering and grain growth. However it has been reported earlier that at high concentrations of solid particles there is no noticeable segregation of particles of different mobilities[3]. This is presumed to be because of particle-particle interaction. Hence, the actual ratio of coarse to fine particles in the coating may be approximately equal to their ratio in the slip (96:3.5 and 82:18 for the two slips). Since the amount of fine particles in both the mixtures was much less than the optimum 60:40 ratio, close packing of particles may not have resulted.

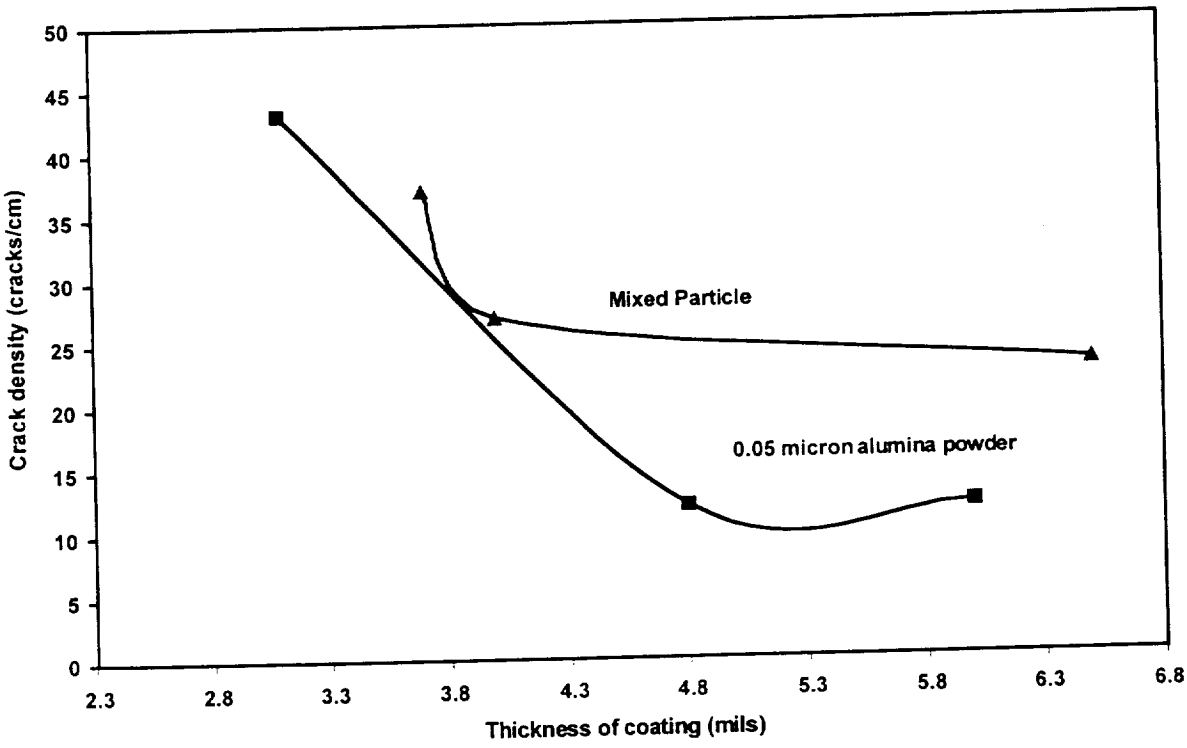

Fig.4.7. Variation of crack density with coating thickness in coatings made from mixed-size alumina slips and single particle size alumina slips. As seen from the plot, the mixed particle slips did not result in a reduction in the crack density.

Double-coated layers could be made. The fact that alumina could be deposited on top of highly insulating sintered alumina coating was attributed to the high voltages used in non-aqueous EPD. The double coatings did show some lamination between the layers (Fig.4.8). The second layer tends to cover the cracks from the first layer and thus reduce average crack width. The average width of the cracks was reduced from 2-3mil to less than 1mil after the second coating. The "covering" up of the cracks is seen in the scanning electron micrograph in Fig.4.9. The double coatings show promise for controlling the cracks, but necessitate the use of two sintering cycles.

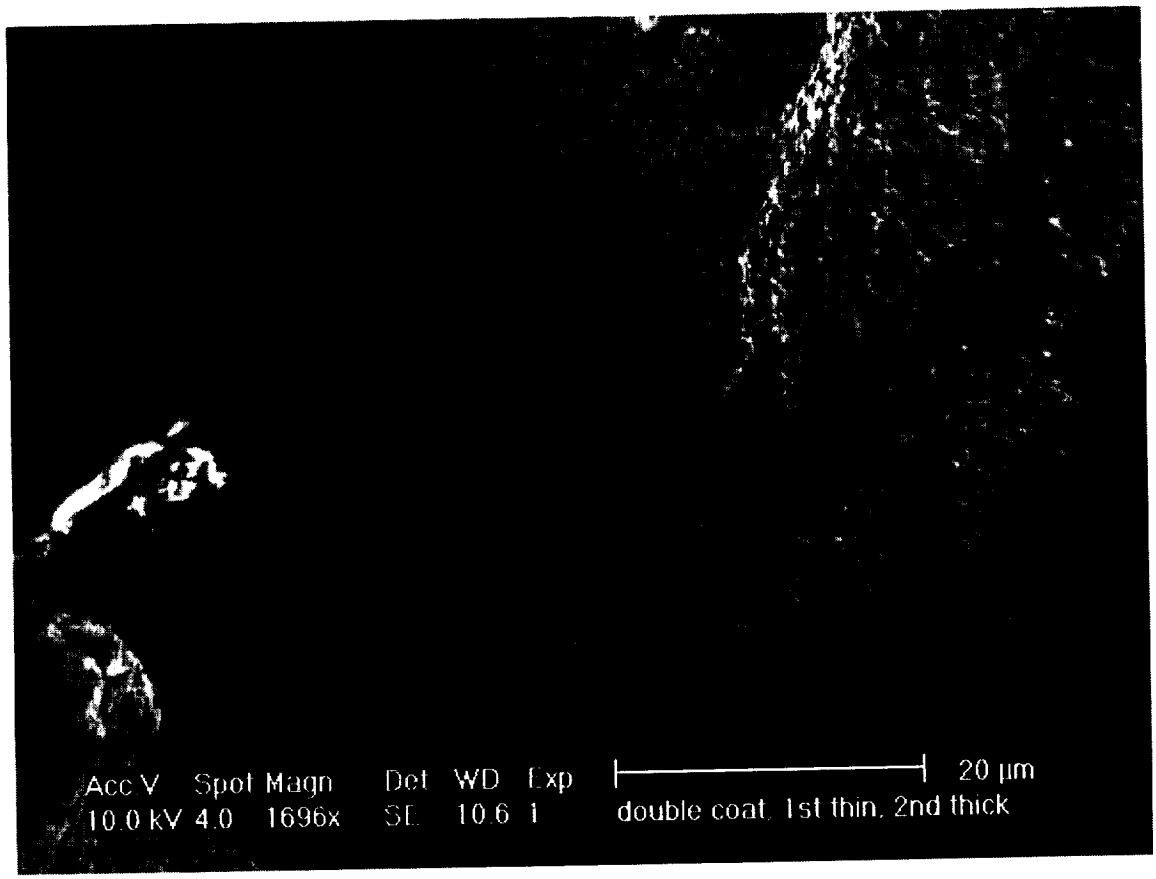

Fig.4.8. An scanning electron micrograph image of the double coated wires showing the laminations in the coatings. The coatings, however, still adhere to each other very well.

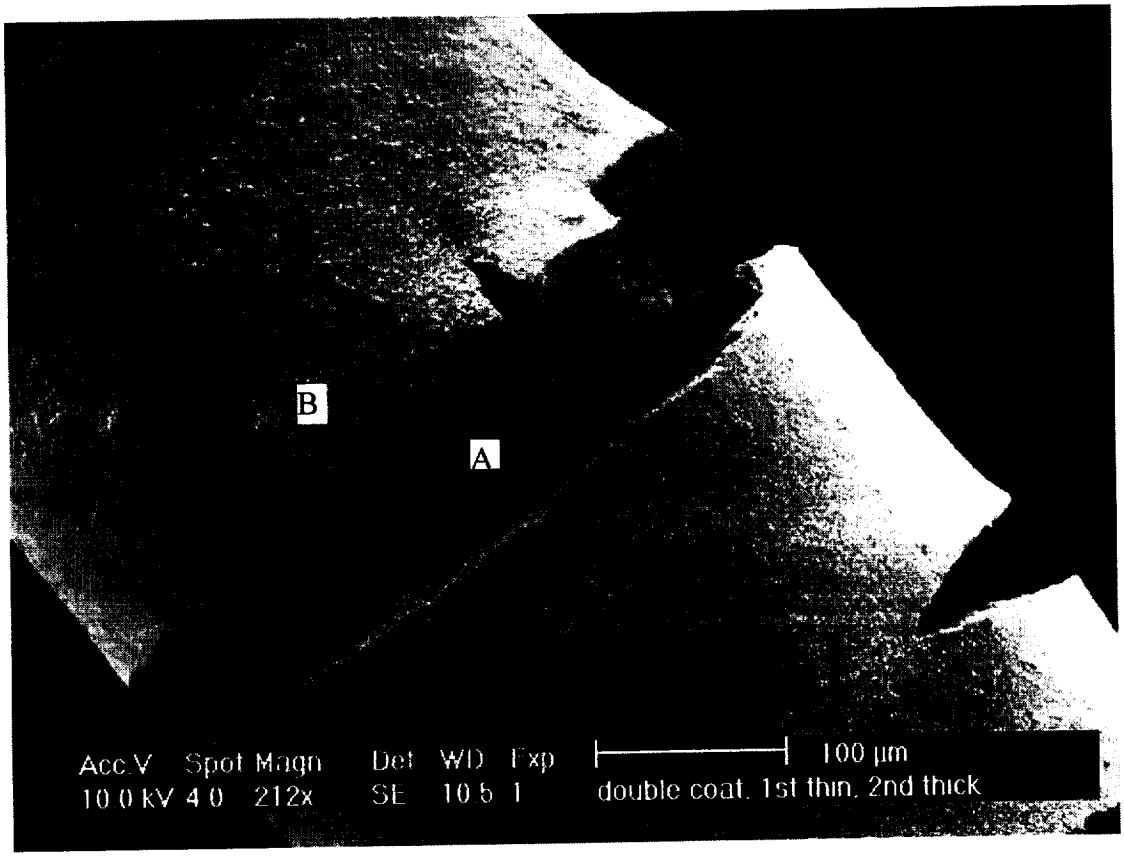

Fig.4.9. A scanning electron micrograph showing the second coating covering the crack in the first coating in a double-coated wire. "A" is the second coating filling the crack in the first coating. "B" is the second coating on top of the first coating. The thickness of the first coating is 1.7 mil, while the second coating is 2.8mil thick.

CHAPTER 5

Slurry Coating

One of the problems with EPD is the low green strength of the deposits in the absence of any organic binder. The deposits are fragile and need to be handled very carefully before they are sintered. This may cause some problems in industrial conditions. Hence another method (Slurry coating) was tried for coating the metal wires with alumina. The problems to be addressed in developing this method were to be able to make thin coatings, which would not have large cracks and which would be flexible.

Slurry coating essentially consists of passing a wire through a ceramic suspension containing a significant amount of binder. The binder, primarily, a large molecular weight organic compound forms a network around the ceramic particles and holds (binds) them together. The result is a viscous slurry. The slurry is very similar to those used in tape casting. When the substrate is drawn through the slurry, some of the slurry adheres to the substrate and forms a coating around it. The adherence is due the binder and due to the wetting of the wire by the fluid. The most important parameters controlling the quality and thickness of the coatings are the rheological behavior of the slurry and the rate of drawing the substrate through the slurry.

The best results will theoretically be obtained when the slip is thixotropic. Thixotropy is a type of non-newtonian flow, which is characterized by a time-dependent shear thinning. Shear-

thinning is the phenomena observed when a suspension is sheared. As the shear rate is increased, the apparent viscosity of the suspension greatly decreases, sometimes by several orders of magnitude. When a thixotropic suspension is sheared after standing still for a long time, the viscosity decreases with time and reaches a minimum value. The minimum value ultimately reached is itself a function of shear rate. When the shearing force is removed, the viscosity returns to its original higher value. Thixotropic behavior is most commonly seen in agglomerated (flocculated) systems. In these flocculated systems as the suspension is sheared, the agglomerates break down and viscosity decreases. The minimum is reached when a balance is established between the rate of structural breakdown and the rate of structure reformation. Finally, on removing the shear force, the system is restored to its original structure and hence its viscosity increases again. A similar effect (shear thinning) is often observed in solutions of high polymers such as organic binders. In this case intermolecular attractions are overcome by shearing and lead to a decrease in viscosity. Upon removal the shear or reduction of original rate, the original conditions are restored by brownian motion and the viscosity recovers to a higher value.

A low viscosity is necessary for obtaining thin coatings. When a wire is being drawn though a thixotropic suspension, the suspension is sheared and its viscosity decreases. This results in thin coatings. Once the coated wire is out of the suspension, the shearing stops and the coated suspensions becomes "thick" (i.e. it regains its high viscosity) again due to thixotropy. This thickening is required to ensure minimal flow of the suspension once the wire is coated. As can be seen, thixotropic behavior for the slurry is very suitable for the present coating method, which in turn implies that the slurry should be flocculated. However if the suspension is too highly flocculated it tends to be of gel like consistency. Such slurries do not flow smoothly, are difficult to handle and also result in non-uniform coatings. They are also difficult to handle.

Hence, an optimal dispersion condition must be established in the slurry if useful coatings are to be made from it. The dispersion is primarily determined by the solvent/solid particle/deflocculent system. The sate of dispersion is determined by the solids loading, binder content, and the presence of dispersants or surface active agents in the slurry

As mentioned, the viscosity of the slurry is related to the thickness of the coatings. A higher viscosity results in thicker coatings. At the same time, slurries with very low viscosity result in a "bead-structure" for the coating. The beads are formed because of the Rayleigh-Plateau's instability criteria[20,21] and their formation is driven by surface tension. For equal volume, the spheres have a lesser surface area than a cylinder. According to the theory, a liquid tends to break up into beads from a cylindrical flow to minimize its surface energy. However, in the case of slurries with already high viscosity, as the viscosity further increases on drying, the coating becomes rigid before the coating can break into beads. However, if the initial viscosity of the coating is too low, it can break up into beads before becoming rigid. Hence the viscosity of the slurries should not be too low. As mentioned earlier, the binder content and the dispersion of the solid particles primarily govern the viscosity. The volume fraction of solids in the slurry also influences its viscosity.

The rate of drawing affects the coating thickness indirectly through its effect on the viscosity of the coated slurry. As the coated wire is drawn out of the slurry, the viscosity of the coating changes due to the removal of the shear force but also due to solvent evaporation. The viscosity of the suspension is related to the volume fraction of the solid particles according to the relation given by Einstein[22]:

$\eta = \eta_0(1+2.5\Phi)$,

where, η is the viscosity of the suspension

η_0 is the viscosity of the pure solvent or dispersing liquid

and Φ is the volume fraction of the solids

As the wire is drawn out of the slurry, solvent evaporates from the layer of slurry adhering to it. Thus from Einstein's equation it can be seen that the volume fraction of the solids increases and that the viscosity must also increase. As solvent evaporates, the binder solution becomes more concentrated and this also results in an increase in viscosity. As the rate at which wire is drawn through the slurry increases, a thicker layer of suspension is withdrawn along with the wire. The thickness of this layer, for any given viscosity of the slurry, is governed by the drawing rate because the drawing rate determines how much time is available for the slurry to flow off the wire and back into the coating bath. At high drawing speeds, the velocity of a coated element of wire away from the surface of the bath is greater than the velocity at which the coating flows back towards the bath. The latter velocity has a maximum value determined by the magnitude of the gravity driven shear force within the coating and the coating viscosity. Any coating which has too little time to flow back to the bath (i.e. coating whose net viscosity is away from the bath) remains on the wire. Whether this coating will be in the form of a smooth cylinder or a string of beads depends upon the rate at which the viscosity of the coating increases after withdrawal from the slurry. If the viscosity increase is very rapid, due either to solvent evaporation or the thixotropic effect, the coating will become rigid before Rayleigh-Plateau instability causes it to bead up, and the final coating will a smooth cylinder having constant diameter along the length of the wire.

Experimental Procedures

The important objectives for the experimental part of slurry coating were to build a machine capable of uniformly and reproducibly coating the wires and to find a good slurry system.

The coater:

A machine capable of continuous operation was built for slurry coating. The schematic of the machine is shown in Fig.5.1. At the top of the machine is a variable speed motor "M" that controls the drawing speed of the wire. Spool "A" has the wire to be coated. The wire after passing through the ultrasonic bath "B" (containing acetone) and passing over Pulley "C" enters a stainless steel u-tube. The u-tube is located inside the glass jar "D" containing the slurry. The wire comes out of an orifice at the other end of the tube and is coated by the slurry. The wire then passes between infra-red lamps "E", which are used to dry the coating. Finally, the dry coated wire is taken up by spool "F", attached to the variable speed motor "M". The motor is capable of wire drawing speeds of less than 1cm/sec to more than 10cm/sec. As mentioned before the speed of drawing the wire through the slurry is a key factor in controlling the thickness and quality of the coatings.

The slurry:

The slurry system was based on a tape casting formulation, reported elsewhere[21]. Two different molecular weight binders were tried. Their specifications are provided in AppendixB. Various aluminas, whose specifications are provided in Table 3.1 were used. Defloc Z-3 was used as a

deflocculant. It was noticed that the slurry had a gel like consistency and high viscosity, which resulted in very thick coatings. Hence the composition was varied, to find a slurry which gave the best results. This was however done qualitatively by observing the consistency and flow property of the slurry. Different milling cycles were also tried to determine the effect of milling on the dispersion. The amount of solvent was varied to obtain a suitable viscosity.

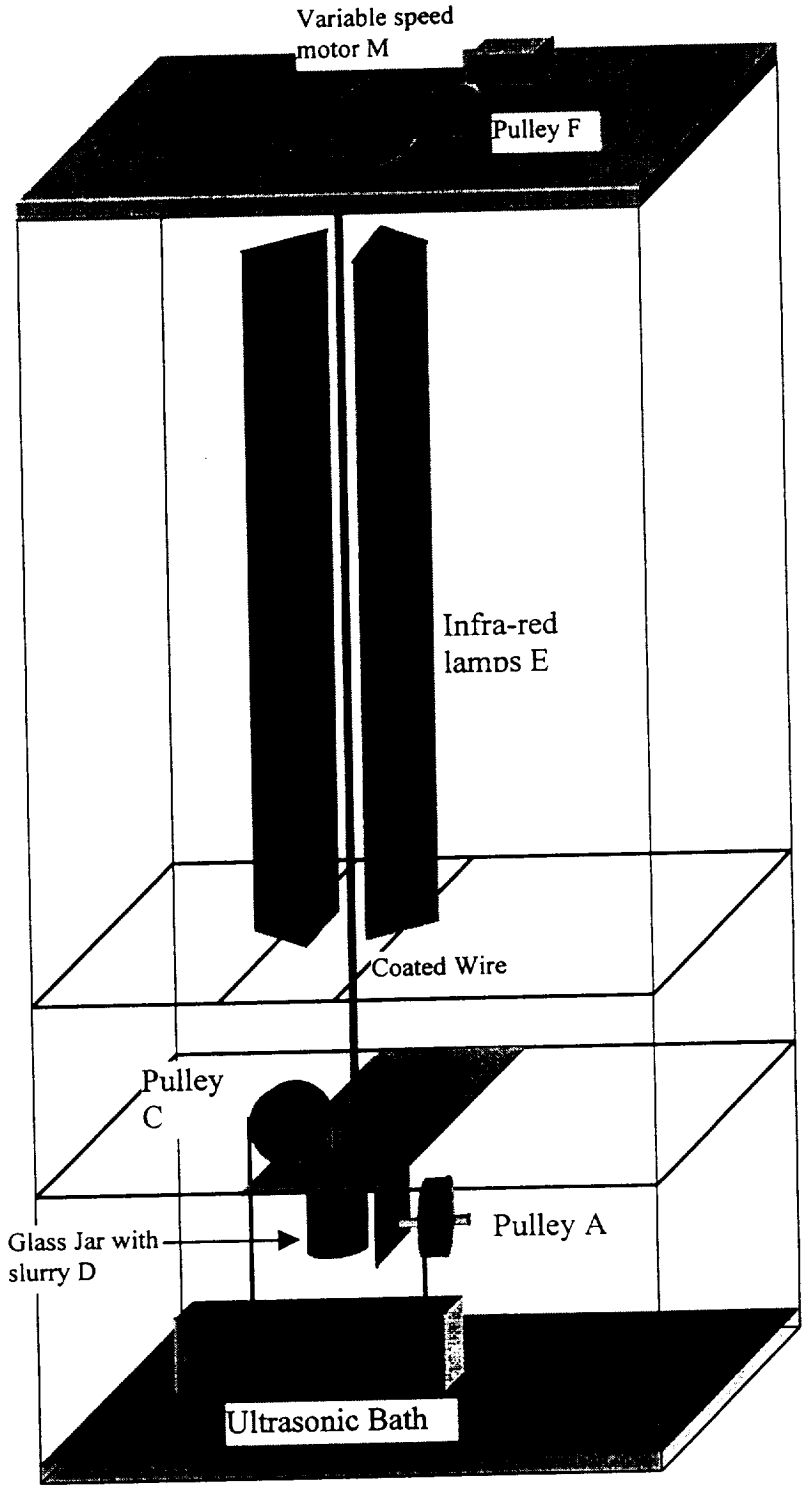

Fig.5.1. A schematic of the slurry coater that was built as a part of the project

The coatings:

Coatings were made on 5.6mil platinum wires. Various speeds were tried and optimal speed was found. Several meters of wire were coated. The coatings were then sintered.

The coatings contain significant amounts of organic compounds, especially the binder. These materials burn out during sintering. If the organic materials do not burn out completely at lower temperatures, they may escape from the coatings at higher temperatures by bursting through the coatings. This typically cracks the coatings or causes them to spall of the wire. Thermogravimetric analysis of dried slurry was done to determine the burn out temperature of the binder. The results are provided in fig.5.2. As can be seen the binder burns out completely by 500°C. To provide adequate time for binder burnout, coatings were heated at the rate of 2°C/min till 500°C. The heating rate was then increased to 10°C and the samples were heated to 1550°C, at which temperature they were sintered for 150min. The coatings were then studied using optical and electron microscopes.

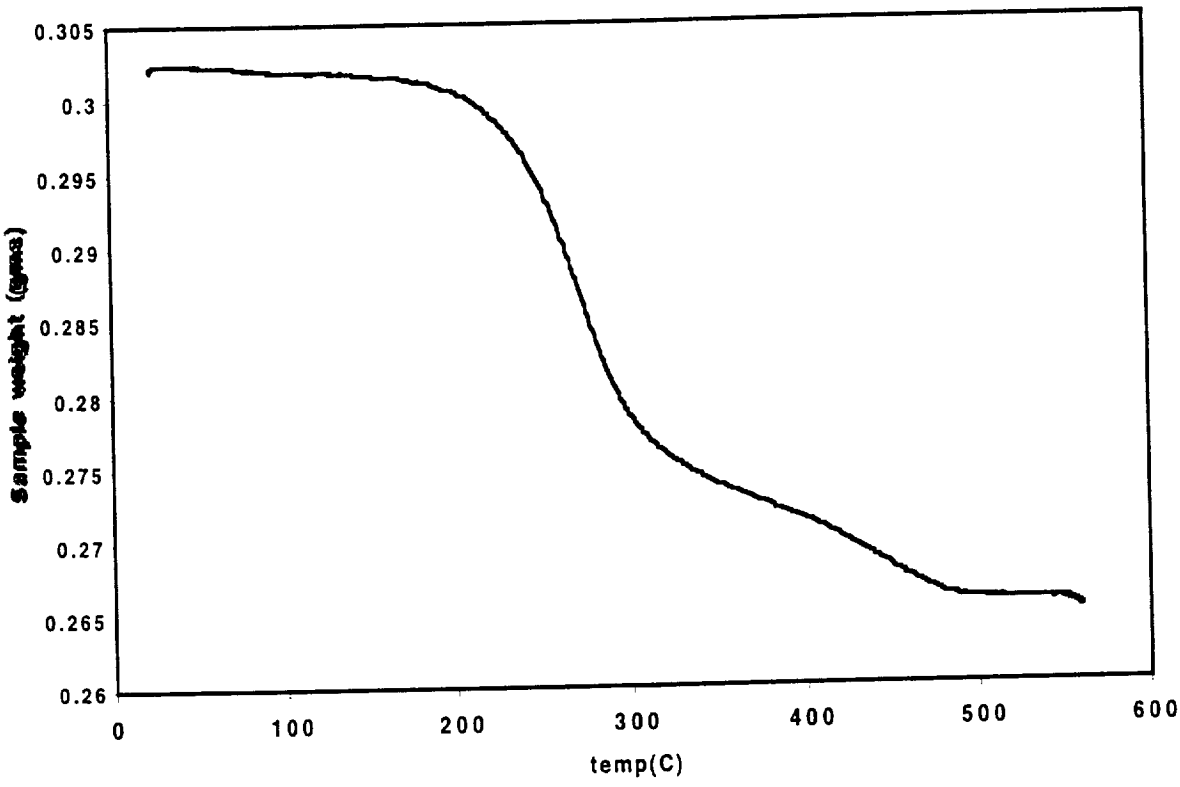

Fig.5.2. The burn-out characteristics of Butvar B-79 binder as determined by TGA analysis in air.

Results

The Initial experiments were done using Butvar B-76 binder. It however resulted in highly viscous slurries that gave very thick coatings. Further the cross section of the coatings was not cylindrical but shaped like the figure "8". The binder formed a "skin "around the coating. The skin collapsed as the solvent evaporated, resulting in the odd cross-section. To counter the skin formation and high viscosity problems a lower molecular weight binder than B-76, Butvar B-79 was tried. An "anti-skinning" agent Cyclo-hexanone was also added to the composition. As expected, the B-79 binder resulted in a slurry of lower viscosity and also gave coatings of lesser thickness. However, the slurry still was highly flocculated and had a viscosity of more than 100,000cps. Hence, The milling cycle was also altered. The milling was done in two stages, 25% of the binder was added to the formulation during the first milling stage. It was thought that the binder was affecting proper milling and adsorption of the deflocculant on to the alumina surface. Hence, the alumina along with the deflocculent and the other constituents, except the binder, was milled first. Then the binder was added and the slurry was milled again. Finally, by adjusting the solvent and deflocculent content, a well dispersed and free flowing slurry was obtained. The final composition that was developed is given in Table 5.1. Appendix C provides a comparison of the various compositions that were tried out. As seen in Table 5.2, it shows thixotropic behavior. The coatings were observed to be too thick above a linear speed of 1cm/sec. Thick coatings have problems with binder burnout and are not very flexible. Speeds below 0.5 cm/sec resulted in the "string of beads" coating structure. A speed of 0.5cm/sec was found to give the best results.

1st milling:

Alumina F:	100gms
Toluene (solvent):	18ml
Methyl Ethyl Ketone (solvent):	18ml
Defloc Z-3 (dispersant):	3gms
Sancticizer (Plasticizer):	4.3gms
Ball milled for:	8hrs

2nd milling

Butvar B-79 (binder):	5gms
MEK:	20ml
Toluene:	20ml
Ball milled for:	24 hrs

Table.5.1. Final composition of the slurry used for coating

Shear Rate (Rpm)	% Torque	Viscosity (cps)
6	99	15180
5	94.3	19660
4	85.3	21880
3	73.5	24830
2	54.7	27350
1.5	49.2	32800

Table 5.2. Viscosity data for the final slip. The measurements were made using a Brookfield DV-E viscometer. A no.3 RV spindle was used for making the measurements.

The coatings made, using the slip mentioned in Table 5.1, at 0.5 cm/sec typically were less than 1 mil thick. As can be seen in Fig.5.3 the sintered coatings contains very few cracks. A high magnification scanning electron micrograph of the slurry coated sample (Fig.5.4) indicates that the coating is well sintered and highly densified. Fig.5.5 shows a bent coated wire. It is seen that although the coating cracks when bent, relatively little of it falls off the wire.

As the sintered sample is cooling down, the Pt wire (thermal expansion co-eff.: $9.1X10^{-6}\,°C^{-1}$) has a tendency to shrink more than the alumina coating (thermal expansion co-eff.: $5.6X10^{-6}\,°C^{-1}$). This thermal expansion mismatch leads to compressive forces in the coating.

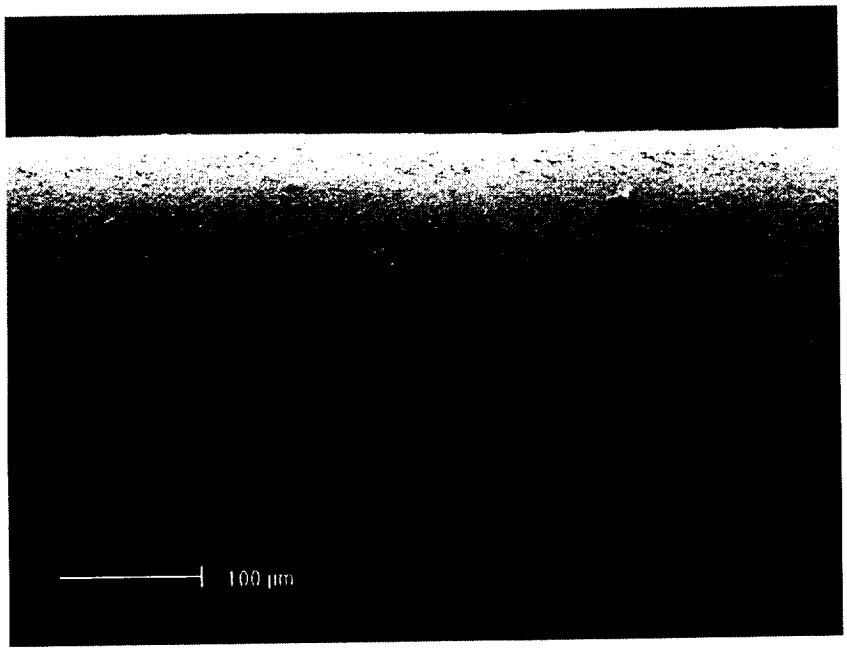

Fig.5.3. Scanning electron micrograph of a sintered slurry coated wire showing a smooth crack free surface.

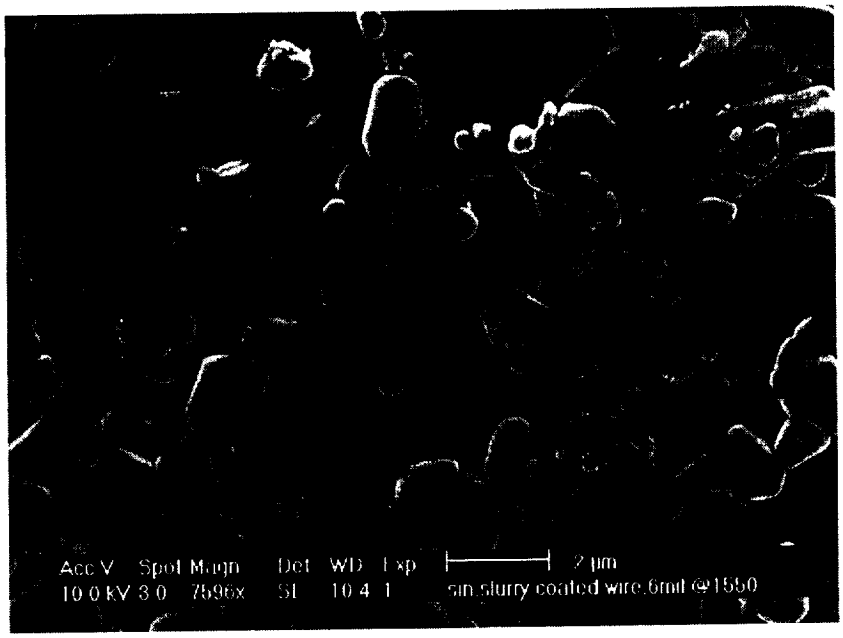

Fig.5.4. High magnification scanning electron micrograph of a sintered slurry coated sample shows that the alumina coatings are well sintered.

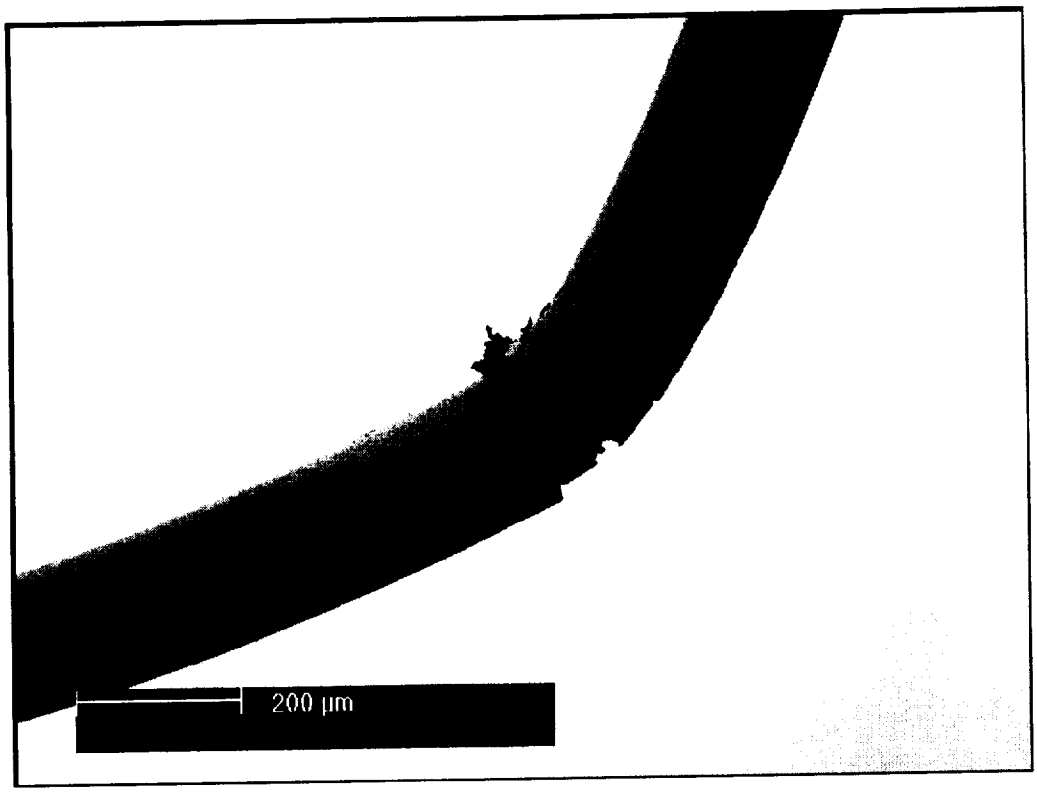

Fig.5.5. Scanning electron micrograph of a slurry coated sample showing that only a small portion of the coating falls off even at sharp bends.

CHAPTER 6

Resistivity Measurements

Since the final application of the coatings is for insulation purposes the resistivity of the coatings is one of the most important properties. Although alumina by nature will be expected to have high resistivity, the exact values of the resistivity will be crucial in determining the exact thickness of the coating required for adequate insulation. The higher the resistivity, the thinner the coating required, which in turn means more flexible wire.

The resistivity values were obtained by first measuring the resistance values of a sample at various temperatures. The details of converting resistance values to resistivity values will be discussed after discussing the methodology for measuring the resistance.

Resistance Measurements

EPD samples:

The cracks and the size of the coatings posed a unique problem for measuring the resistivity. The conventional method of applying metal electrodes could not be used. These electrodes are applied in the form of a paste and have to be cured at a high temperature. However, they flowed into the cracks on heating and caused a short circuit. Several approaches were tried and the following was found most suitable.

Fig.6.1 shows the configuration used for the resistivity measurement. A coating was made on a U-shaped wire sample with enough wire left at the top to take out the leads. The samples were sintered in the same way as the other samples. Then the bottom of the coatings was cut, resulting in two metal wires separated by the ceramic coating. However, there were numerous problems in making samples even in this configuration. The samples had a tendency to crack longitudinally (along the length) halfway between the two wires. Some samples also developed cracks when the bottom was being cut. The resistance of these samples was then measured 950-1050°C in a Keithley Electrometer, Model 6517. The sample was heated in a furnace and maintained for 30mins at a particular temperature for temperature stabilization. Then the resistance value was read from the electrometer. The value was not stable. The most frequent reading was noted.

Slurry coated samples:

The resistivity measurements of slurry coated samples were done in a more conventional configuration as shown in Fig.6.2. This was possible due to absence of cracks in the coatings. The resistance of the samples was measured using a Hewlett Packard Mutimeter. The thickness of the coating and the length of the coating covered with platinum paste were measured using a graduated microscope and digital calipers. The sample was heated in a furnace. For making a measurement, it was held at a particular temperature for 20-30 mins for the temperature to stabilize. The measurements were

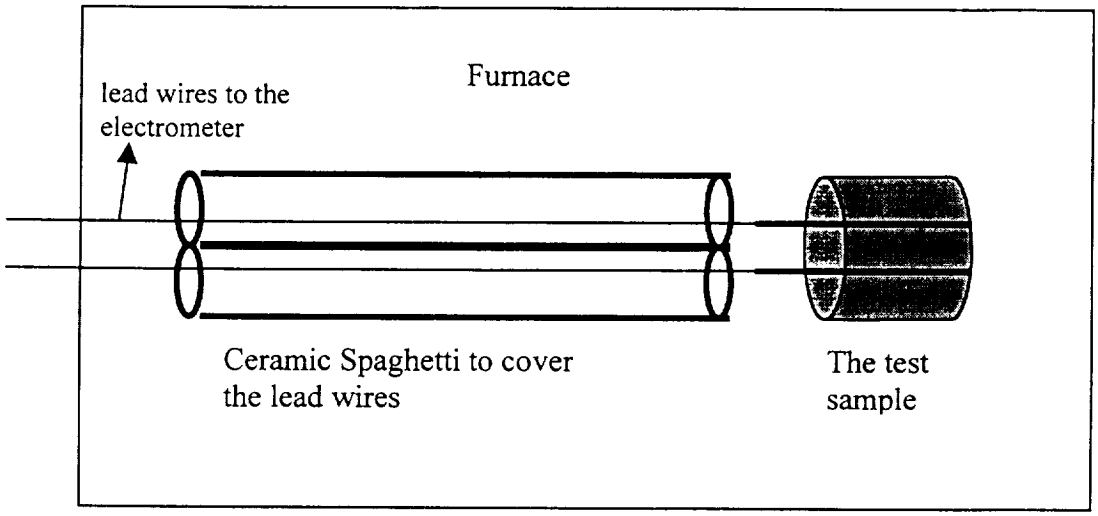

Fig.6.1. The configuration used for making resistivity measurements of the samples made by EPD.

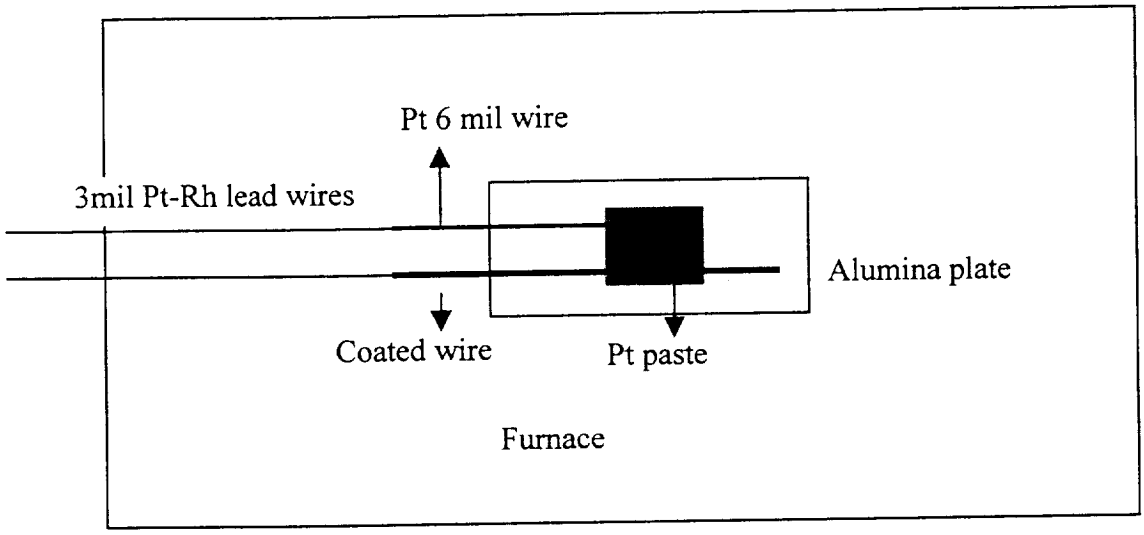

Fig6.2. The configuration used for measuring the resistivity of the slurry coated samples

recorded by on a computer. Readings were taken every two seconds and approximately 200 readings were taken at each temperature. Then the average and standard deviation of the readings were found for each temperature.

Results and conversion to resistivity

EPD Samples:

Due to the problems mentioned in the experimental section, only one sample could be satisfactorily prepared. The measured resistance values at various temperatures are given in Table 6.1. The resistivity of the samples was calculated by assuming the resistance to be primarily due to the material between the wires. This assumption should be valid for a highly resistive material like alumina and for the small voltages used for the resistance measurements as the electric field will not extend far from the wire. The resistivity was then determined by using the following formula:

$\rho = RDh/L$

Where, R is the measured resistance

D, the diameter of the wire

h, the length of the coating

and L, the distance between the two wires

Slurry coated samples:

The resistance values at various temperatures are shown in Table 6.2. The resistance was converted to resistivity by measuring the length of the coating under the electrode. It was calculated using the following formula:

Resistivity, $\rho = RA/r$

Where R is the measured resistance and,

A, the area for the current flow, was taken as the average of the area at the wire surface and the area at the coating surface. Hence

$A= 2\pi[r_0+(r/2)]h$,

Where, r_0 is the radius of the wire,

r, the thickness of the coating

and h, the length of the coating covered by the electrodes

The final calculated resistivity values for both kinds of sample are given in Table.6.3. It can be seen that samples coated by both the methods have very high resistivity at high temperatures and should satisfy the requirements for the application in advanced turbine engines.

Temperature (°C)	Resistance(10^6 ohms)
1050	10
1000	17.5
950	48.1
900	222

D = .254mm, h = 6.84mm, and L = 0.55mm

Table.6.1: measured resistance values at various temperature for the EPD coated sample

Temperature (°C)	Resistance* (10^6 ohms)	Standard Deviation (10^6 ohms)
1050	0.66	0.28
1000	1.09	0.39
950	1.23	0.41
900	4.14	1.30
850	5.60	1.40
800	9.60	2.00

* Average of 200 readings

the radius of the wire, r_0 = .071mm

the thickness of the coating, r = .022mm

the length of the coating covered by the electrodes, h = 1.5 cm

Table.6.2: Measured resistance values for slurry coated samples

Temperature (°C)	Resistivity (10^6 Ω-cm) of EPD samples	Resistivity (10^6 Ω-cm) of slurry coated samples
1050	3.16	22.8
1000	5.53	37.9
950	15.3	42.6
900	70.1	143
850		194
800		332

Table 6.3. Resistivity of the coatings made by EPD and slurry coating at various temperatures

CHAPTER 7

Conclusions and Summary

EPD and slurry coating have been studied for applying alumina coatings on metal wire substrates. Experiments were done to study the deposition conditions and adherence of the coatings to the wires.

Studies on the effect of deposition current, solids content and particle size on EPD from aqueous alumina slips indicated the highest rates of deposition correspond to 3mA current, 40 weight percent solids content and 0.23 micron particle size. The deposition rate was found to increase substantially beyond 1mA deposition current. However, as the current increases the dissociation of water at the electrodes also increases. The dissociation of water leads to gas evolution at the electrodes, which is released through the coatings and forms large pores in the coatings. Hence a current of 1mA was found to be more suitable. The coating thickness increases linearly with the time of deposition. The effect of pH and conductivity were also studied. Since it is difficult to vary them individually, their effects were studied together. Since the pH primarily influences the zeta-potential and hence the electrophoretic mobility, the variation of electrophoretic mobility with pH was also studied. The conductivity has an indirect effect on the deposition rate due to its relation with the electric force acting on the

particles. Electrophoretic mobility of 8.16 $X10^{-3}$ m/V.s and low conductivity of 16280 $10^{-6}(\Omega.cm)^{-1}$ were found to give the maximum deposition rate.

The adhesion of the coatings was found to increase with the sintering temperature. Although coating weight loss on coiling was observed only for samples sintered at 1100°C and not in samples sintered above this temperature, the adherence is expected to increase with sintering temperature due to the increased interdiffusion at the interface. Hence a sintering temperature above 1500°C or higher is recommended. Thinner coatings were found to adhere better and adherence was better in thinner wires. The larger crack densities observed in thin coatings, and in coatings made on thinner wires explained these results.

The effect of the wire substrate on crack density is primarily dependent on it surface roughness. The crack density increases with the roughness of the wire. Heating in air and vacuum at high temperatures had varying effects on different wires. They usually increased the roughness and hence the crack density. The maximum effect was seen in chromel-p wires, while the least effect was seen in platinum wires. Also, since the roughness resulting from the heat treatment is irregular, the cracking pattern is also expected to be irregular. Hence, an untreated wire is preferred as a substrate.

Non-aqueous EPD offers a better alternative. The rate of deposition is much higher compared to that of aqueous EPD. The more important advantage, though, is that the coatings made by non-aqueous EPD do not show any drying cracks. On sintering, they show uniform transverse cracks, which aid flexibility of the coatings. Coatings of mixed particle sizes did not show any significant effect on crack density or crack width. This may be due to the proportion of fine to

coarse particles in the coatings. Double coatings show some promise in reducing the crack width. The second coating adheres well to the first coating and tends to cover the cracks in the first coating. The average crack width reduced from 2-3 mil for single coating samples to less than one mil in the double-coated samples. However they require two sintering cycles.

A machine was built to continuously coat wires by slurry coating. Since they contain a polymeric binder, the green slurry coatings are much less fragile than those made by EPD. The green slurry coatings could be spooled without damage. Hence the sintering can be done independently of the coating and drying. In case of EPD samples great care has to be taken if the samples are not sintered immediately after drying. Hence slurry coating offers an advantage from a commercial point of view.

A slurry composition was developed (Table.5.4) to avoid skin formation on the coatings and to control the thickness of the coatings. Lower molecular weight binder worked better for countering the skin formation. About one mil thick coatings gave the best results. They were flexible and did not have any cracks in them. The coating was found to adhere to the wire even when it was bent sharply. The quality of the coatings and their thickness was also found to depend on the rate of drawing the wire through the slurry. A linear speed of 0.5cm/sec gave the best results. It gave thin coatings and did not result in a "bead structure".

Finally, the resistivity of the coatings made by, both EPD and slurry coating, is very high even at 1050°C. The resistance of even the thinner slurry coatings is of the order of a mega ohm at 1050°C. Such a high resistance should suffice for the applications these coatings are intended for.

To summarize, the suitable parameters for coating metal wires by EPD have been identified. The various parameters affecting the adherence and crack density of the coatings have been qualitatively examined. Non-aqueous EPD offers a better alternative for controlling the cracks. Slurry coating has advantages due to the better green strength of the coatings. Also, thin coatings, which do not have cracks, can be made with good thickness control. The various parameters affecting the slurry coating process have also been studied and useful coating conditions have been found.

LIST OF REFERENCES

1. Kreidler, E.R - "Research on high temperature insulation for electrical conductors"- Proposal submitted to NASA Lewis, , Sep. 1997

2. CRC Materials Science and Engineering Handbook, Ed.- Shackelford, J.C et.al, 2nd ed., CRC Press Inc., 1994

3. Gani, M.S.J -"Electrophoretic deposition- A review"; Industrial Ceramics, 14[4], 162-174 (1994)

4. Ferrari, B., et.al -"Electrophoretic forming of Al_2O_3/Y-TZP layered ceramics from aqueous suspensions" Mats. Res. Bull., 33[3], 487-499 (1998)

5. Narisawa, T, et.al -"Formation of alumina insulation films for a CRT heater by constant current elctrophoretic deposition method"; J. Ceram. Soc. Japan, 103[1], 54-58 (1995)

6. Woolf, L.D, et.al - "Continuous fabrication of high-temperature superconductor coated metal fiber and multifilamentary wire"; Appl. Phys. Lett. 58[5] 534-536 (1996)

7. Hunter, R.J - "Zeta-Potential in colloid science-Principles and Applications"; Colloid Science Series, Academic press (1981)

8. Sarkar, P., Nicholson, P.S. - "Electrophoretic Deposition(EPD): Mechanisms, Kinetics, and Applications to Ceramics"; J.Am.Ceram.Soc, 79[8], 1987-2002 (1996)

9. Hamaker, H.C, Verwey, E.J.W -"The role of the forces between the particles in the electrodeposition and other phenomena"; Trans. Faraday Soc., 180-185 (1940)

10. Hamaker, H.C- "Formation of deposit by electrophoresis"; Trans. Faraday Soc., 279-287 (1940)

11. Weise, G.R., Healy, T.W.; J.Colloid and Interface Sc., 51, 427 (1975)

12. Olivier, J.P. and Senett, P.- "Electrokinetic effects in kaolin-water systems I - Measurement of electrophoretic mobility"- Clay and Clay Minerals, 15, 345-46 (1996)

13. Binary alloy phase diagrams; ed.- Massalski, T.B et.al, ASM, (1986)

14. Nsongo, T. and Gillet, M. -" Adhesion characteization of titanium and titanium nitride thin coatings on metals using stratch test"; Int. J. Adhesion and Adhesives, 15, 191-196 (1995)

15. Attar, F. and Johannesson, T.-" Adhesion evaluation of ceramic coatings in tool steel using the scratch testing technique"; Surf. Coatings.Tech., 78, 87-102 (1996)

16. Dimitrova, V.I -" Influence of ion-implantation of the properties of coatings deposited by electro-arc evaporation on to steel"; Vacuum, 49[3], 199-204 (1998)

17. Chiu, R.C et.al- " Drying of granular ceramic films: I, Effect of processing variables on cracking behavior"; J.Am.Ceram.Soc, 76[9], 2257-2264 (1993)

18. Chiu, R.C et.al- " Drying of granular ceramic films: II, Drying stress and saturation unniformity"; J.Am.Ceram.Soc, 76[11], 2769-2277 (1993)

19. CRC handbook of Chemistry and Physics 1995-96, Ed.- Lide, D.R, 76th ed., CRC Press Inc., 1995

20. Paik, U. et.al-" The effect of electrostatic repulsive forces on the stability of Ba_2TiO_3 particles suspended in non-aqueous media"; Colloids and Surfaces A, 135, 77-87 (1998)

21. Faber, T.E- " Fluid dynamics for the physicists"; Cambridge University Press, 295, (1995)

22. Shaw Duncan J - "Introduction to colloid and surface chamistry"; Butterworth-Heinemann, (1992)

23. Ferrari, B., Moreno, R. -"The conductivity of aqueous Al_2O_3 slips for electrophoretic deposition"; Materials Letters, 28, 353-355 (1996)

24. Choudhary, R.Y, et.al- "Electrophoretic deposition of alumina from aqueous suspensions"; Trans. J. Br. Ceram. Soc., 81, 189-193 (1982)

25. Sarkar, P., Nicholson, P.S., - "Mechanisms and Kinetics of Electrophoretic Deposition" in Science, technology, and commercialization of powder synthesis and shape forming processes / edited by J.J. Kingsley, Christopher H. Schilling, James H. Adair, Ceramic transaction, V.62, 271-279 (1995)

APPENDIX A

Details of the instrument built for measuring zeta-potential

Schematic of the equipment:

A: The main chamber of the instrument. It is made of delrin

B: The test chamber, also made of delrin.

C: Delrin cap with a pin hole to cover the front of the test chamber

D: A tantalum sheet used as a part of the electrode, used for corrosion resistance

E: An alumina cap used as a lid to prevent the liquid from flowing out when the steel caps are removed

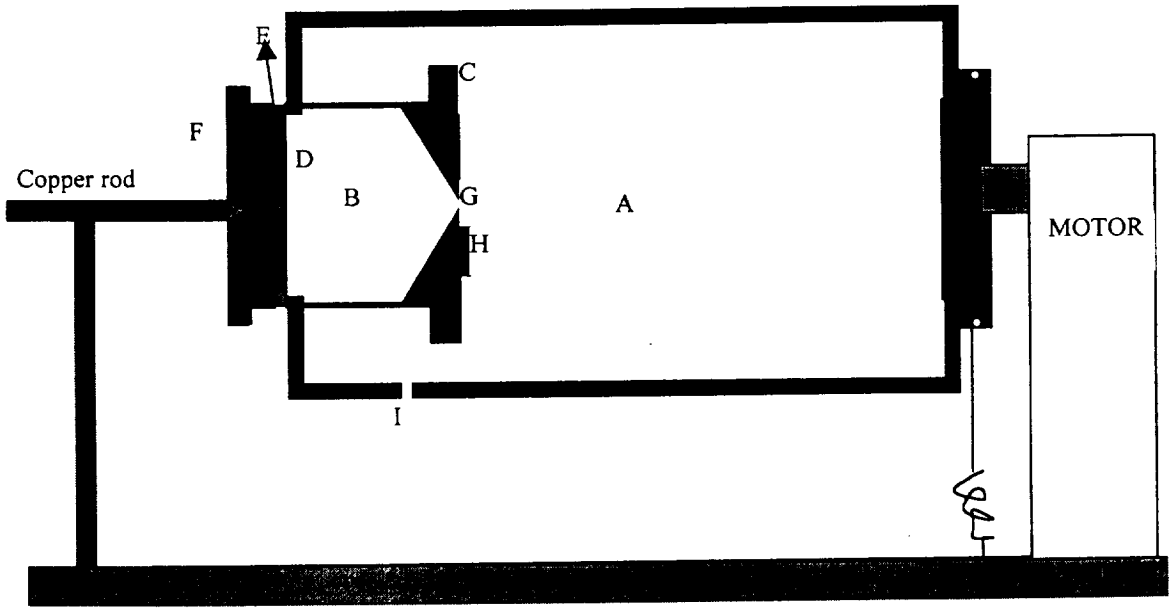

F: Stainless steel caps, which also act as a electrodes.

G: A pin-hole in the test chamber through which mass transport takes place

H: A rubber strip used for covering G during weight measurements

I: An orifice, closed during electrophoresis. Used for venting the vacuum before the test chamber is removed from or inserted into the main body.

Operation of the instrument:

80% of the main chamber was filled with the suspension. Then the suspension was separately filled into the test chamber. When the lid C was put on the chamber, excess suspension comes throughout the hole G. Some suspension flowed out from the sides as well. The overflow was carefully wiped using a tissue. The test chamber was tapped to remove any air that may be trapped inside. The weight of the test chamber was measured with the tantalum sheet and alumina cap on it. This was the initial weight. The steel cap being too heavy reduces the sensitivity of the weight measurement. Hence it was removed during weight measurements. The test chamber was then inserted into the main chamber. The orifice "I" was kept open to facilitate easy insertion and the out flow of any suspension due to the vacuum that may be created. It was closed with the screw during elctrophoresis.

Then the entire assembly was hung on the support structure to do electrophoresis. The steel cap on the main chamber has a groove on it. A copper wire running through this groove provides a sliding electrical contact for one electrode. The other contact is provided at the copper rod on which the steel cap rides. The motor rotated the entire assembly at 28 rpm during electrophoresis. This was done to ensure that the slip did not settle out during the process. After electrophoresis was done, the orifice I was opened to vent the chamber. Then, the test chamber was removed. It was carefully wiped to remove all the liquid on its walls. It was then

reweighed. The difference in weight was calculated and the conductivity of the slips measured. Using these data, the electrophoretic mobility was calculated.

Two-three readings were made for each pH value. The final calculated mobilities with the standard deviations are given below:

PH	Average Electrophoric Mobility (10^{-3}cm2/V.sec)	Standard Deviation (10^{-3}cm2/V.sec)
6.87	40 (Average of three readings)	38.2
8	16 (Average of two readings)	2.83
9.2	13 (Average of two readings)	2.83

APPENDIX B

Specifications of the Butvar binders used for slurry coating (from http://www.coatings-solutia.com/docs/Butvar.htm)

Butvar B-76:

Property	Limits	Test Method
Hydroxyl Content, % (Expressed as % Polyvinyl Alcohol)	11.0-13.0	Titration WS-03-76-09B
Solution Viscosity, cps (5% solids in ethanol @ 25°C)	18.0-28.0	Ostwald Viscometer WS-03-76-01D
Volatile Content, %	5.0 max.	Thermogravimetric WS-03-76-03B

Useful Information

Form	White, free-flowing powder
Acetate Content, (% Polyvinyl Acetate)	1.5 max
Butyral Content, (% Polyvinyl Butyral)	88 (approximate)
Molecular Weight* (Mw)	90,000-120,000
Specific Gravity	1.083
Glass Transition Temperature (Tg), °C	62-72
* Size exclusion chromatography with low angle laser light scattering standard	

Butvar B-79:

Property	Limits	Test Method
Hydroxyl Content, % (Expressed as % Polyvinyl Alcohol)	10.5-13.0	Titration WS-03-79-09B
Solution Viscosity, cps (5% solids in ethanol @ 25°C)	9.0-16.0	Ostwald Viscometer WS-03-79-01B
Volatile Content, %	5.0 max.	Thermogravimetric WS-03-79-03B

Useful Information

Form	White, free-flowing powder
Acetate Content, (% Polyvinyl Acetate)	1.5 maximum
Butyral Content, (% Polyvinyl Butyral)	88 (approximate)
Molecular Weight* (Mw)	50,000-80,000
Specific Gravity	1.083
Glass Transition Temperature (Tg), °C	62-72
* Size exclusion chromatography with low angle laser light scattering standard	

APPENDIX C

The various recipes tried out for slurry coating:

Constituent	Amount of material				
	from literature	1st trial	2nd trial	3rd trial	4th trial
1st Milling					
Alumina	100gm (Unknown)	100gm (D)	100gm (D)	100gm (A)	100gms (F)
Toluene	14.4gm (20ml)	26ml	26ml	33ml	18ml
MEK	14.4gm (20ml)	18ml	18ml	29ml	18ml
Defloc Z-3	2.00gm	2.00gm	2.00gm	2.00gm	3.00gm
Sancticizer 160	4.30gm	4.30gm	4.30gm	4.30gm	4.30gm
Butvar Binder	5.00gm (B-79)	1.25gm (B-76)	1.25gm (B-76)	1.25gm (B-79)	-----
C-Hexanone	-------	-------	1.25µl	1.25 µl	-----
Ball milled for	Not available	18hrs		15hr	8hr
2nd milling	-----				